1-1-2010

Static And Transient Voltage Stability Assessment Of Hybrid Ac/ Dc Power Systems

Minglan Lin

STATIC AND TRANSIENT VOLTAGE STABILITY ASSESSEMENT OF HYBRID AC/DC POWER SYSTEMS

By

Minglan Lin

A Dissertation
Submitted to the Faculty of
Mississippi State University
in Partial Fulfillment of the Requirements
for the Degree of Doctor of Philosophy
in Electrical Engineering
in the Department of Electrical and Computer Engineering

Mississippi State, Mississippi

December 2010

STATIC AND TRANSIENT VOLTAGE STABILITY ASSESSEMENT OF HYBRID AC/DC POWER SYSTEMS

By

Minglan Lin

Approved:

Stanislaw Grzybowski Professor of Electrical and Computer Engineering (Major Professor)	Noel N. Schulz Professor of Electrical and Computer Engineering (Co-Major Professor and Dissertation Director.)
Anurag K. Srivastava Assistant Professor of Electrical Engineering and Computer Science (Dissertation Co-Director and Committee Member)	Randolph F. Follett Assistant Professor of Electrical & Computer Engineering (Committee Member)
James E. Fowler Professor and Director of Graduate Studies Electrical and Computer Engineering	Sarah A. Rajala Dean of the Bagley College of Engineering

Name: Minglan Lin

Date of Degree: December 10, 2010

Institution: Mississippi State University

Major Field: Electrical Engineering

Major Professor: Dr. Stanislaw Grzybowski

Title of Study: STATIC AND TRANSIENT VOLTAGE STABILITY ASSESSEMENT OF HYBRID AC/DC POWER SYSTEMS

Pages in Study: 135

Candidate for Degree of Doctor of Philosophy

Voltage stability is a challenging problem in the design and operation of terrestrial and shipboard power systems. DC links can be integrated in the AC systems to increase the transmission capacity or to enhance the distribution performance. However, DC links introduce voltage stability issues related to the reactive power shortage due to power converters. Multi-infeed DC systems make this existing phenomenon more complicated. In addition, shipboard power systems have unique characteristics, and some concepts and methodologies developed for terrestrial power systems need to be investigated and modified before they are extended for shipboard power systems.

One goal of this work was to develop a systematic method for voltage stability assessment of hybrid AC/DC systems, independent of system configuration. The static and dynamic approaches have been used as complementary methods to address different aspects in voltage stability. The other goal was to develop or to apply voltage stability indicators for voltage stability assessment. Two classical indicators (the minimum eigenvalue and loading margin) and an improvement (the 2nd order performance indicator) have been jointly used for the prediction of voltage stability, providing

information on the system state and proximity to and mechanism of instability. The eliminated variable method has been introduced to calculate the partial derivatives of AC/DC systems for modal analysis. The previously mentioned methodologies and the associated indicators have been implemented for the application of integrated shipboard power system including DC zonal arrangement.

The procedure of voltage stability assessment has been performed for three test systems, the WSCC 3-machine 9-bus system, the benchmark integrated shipboard power system, and the modified IEEE RTS-96. The static simulation results illustrate the critical location and the contributing factors to the voltage instability, and screen the critical contingencies for dynamic simulation. The results obtained from various static methods have been compared. The dynamic simulation results demonstrate the response of dynamic characteristics of system components, and benchmark the static simulation results.

DEDICATION

I would like to dedicate this work to my beloved family and all friends who support me.

ACKNOWLEDGEMENTS

I express my deep gratitude to my dissertation directors, Dr. Noel N. Schulz and Dr. Anurag K. Srivastava, for their valuable guidance, assistance, encouragement and financial support throughout the course of my stay at Mississippi State. They not only made me academically sound but also enlightened my personality. They gave me opportunities to present at several conferences, which widened my view and gave me recognition.

I thank my major professor, Dr. Stanislaw Grzybowski, and committee member, Dr. Randolph F. Follett, whose comments and suggestions were very helpful. Also their classes gave me the necessary knowledge and skills to fulfill my research work.

I gratefully acknowledge the financial support of the Office of Naval Research and the Electric Ship Research and Development Consortium. Special thanks to all the technical staff and graduate students working on the MSU E-ship project.

I thank my parents and my family for their love, affection and encouragement throughout my life, which is so deep that I can feel it in spite of the time and space between us. I owe all my achievements to the guidance of my parents.

Special thanks to my husband, whose love and encouragement have helped me to this stage, and permitted me to achieve my goal in this record time.

TABLE OF CONTENTS

LIST OF TABLES

LIST OF FIGURES

LIST OF SYMBOLS

SYMBOLS

The symbols below summarize the quantities used in equations and figures of Chapters 3 and 5 to describe the DC features and architecture. All quantities are given in pu. Subscript t refers to the converter ac terminals; subscript r refers to the rectifier and i to the inverter.

1) Voltages and Currents

V	Nodal Voltage Magnitude
θ	Nodal Voltage Angles
V_d (V_{dr}, V_{di})	Voltage at Converter DC Side
V_t (V_{tr}, V_{ti})	Voltage at Converter AC Side
V_C	Capacitor Voltage
I_d (I_{dr}, I_{di})	Direct Current
I_0	Measured Direct Current
I_m	Current Margin
I_{ord}	Current Order

2) Powers

ΔP	Active Power Mismatches

ΔQ	Reactive Power Mismatches
P_d (P_{dr}, P_{di})	Active Power Consumed by Converters
Q_d (Q_{dr}, Q_{di})	Reactive Power Consumed by Converters and Transformers
S_d (S_{dr}, S_{di})	Apparent Power Consumed by Converters and Transformers
P_t^{spec}, Q_t^{spec}	Specified Active/Reactive Power at Converter Terminals
P_t^{ac}, Q_t^{ac}	Active/Reactive Power Transmitted by AC Side of Converter
P_I	Active Power Transmitted by DC Side of Converter
Q_c (Q_{cr}, Q_{ci})	Var Compensation Connected to Converter Terminals
P_{si}, Q_{si}	Active/Reactive Power Injected from Power Sources
P_L (P_{Lr}, P_{Li})	Active Power Loads Connected to Converter Terminals
Q_L (Q_{Lr}, Q_{Li})	Reactive Power Loads Connected to Converter Terminals

3) DC Line Parameters

X_c	Commutating Reactance
R_d	DC Line Resistance
R_r, R_i	Converter Resistance
b_c (b_{cr}, b_{ci})	Susceptance Connected to Converter Terminals
T (T_r, T_i)	Converter Transformer Tap Ratio
α	Firing Angle
γ	Extinction Angle
μ	Overlap Angle

CHAPTER I

INTRODUCTION

1.1 Introduction to Voltage Stability

Voltage stability is the system's ability to control its voltage following small disturbances or big disturbances, which is a challenging problem in the design and operation of power systems, including terrestrial and shipboard power systems. In terrestrial power systems, voltage stability is gaining importance as the trend of operating power systems closer to their limits continues to increase. Voltage instability and collapse can be related to stresses on the power system, caused by lack of sufficient reactive power reserves to compensate for the increased loading level. The economic and societal consequences of voltage collapse and blackout are significant, compounded with deregulation and emerging competition in the electric utility industry. Therefore, voltage instability has become a serious concern in the planning and operation of power systems. Voltage collapse incidents have prompted the investigation of various techniques, such as PV and VQ curves, modal analysis, and dynamic analysis, to minimize the potential of voltage instability. Knowledge of voltage stability can help system operators to estimate the limits of power systems, which have major service quality and economic implications.

On the other hand, the integrated shipboard power system with a DC Zonal Electric Distribution System (DC ZEDS) is under investigation for possible implementation on the next generation of surface combatants. Though significant gains

can be realized in terms of survivability, weight, manning, and cost, voltage stability is a big concern for the integrated shipboard power system with a DC zonal architecture, since such a system has power electronic devices, which may result in a reactive power shortage and voltage instability. Understanding the voltage stability and working to maintain the integrity of this system's operation is vital.

1.2 Introduction to Hybrid AC/DC Power Systems

DC links are widely recognized as being advantageous for long-distance, bulk power delivery, and asynchronous interconnection. Newer conversion technologies permit the wider use of DC links in additional applications.

1.2.1 DC Links in Terrestrial Power Systems

Traditionally, DC links have been built as single point-to-point AC/DC interconnections, or single-infeed DC systems. However, as the use of DC links continues to develop, more links are under construction, and two or more converters have been added into AC system locations. Thus, various system configurations, termed as multi-infeed DC systems, are expected to be integrated in advanced power systems.

DC power is independent of the frequency and relative phase of power systems, and can be transmitted between two independent AC systems without applying any operational restrictions to either system. When updating an AC system with additional DC transmission lines, the controllability of DC means that the power delivered can be modulated to give improved damping to the AC transmission. The maximum angular displacement of voltage vectors between the ends of parallel AC lines can be changed to increase the power transmission capacity of the line. However, voltage stability has been a limiting factor for the operation of DC links during the weak AC conditions, and multi-

infeed DC systems make this existing phenomenon more complicated. This necessitates the development of appropriate computational tools, which take into account the incorporation of DC lines, converters and control equipment for analyzing power flow in hybrid AC/DC power systems as well as for assessing voltage stability in AC/DC systems.

1.2.2 DC Links in Shipboard Power Systems

The U.S. Navy has proposed two alternative distribution architectures for their future shipboard power systems [2]. One is based on Medium Voltage DC (MVDC) distribution, and the other is based on High Frequency AC (HFAC) distribution. In replacing the low voltage AC distribution systems, the implementation of DC Zonal Electric Distribution Systems (DC ZEDS) provides several advantages with regards to comparisons with its AC counterparts. DC ZEDS facilitates isolating faults to an electrical zone. The current sensors and algorithms required to detect fault conditions are both simpler and faster. Most of the distribution transformers and AC switchgears may be eliminated in DC ZEDS, which offer a considerable benefit in terms of both weight and size. The generation frequency is decoupled from the distribution requirements. The enhanced performance and improved flexibility motivate the selection of DC ZEDS over an AC counterpart. However, DC ZEDS introduces several stability issues related to the interconnection of a number of high-bandwidth, nonlinear power converters, which is an ongoing research area in terms of system characterization, analysis and control.

1.3 Voltage Stability Assessment

The objective of voltage stability assessment is to determine the current system state as well as the proximity to instability. If instability occurs, the proper analysis needs

to identify the involved areas and contributing factors. Furthermore, the associated measures will be applied to mitigate or control instability. In summary, voltage stability assessment must provide information on system state, proximity to, and mechanism of instability.

Many aspects of power system problems including voltage stability can be effectively analyzed by using steady-state and dynamic approaches.

1.3.1 Steady-State (Static) Analysis

Static analysis is concerned with the existence and/or stability of equilibrium under small disturbances in power system parameters. Such static approaches are based on the steady-state model or on the linearized system model, which only considers algebraic equations and time is handled implicitly.

Static analysis requires much less CPU, and provides much more insight into system state, proximity to, and the mechanism of instability. It can be used for examination of a wide range of system conditions and a large number of contingencies in the bulk of system studies. Though modeling simplifications are usually applied in analysis, the essential mechanics are required to retain in this research. In addition, time trajectory is not computed, which may cause difficulties to predict certain characterizations of instability.

1.3.2 Dynamic Analysis

Dynamic analysis is concerned with the stability of the system state and equilibrium under large disturbances in system parameters. Consequently, dynamic approaches are based on the complete power system models by taking into account the

dynamic characteristics of system components. This analysis considers differential equations, and uses enhanced time-domain simulations (time is explicitly handled).

Dynamic analysis captures the events and timeline leading to voltage instability, which accurately replicates the actual dynamics of voltage instability. It also provides the performance of system and individual devices. However, dynamic analysis is time consuming in terms of CPU, even with state-of-the-art techniques, which makes multiple contingency analyses impractical. Dynamic simulations do not readily provide sensitivity information or the degree of stability. Thus, dynamic analysis is essential for the detailed study of special voltage collapse situations, involving the coordination of protection and control, and the testing of remedial measures. Dynamic analysis can also provide benchmarks for steady-state analysis.

Therefore, the most effective solution for voltage stability assessment is to use a variety of complementary methods to address different aspects of the phenomena or analysis requirements.

1.4 Research Motivation

A number of methods and tools for studying voltage stability in power systems have been proposed. Much of the work has been made focusing in one of two specific systems, either a "pure" AC system or a DC system with only the converter AC buses connected by the equivalent impedance. However, many aspects of the voltage stability problem are similar for both "pure" AC systems and DC systems. This research works to develop a comprehensive and systematical analysis method for hybrid AC/DC systems. Several methods traditionally applied to AC systems will be extended to voltage stability analysis of hybrid AC/DC systems.

In addition, though various DC configurations exist, the previous concepts and methods were introduced mainly based on the single-infeed DC configuration. There is some belief that the interaction phenomena and associated problems for single-infeed and multi-infeed configurations are closely related. Many conceptual ideas developed for single-infeed DC systems are similar to those for multi-infeed DC systems since the multi-infeed evolved from the single-infeed. Although the single-infeed DC systems are the most common occurrence in AC/DC interconnections, it is necessary to develop an analytical technique which is valid for both single-infeed and multi-infeed DC configurations integrated with AC systems scenarios.

Various voltage stability indicators have been proposed in the previous research which will be reviewed in Chapter 2. Most of these indicators were developed for static analysis, and are limited for dynamic analysis. Voltage stability indicators for dynamic analysis, though affected by system dynamics, preserve the same relationship as their static counterparts. This motivates the idea of the development of indicators for dynamic analysis, which combines the static indicators with the effects of dynamic components, such as synchronous machines and their voltage control. Thus, static assessment approaches may be extended to transient voltage stability assessment, and the associated dynamic indicators may also be developed.

Voltage stability of AC systems, whether stiffly connected or following an infinite bus assumption, is well understood. Less is known about networks of power converters in such a stiffly-connected platform as a shipboard power system. Since the power system may be quickly reconfigured because of equipment failure or enemy damage, understanding voltage stability is a prime issue to guarantee the integrity and survivability of shipboard power systems. Some of the concepts developed for terrestrial

power systems can be modified and extended to shipboard power systems. Increasing usage of AC/DC systems requires investigation for several issues including voltage stability for such a hybrid system.

1.5 Objectives and Outline of Thesis

This thesis contains two fundamental, interrelated, and overlapping tasks. The first task is to propose a methodology for analyzing hybrid AC/DC power systems independent of system configuration. The second task is to develop and implement voltage stability indicators for static and transient voltage stability assessment. The goal of these two tasks is to develop a systematic method for voltage stability assessment of hybrid AC/DC power systems, providing information on system state, proximity to instability, and mechanism of the instability. Finally, the assessment method developed for terrestrial power systems will be extended to application of integrated shipboard power systems with DC zonal architecture.

Chapter 2 provides background information on voltage stability assessment and hybrid AC/DC systems as well as the associated analysis methods. Section 2.1 gives the definition and classification of voltage stability. Section 2.2 provides a glimpse of steady-state and dynamic approaches for voltage stability assessment. The corresponding indicators are described in Section 2.3. Section 2.4 provides a review of hybrid AC/DC characteristics and load flow methods. Section 2.5 introduces the unique characteristics of shipboard power systems. Section 2.6 is a concise statement of problems for voltage stability assessment of hybrid AC/DC power systems.

Chapter 3 provides a detailed description of system model and simulation considerations. The overall power system model is given in the form of the basic

differential and algebraic equations, and the detailed description of each model follows. Section 3.1 describes the network model based on appropriate assumptions. Sections 3.2 and 3.3 introduce the various static and dynamic models of system devices, including generators, loads, DC links and other devices. Section 3.4 describes disturbance and fault control. Section 3.5 summarizes the models in the notional E-ship power system. Section 3.6 provides a numerical solution to the Differential-Algebraic Equations.

Chapter 4 discusses the generalized guidelines for applying voltage stability assessment methods. The basic functions in assessment package are introduced in Section 4.1, and the main module of voltage stability assessment is also discussed in this section. The main steps of static and transient assessment are discussed in Sections 4.2 and 4.3, respectively. Section 4.4 introduces the main tools used in this work.

Chapter 5 discusses two classical indicators for voltage stability assessment and proposes the 2nd performance indicator as an improvement. Section 5.1 provides the detailed description of modal analysis and loading margin, and presents the development of the 2nd order performance indicators. Section 5.2 illustrates two DC configurations, and derives the associated Jacobian matrices. Section 5.3 makes a summary and a comparison of the discussed indicators.

Chapter 6 demonstrates the procedure of static voltage stability assessment. Section 6.1 gives the description of WSCC 3-machine 9-bus system and a small disturbance to trigger the assessment. This section also contains the discussion of implementation of modal analysis, loading margin and the second order performance indicator, and gives a comparison of voltage stability assessment for WSCC with different control modes. Section 6.2 describes a benchmark shipboard power system.

Modal analysis and loading margin are deployed for base case and the selected contingency.

Chapter 7 demonstrates the procedure of transient voltage stability assessment. Section 7.1 gives a description of modified IEEE one-area RTS-96 system, and performs load flow and AC contingency analysis to screen the specified list. Modal analysis, PV and QV plots, and the second order performance indicator are implemented for base case and the selected contingencies. Section 7.2 discusses the dynamic simulation of the most critical contingency, and shows the response of dynamic characteristics to voltage stability.

Chapter 8 contains the conclusion and future work regarding this research. References and appendices follow.

CHAPTER II

LITERATURE REVIEW

Voltage stability problems have been known for long time. The first paper related to voltage instability by B.M. Weedy was appeared in 1968 [3], and the first criteria for detecting the point of voltage collapse was proposed by Wenikov in 1975 [4]. But active work involving voltage stability started in the 1980's [5]. Since then many methods and indicators have been proposed and used throughout the world for voltage stability analysis. The first commercial application of DC transmission was built between the Swedish mainland and the island of Gotland in 1954 [6]. In the later 1990's a number of newer converter technologies boosted the more construction of DC transmissions [7]. This increase is likely to continue with advancing solid state technology, increasing DC expertise, and lower costs for conversion equipment. Although DC lines can improve the transfer capability and performance of AC systems, they make the problem of voltage stability even worse because of their requirement of reactive power, especially for the weak AC systems.

This chapter provides the background definition and classification of voltage stability, reviews the existing static and dynamic approaches for voltage stability assessment as well as the associated voltage stability indicators. This chapter also provides a review of the features, modeling and analysis approaches of hybrid AC/DC systems.

2.1 Definition and Classification of Voltage Stability

The definition for voltage stability has been given by IEEE/CIGRE Joint Task Force [8] as "*Voltage stability* refers to the ability of a power system to maintain steady voltages at all buses in the system being subjected to a disturbance from a given initial operation condition". More often, people are interested in the phenomena and mechanism of voltage instability, and use the definition in [9], "*Voltage instability* stems from the attempt of load dynamics to restore power consumption beyond the capability of the combined transmission and generation systems". As indicated by this description, loads are the driving force of voltage instability. The transfer capability of transmission and the performance of generation affect voltage stability. As a result voltage stability is a condition of equilibrium depending on network topology, system operating conditions and the disturbance.

Table 2.1 Classification of Voltage Stability Scenarios and Approaches

Subcategory		Phenomena	Time frame	Approach
Small disturbance voltage stability		Incremental changes in system loads	An instant of time	Linearization, static approach
Large disturbance	Short term	Unfavorable fast-acting loads (induction motors, electronically controlled loads, HVDC converters)	0 –10 seconds	Dynamic approach
	Mid-term	Loss of generators Loss of major transmission lines	2-3 minutes	Dynamic approach
	Long term	Large load buildup, large rapid power transfer increase	Longer time, may extend to hours	Quasi Steady State approximation

For convenience in analysis as well as for gaining insight into the nature of voltage stability problems, it is useful to characterize voltage stability in terms of subcategories, which are specified according to disturbance or time frame of interest [8]. The subcategories of voltage stability associated with the involved scenarios and analysis

approaches are summarized as Table 2.1. More information of the classification and the separation of time frame can be found in [1].

Dynamic stability has been used to denote different phenomena by different authors. In the North American literature, it has been used mostly to denote a small-disturbance stability in the presence of automatic controls (particularly, the generation excitation controls) as distinct from the classical "steady-state stability" with no generator controls. In the European literature, it has been used to denote transient stability. Since much confusion has resulted from the use of the term of dynamic stability, reference [8] recommended against its usage. Transient stability will be used to represent the stability of power system to maintain synchronism when subjected to a severe disturbance. Transient stability depends on both the initial operating state of the system and the severity of the disturbance.

In this research, static voltage stability (or small-disturbance voltage stability [8]) refers to the system's ability to maintain steady voltages when subjected to small disturbances, such as incremental changes in system loads; while transient voltage stability (or large-disturbance voltage stability [8]) refers to the system's ability to maintain steady voltages following large disturbances, such as system faults, loss of generation, or circuit contingencies.

2.2 Static and Dynamic Assessment Approaches

A number of algorithms have been proposed in the literature for voltage stability assessment. The most common and widely used algorithms have been categorized, based on analysis methods, whether a static or dynamic approach is taken. Electric utilities still tend to depend largely on the conventional power flow method to determine voltage

collapse buses. The simplest and most widely used method is to define the bus voltage range (typically 0.95 to 1.05 pu) [10, 11]. The problem with this method is that voltage range is specified somewhat arbitrarily, and in some cases, too restrictive since the system may actually remain stable at lower voltage level.

2.2.1 Steady-State (Static) Approaches

Most of static approaches deal with results from power flow programs, and can further be categorized into one of two groups. One is the technique that requires an assumption on the path to system collapse. System snapshots are calculated by the conventional power flow studies to capture the voltage evolution toward collapse through slow parameter variation (usually system loading level) [12]. Continuation power flow [13, 14] was introduced to overcome the divergence which occurs in the conventional power flow algorithms at operating conditions near the stability limit. These methods are robust and powerful, but computationally expensive, and require the assumption of a particular trajectory to collapse. Moreover, they only trace the voltage curve at the individual buses, so it is difficult to locate the critical or weak area among the large system.

The other category of techniques uses information only pertaining to the current system states, such as eigenvalues of the power flow Jacobian [15, 16]. The relationship between the magnitude of eigenvalues and characteristics of voltage stability was investigated [17, 18]. This method is suitable for applications of large systems, and provides additional information about buses, branches, and generators. Unfortunately, such quantities as eigenvalues or participation factors exhibit large discontinuities and nonlinearities, particularly when device limits are enforced. This method may provide a

false sense of stability. As a result, a derivative category has been proposed, where the techniques represent a hybrid of two groups aforementioned. This method predicts the proximity to collapse in terms of relationships derived from multiple power flow solutions [19], [20]. Some of these techniques were described in the IEEE/PES special publication [21]. In general, most of them have not found widespread practical application.

2.2.2 Dynamic Approaches

Although many static approaches have been proposed, none has clearly demonstrated results consistent with the performance of practical power systems since power systems are naturally complex, nonlinear systems. If dynamic characteristics are not considered, the credibility of analysis results is negatively affected.

There are a limited number of dynamic approaches which have been proposed in the existing literature, such as bifurcation dynamic method [22, 23] and time-domain simulation method [24, 25]. Based on the small signal method, the differential bifurcation, such as saddle node bifurcation, Hopf bifurcation and singularity induction bifurcation, can be obtained from the differential algebraic equations of power systems [26]. The region of dynamic stability is identified by modal participation factors of state variables [27]. However, the dynamic bifurcation method is effective only if systems under consideration are low order and simple. The time-domain simulation method is the most popular one for dynamic analysis, and can provide the most accurate replication of the actual dynamics of voltage stability. If provided appropriate models, the time-domain simulation can capture the events and their timeline, leading to voltage instability. Though the time-domain simulation method is time-consuming in terms of CPU, many

numerical methods [6] have been greatly enhanced in recent years to make them suitable for voltage stability assessment.

Using complete dynamic approach means that the model must reflect all dynamic phenomena which have the potential to cause unacceptable operating conditions. Since almost all phenomena are coupled, it is not clear which dynamic model can be ignored. One solution is to eliminate those dynamic states which do not contribute to the critical points. Voltage stability is basically load stability [1]. Fast acting load components [28], such as induction motors, electronically controlled loads and DC converters, are critical in voltage stability analysis, and their dynamic modeling is essential. The composite load comprising residential, commercial and industrial loads [29], loads consisting of a static load plus an aggregate of induction motors [30], and a DC link in parallel operation with an AC transmission [31] have been discussed in the previous literature. This type of voltage stability is specified as short-term voltage stability [32], and the study period of interest is in the order of several seconds. Short-term voltage stability is also of interest in this research.

2.3 Voltage Stability Indicators

To evaluate voltage stability, various indicators have been proposed in the previous literature, involving system physical parameters, such as voltage level [33], load capacity [34, 35], and reactive reserves [36, 37]. Corresponding to static approaches discussed in Section 2.2.1, indicators are further separable into two types, namely "direct" and "indirect" measurements. These two types of indicators play mutually complementary roles in static voltage stability assessment. In general, "direct" measurements focus on the variation of only one system parameter of interest,

constraining other parameters to be constant; while "indirect" measurements provide a system wide assessment.

Loading margin [21] is a prominent "direct" indicator, the most basic and widely accepted one. Loading margin can in principle be calculated by starting at the current operating point, making small increases in loading and re-computing load flow at each increment until the nose of curve (P-V or Q-V curve) is reached by using the conventional [38] or continuation [13] power flow method. The maximum loadability can be observed from the curve. The similar concept in DC links is maximum available power, which is defined as DC power corresponding to a direct current, where $\frac{dP_d}{dI_d} = 0$ [39]. Such performance indicators should have a predictable shape or be smooth so that an acceptable prediction may be made. Though straightforward, the computational cost is the most serious disadvantage, and this method requires the assumption of a direction of load change.

The representative of "indirect" measurement is an eigenvalue or singular value [40, 41], which is to define a scalar magnitude that can be monitored as system parameters change. This is a bus-oriented index, based on the Jacobian matrix and applied to power flow models. The fundamental idea is to detect the collapse point by monitoring the minimum eigenvalue or singular value of the system Jacobian matrix, which approaches zero at collapse point. In addition, the maximum entries in the right eigenvector correspond to the critical buses (the most sensitive voltage) in the system; The maximum entries in the left eigenvector pinpoint the most sensitive direction for changes of power injections, and the associated participation factors can be used to identify the critical bus, branch and generator [42, 43]. The corresponding concept of "indirect" measurement in DC links is voltage stability/sensitive factor, which is defined

as the sensitivity of the converter AC bus voltage to a small reactive power injection at the same bus, and assumes $\Delta P = 0$, $VSF = \frac{\Delta V}{\Delta Q}$ [39]. This index is useful but highly nonlinear.

Corresponding to dynamic analysis, only few dynamic indicators have been proposed in the literature. Dynamic maximum available power and dynamic voltage stability factor for DC links have been discussed [39], which can be regarded as the extension of static indicators by incorporating with the characteristics of dynamic components. Hence, a dynamic indicator is expected to be developed in this research.

There are other indicators, such as voltage instability proximity index (VIPI) [44], reduced determinant [45], and tangent vector index (TVI) [46], which have been discussed in the existing literature and summarized in Chapter 4 of the IEEE special publication, "Voltage Stability Assessment: Concepts, Practices and Tools" [21]. In this research, two of the most popular indicators will be described, compared and verified. These indicators will be revised as new methodologies and solutions develop, and their development is an on-going process with future additions, changes and deletions.

2.4 Hybrid AC/DC Power Systems

DC links were introduced to solve the technical problems inherent in AC systems, such as long distance transmission and asynchronous interconnection. The technological improvements in hardware and control methods have made DC a major element in power systems. Various characteristics, theoretical analysis, modeling and computational techniques of AC/DC interactions have been investigated in the literature.

This section reviews the basic principles and features of operation and control of DC systems and introduces their modeling and analysis methods for power flow and stability studies.

2.4.1 Features of Hybrid AC/DC Systems

There are advantages of transmitting power by DC rather than by AC, which are summarized as follows [7, 47, 48].

- For terrestrial power systems, DC power can be transmitted in cables over great distances. Power transmitted depends upon line reactance and the phase angle between the voltages at each end of the line. But when power is transmitted by DC, frequencies and phase angles have limited impact, and line reactance does not limit the steady-state DC power flow. Theoretically, there is no limit to the distance that power may be carried this way. If anything, it is only the resistance of the line that limits the flow. Moreover, overhead DC transmission lines become economically competitive with AC lines when the length of line exceeds several hundred kilometers. The width of the power corridor is less, and experience to date has shown that outages due to lightning are somewhat reduced.

- At the opposite extreme of great distance are back-to-back converters, for example, in shipboard power systems, a DC line is used to interconnect adjacent AC systems which may be only a few meter apart. Back-to-back converters enable the two systems to operate at their respective frequencies and phase angles. As a result, disturbances on one system do not tend to destabilize the other system. Furthermore, the power flow between the systems can be modified and even reversed in a matter of milliseconds, much faster than can be achieved on AC systems. Most of the distribution transformers and AC switchgear can be eliminated in DC systems. Therefore, the substantial gains in size and weight, efficiency and enhanced performance, and improved flexibility motivate the selection of DC over an AC counterpart.

- DC power can be controlled much more quickly. This feature makes it useful to operate DC transmission lines in parallel with existing AC networks. When instability is about to occur (due to disturbances on the AC system), the DC power can be changed in amplitude to counteract and dampen the power oscillations. Quick power control also means DC short-circuit currents can be limited to much lower values than those encountered on AC network. Sometimes, this controllability allows additional power to be transmitted safely through an AC interconnection by enabling the maximum angular displacement of voltage vectors between the end of parallel AC line.

However, unlike AC transmission lines, it is not easy to tap power off at different points along a DC line. In effect, DC lines are usually point-to-point systems, tying one large generating station to one large consuming center. Multi-terminal DC lines have been introduced to make this transmission more flexible.

2.4.2 Hybrid AC/DC Modeling and Analysis Approaches

The detailed modeling of a DC system was firstly proposed within a stability based AC system framework [49], where the DC system was modeled using state variable techniques while the AC system was represented by a conventional stability program. An EMTP solution was used for such detailed analysis. This hybrid idea was modified by moving the interface location away from the converter terminals where distortion and phase imbalance were less prevalent [50]. A type of hybrid approach was used in NETOMAC [51], a digital program for dynamic network calculation provided by Siemens PTI. In this program, two separate modes have been used for modeling to reduce the computational requirements, namely an instantaneous mode and a stability mode. The first mode models components in three phase detail with small time steps, and the second mode models the system in *rms* quantities at fundamental frequency, with increasing time step lengths.

Two different approaches have been introduced to solve the load flow in AC/DC interconnections. The first one is the sequential method [52, 53], in which AC and DC equations are solved separately each iteration. This method is easy to implement, but convergence problems may occur in certain situations. The second one is the unified method [54, 55], in which the solution vector is extended with DC variables. The drawback of this method is that it is complex to program and difficult to combine with

AC power flow solution techniques. To overcome the difficulties of both methods, the eliminated variable method was proposed [56], in which the real and reactive powers consumed by converters were treated as voltage dependent loads. Thus, it is unified since the effect of DC links is included in the system Jacobian matrix. At the same time, it handles AC and DC power flow separately simplifying the implementation and modification.

DC dynamic characteristics arise from DC lines and DC controllers. It is very important to know the preliminary range of DC control settings and system parameters to avoid the exhibition of the different modes of instability. A fundamental and rudimentary analysis of the nonlinear phenomena in DC systems was presented in [57]. DC control modes have been explained in details [6], and can be summarized as follows.

- The rectifier is provided with a current control and an α limit control.
- The inverter is provided with a constant extinction angle (CEA) control and a current control, while CEA control is the norm, there are variations which include voltage control and β control.
- Under normal conditions, the rectifier is on current control mode and the inverter is on CEA control mode. When the AC voltage at the rectifier end is reduced until the rectifier firing angle hits the $\alpha_{\min}$ limit, the rectifier will switch to $\alpha_{\min}$ control, and the inverter will assume current control.

The hybrid simulation is very useful in studying the impact of an AC dynamic system on DC system dynamic performance, which takes advantages of the computationally inexpensive dynamic representation of AC system in the stability program. The slow dynamics of AC systems are sufficiently represented by the steady-state program, while the fast dynamic response of DC systems is accurately modeled by electromagnetic means. Disturbance response studies and control assessment are typical examples for the hybrid simulation package.

2.5 Shipboard Power Systems

The terrestrial power systems are optimized for reliability and the minimal operating cost; while the function of shipboard power systems has determined the survivability and minimal weight and volume as the principal priorities, which lead to different architecture and the design consideration.

The unique characteristics of shipboard power systems, with regards to how they contrast with terrestrial power systems are summarized as the following [70].

- Faster prime movers than utilities relative to dynamic times of interest.
- Very little rotational inertia relative to loads.
- Transmission lines are not as significant as for utilities
- Fast controls maintain frequency
- Large, dynamic loads relative to generation
- Generators share loads in proportion to rating
- Very fast load-sharing information is provided to all generators

These different characteristics come to two specific implications for shipboard power systems. One is that typical terrestrial power system models may not appropriate for analyzing shipboard dynamics. Higher-order models are necessary for both generation and loads. “Swing” equation assumption may not be met. The other is that some of the mathematical expediencies used in terrestrial power system analysis cannot be used with shipboard power systems. “Infinite” buses do not have manifestations in shipboard power systems. “Constant voltage”, “constant frequency” and “constant power” simplification may be invalid. This discussion offers insight into approaches for the design of future shipboard power systems.

The U.S. naval electric shipboards currently employ the radial AC distribution system architecture [71]. There are several other architectures possible for AC shipboard power distribution systems [70, 72]. Additionally, in order to maximize survivability, enhance operational flexibility, minimize size and weight, and decrease the overall cost, the U.S. Navy has proposed two alternative distribution architectures for their future shipboard power systems [73], which have been discussed in Section 1.2.2.

Voltage stability is a concern for shipboard power system architectures. Two methods for voltage stability analysis have been discussed and tested on the benchmark shipboard power system [74]. One is the voltage sensitivity method with P-V sensitivity. The other is the hybrid probabilistic/deterministic index in the form of the expected voltage stability margin. The effects of changing network impedance and loading level were also studied in this literature.

2.6 Summary and Statement of Problems

As a summary of previous research, much of work has been done with various aspects of AC/DC power systems, including their modeling, control technologies, and stability assessment by considering different simulation emphases. However, most previous work has been done with either "pure" AC system or DC system; this work is to present a general and systematic method for AC/DC systems. While many concepts or methodologies are based on the single-infeed DC configuration, the method proposed here is independent of system configuration, which means it is suitable for multi-infeed configuration, and uses the computational efficiency of a hybrid simulation. The steady-state and dynamic simulation methods are used as complements to address the problems of voltage stability. Some typical indicators have been applied to estimate the margin and

to determine the mechanism of voltage instability, but there is the limited discussion about dynamic indicators. In this research, a static indicator is extended to the dynamic application and an effective indicator is developed to overcome the shortages in the previous static indicators. Moreover, the voltage stability assessment procedure and the developed indicator will be used to investigate the voltage stability for shipboard power systems.

CHAPTER III

SYSTEM MODELS AND SIMULATION CONSIDERATIONS

To assess static and transient voltage stability of hybrid AC/DC systems, the modeling and data requirements first should be decided in both static and dynamic analysis. Generally, the model of power systems is given in the form of differential and algebraic equations as shown in Equation 3.1 [21], where x corresponds to system state variables, y represents the "algebraic" variables, and λ stands for parameters that "slowly" change in time so that system moves from one equilibrium point to another until reaching collapse point.

$$\begin{cases} \dot{x} = f(x, y, \lambda) \\ 0 = g(x, y, \lambda) \end{cases} \tag{3.1}$$

An understanding of system characteristics and accurate modeling of their performance are of fundamental importance to the study of voltage stability. However, the problem of defining accurate modeling is very challenging even in the theoretical realm. The proper way to address this problem is selecting an appropriate stability definition, making proper assumptions, formulating a mathematical model of phenomena of interest, and simplifying the complex system to meet the simulation objectives.

According to the definition of voltage stability, it is obvious that voltage stability closely depends on the initial operating conditions as well as the nature of disturbance. Normally voltage instability occurs in heavily stressed systems. Hence, load modeling,

specially the voltage dependent type, is a critical aspect of voltage stability assessment. The other devices such as generators, voltage regulators, AC/DC transmission lines, reactive power compensators, and disturbances/controllers also play important roles in voltage stability analysis.

In this chapter various models required for voltage stability analysis, as well as their simulation considerations, are discussed below, which include:

- Network Model
- Load Model
- Device Static/Dynamic Models
- Disturbances/Control Models

3.1 Network Model

The network model used here is the conventional steady-state power flow equations, which rely on two basic assumptions:

- The quasi-sinusoidal and nominal frequency allows the representation of network with constant impedances at nominal frequency instead of resorting to differential equations.
- The definition of a single, common reference takes on the form of two orthogonal axes rotating at the synchronous speed, for all phasors.

Based on the above assumptions, the voltage-current relationships relevant to an N-bus system can be written in a vector form as Equation 3.2, where $\bar{I}$ is the N-dimensional vector of complex injected currents; $\bar{V}$ is the N-dimensional vector of complex bus voltages; Y is the $N \times N$ bus admittance matrix of the network (with the ground node taken as the voltage reference). This form of relationship is suitable for both static and dynamic analysis.

$$\bar{I} - Y \cdot \bar{V} = 0 \tag{3.2}$$

Two types of network models, namely internal and external models, have been presented in this work. The internal model adequately represents various devices, such as generators, transformers, lines and loads. The external model is the area/zone where equivalent models are used depending on arrangements for data exchange with other transmission systems. More than one external model may be required to account for various operating conditions.

3.2 Load Model

Most components in power systems can be modeled quite accurately, however, loads present a difficulty because of limited available resource to identify model parameters. For research purposes, the term "load" refers to the equivalent representation of the aggregate effect of many individual load devices and the interconnecting distribution and subtransmission systems, which are typically represented as simple functions of voltage. Lack of data and the requirement for detailed representation of major components influencing load behavior, make a simplified load model essential. Recently, loads have been modeled as combinations of constant impedance (Z), constant current (I) and constant power (P) (ZIP model) as Equation 3.3 [21].

$$\begin{cases} P_L = P_{L_P}(1+K_{pc}\lambda) + P_{L_I}(\frac{V}{V_0})(1+K_{pi}\lambda) + P_{L_Z}(\frac{V}{V_0})^2(1+K_{pz}\lambda) \\ Q_L = Q_{L_Q}(1+K_{qc}\lambda) + Q_{L_I}(\frac{V}{V_0})(1+K_{qi}\lambda) + Q_{L_Z}(\frac{V}{V_0})^2(1+K_{qz}\lambda) \end{cases} \quad (3.3)$$

Where, P_L and Q_L represent the load at bus L.

K_{pc}, K_{qc} are per unit of constant MVA active/reactive load;

K_{pi}, K_{qi} are per unit of constant current active/reactive load;

K_{pz}, K_{qz} are per unit of constant impedance active/reactive load.

There exist such relationships that $K_{pc} + K_{pi} + K_{pz} = 1$ and $K_{qc} + K_{qi} + K_{qz} = 1$.

Some simplifications are made that the frequency-dependent exponents are neglected since the frequency effect is not an issue in this research. Nominal (initial) voltage V_0 is assumed to be 1.0 per unit, and 100% of all initial loads are modeled.

Several aspects involving in the representation of a dynamic load model for voltage stability assessment include longer-term dynamics and nonlinearities in the voltage characteristics at low voltage [21]. The modeling of these effects is not well-established and beyond the scope of research in this thesis. More information regarding the nature of load and various approaches of modeling can be found in IEEE Task Force papers [58, 59].

3.3 Device Static/Dynamic Models

Device static models are power flow models of device representations for steady-state operation conditions or after being subjected to small disturbances, while device dynamic models are normally used to represent systems subjected to large disturbances. The typical static/dynamic models are necessary to evaluate the AC/DC voltage stability as described below.

3.3.1 Generators

Under balanced steady-state conditions, the performance of synchronous machines can be readily analyzed by only applying algebraic equations, since rotor quantities are constant and all time derivative terms drop out of the machine equations. Thus, generators can be regarded as points of power injection, and the power flow equations yield adequate results. In other words, the generator static model can be

represented as a real-power source together with a reactive power capability curve as a function of terminal voltage.

Generator dynamic models include the machine mechanical and electrical dynamic equations, and various types of excitation and governor systems. Generator dynamic models range from the simplest to highly elaborate representations of the synchronous machine [60]. All models share certain common features. Usually, hydro turbine units are represented by the salient pole machine model, and thermal units are represented by the round rotor machine model. Detailed electromagnetic models of various generators as well as saturation effects are illustrated and discussed in Chapter 13 of reference [61].

The proper representation of excitation systems requires careful consideration of both the gains and time constants assigned to the voltage regulators and of the characteristics of the excitation power components, which are influential in determining overall dynamic behavior of systems. The turbine-governor model applied here just presents the principal effects in conventional plants. More information are available in [61].

3.3.2 DC Links

The modeling of DC systems in power-flow and stability studies requires consideration of such components as converter model; DC line; DC control model; and the interface between AC and DC systems. The symbols in the following figures and expressions are defined in List of Symbols.

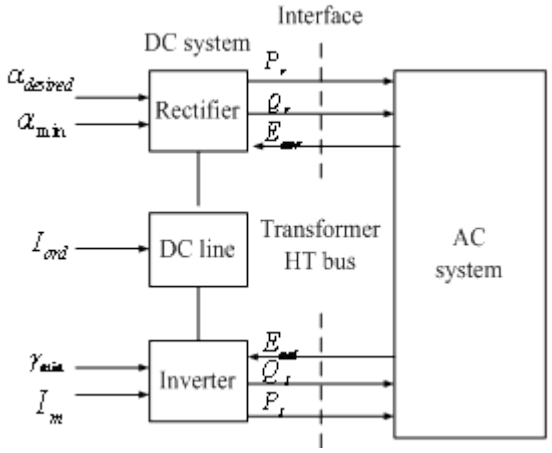

Figure 3.1 The Interface of AC and DC Systems

The interface of AC/DC systems and the relationship of power flow between AC and DC systems, which contains two sets of AC and DC equations, are illustrated in Figure 3.1, where a two-terminal DC line is added in the AC system.

The steady-state behavior of DC links can be represented as Equations 3.4-3.12.

$$V_{dr} = \frac{3\sqrt{2}}{\pi} T_r V_{tr} \cos\alpha_r - \frac{3}{\pi} X_c I_d \tag{3.4}$$

$$V_{di} = \frac{3\sqrt{2}}{\pi} T_i V_{ti} \cos\gamma_i - \frac{3}{\pi} X_c I_d \tag{3.5}$$

$$V_{dr} = V_{di} + R_d I_d \tag{3.6}$$

$$P_{dr} = V_{dr} I_d \tag{3.7}$$

$$P_{di} = V_{di} I_d \tag{3.8}$$

$$S_{dr} = k \frac{3\sqrt{2}}{\pi} T_r V_{tr} I_d \tag{3.9}$$

$$S_{di} = k \frac{3\sqrt{2}}{\pi} T_i V_{ti} I_d \tag{3.10}$$

$$Q_{dr} = \sqrt{S_{dr}^2 - P_{dr}^2} \tag{3.11}$$

$$Q_{di} = \sqrt{S_{di}^2 - P_{di}^2} \tag{3.12}$$

Where k is constant, $k \approx 0.995$ [56]. It is sufficient to find P_d and S_d at each converter, since Q_d can be computed with P_d and S_d.

DC dynamics arise from DC lines and controllers. The converters are represented by the same expressions as the conventional steady-state Equations 3.4-3.12. For simplicity, the DC line model does not include the DC capacitance but in general its inclusion does not pose any conceptual problem in this study.

DC line dynamic characteristics are described as Equations 3.13-3.16.

RL model (without DC capacitance):

$$\frac{dI_d}{dt} = \frac{1}{L}(V_{dr} - V_{di} - RI_d) \tag{3.13}$$

RLC model:

$$\begin{cases} \dfrac{dI_{dr}}{dt} = \dfrac{1}{L_r}(V_{dr} - V_C - R_r I_{dr}) \\ \dfrac{dI_{di}}{dt} = \dfrac{1}{L_i}(V_C - V_{di} - R_i I_{di}) \\ \dfrac{dV_C}{dt} = \dfrac{1}{C}(I_{dr} - I_{di}) \end{cases} \tag{3.14}$$

$$V_{dr} = \frac{3\sqrt{2}}{\pi} T_r V_{tr} \cos\alpha_r - \frac{3}{\pi} X_c I_d \tag{3.15}$$

$$V_{di} = \frac{3\sqrt{2}}{\pi} T_i V_{ti} \cos\gamma_i - \frac{3}{\pi} X_c I_d \tag{3.16}$$

The dependent and independent variables in the solutions of DC equations depend on the rectifier and inverter control modes. Some possible operating modes are discussed in [6]. PI controllers are used to control the firing angles of both rectifiers and inverters.

For example, the rectifier constant current controller is described as Equations 3.17 and 3.18.

$$\frac{dX}{dt} = k_i (I_0 - I_d) \tag{3.17}$$

$$\alpha_r = X + k_p (I_0 - I_d) \tag{3.18}$$

For constant current control, the difference between the measured DC current (I_0) and the desired current (I_d) is used as the input, while for constant power control, I_0 is replaced by P_0 / V_{di}.

In this study, the bridge control angles (alpha α or gamma γ) and transformer tap positions can be adjusted to control DC voltage and current to meet the scheduled power output. Of course this adjustment is subject to control angle limits, two basic control regimes [6] are considered here.

Normal operation: Rectifier and inverter AC voltages are near to normal such that the rectifier is able to maintain current control and the inverter is able to regulate DC voltage.

Depressed voltage operation: When AC voltage at the rectifier is depressed, such that the rectifier reaches its limit (by reducing the firing angle in order to raise the voltage), DC voltage control is abandoned and the inverter adjusts its margin angle to control DC current below the desired value.

Data are required to characterize the DC line for load flow solution, and form the necessary initial "state" for dynamic analysis. Data should be specified for the components such as: 1) power set points and firing angle limits for both the rectifier and the inverter; 2) commutating reactance and tap limits for the converter transformers; and 3) resistance and scheduled DC voltage for the DC line.

3.3.3 Other Devices

Other devices should be also considered and supported at a minimum. In power flow calculations, lines and transformers are represented as pi-sections, shunt elements are represented by impedances or admittances, and Static Var Compensators (SVCs) by static gain and maximum/minimum limits [21].

Modeling to account for dynamics includes generator Maximum Excitation Limiters (MELs). MEL model corresponds to a MEL that acts at the voltage reference of the excitation system with an inverse time characteristic.

3.4 Disturbance/Control Models

The disturbance discussed here includes the trip of the cable without any fault, or the trip of the cable to clear a short circuit. The control modeling requirement simply considers relay model, which may operate due to a disturbance (e.g. load shedding), and modeling of control actions in remedial action schemes.

3.5 Models in Shipboard Power Systems

An integrated power system is commonly used for a wide range of ship applications, including submarines, surface combatants, aircraft cruise and high value commercial ships [74]. The models discussed here include generators, cables, loads and converters, which are common to the integrated shipboard power system shown as Figure 3.2.

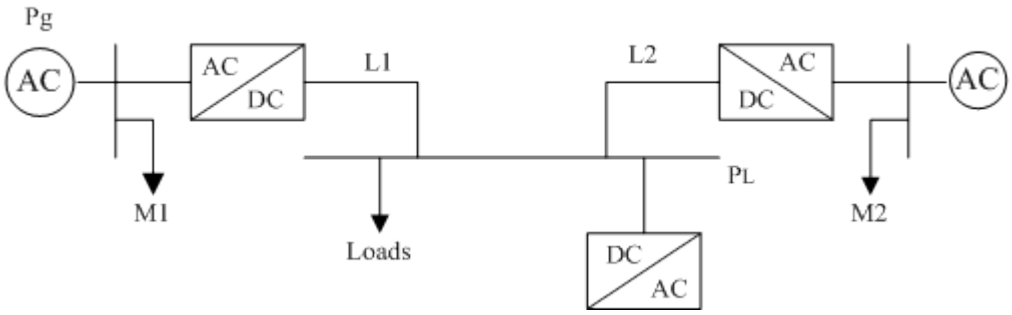

Figure 3.2 Integrated Power System Architecture

The description of each model is based on the concept for the integrated shipboard power system of a notional destroyer, which has been built using RTDS by Center for Advanced Power Systems of Florida State University [75] as part of the Electric Ship Research and Development Consortium.

3.5.1 Generators

This model consists of a synchronous machine, a voltage regulator, and a governor. The synchronous machine uses the standard three-phase synchronous machine model, where the stator, the rotor field and the damper windings can be represented by d- and q-axis windings. A generic AVR/exciter model has been used as the voltage regulator, and the IEEE AC1A exciter has been chosen for the E-ship model. The prime mover for generators may be modeled as aero-derivative gas turbine engines.

3.5.2 Loads

The propulsion loads consist of the propulsion transformer, the propulsion motor, the motor drive, and the motor speed controller. A standard transformer model and a standard three-phase induction motor model can be used to represent the propulsion transformer and the propulsion motor, respectively. Five different models have been used for the propulsion motor drives, which differ principally by the type of front-end

converter employed [75]. The propulsion motor speed/power controller makes use of five PI controllers tracking the motor speed (ω), power (P), flux torque (T), D-axis current (I_d), and Q-axis current (I_q).

The non-propulsion loads include a high power ship's radar, electromagnetic aircraft launchers (EMALs), high power weapons, a line-commutated energy storage system, and ship's service loads. These loads may be represented by using three-phase dynamic load model, a pulsed load charging model, an energy storage capacitor, and the lumped loads, respectively.

3.5.3 Converters

All converters have been represented by switching power electronic models employing idea switches. AC-DC converters can be modeled as 12-pulse rectifiers; DC-DC converter can be modeled as a one-GTO, one-diode, buck converter; and a DC-AC inverter controller employs PWM modulation.

3.5.4 Cables

The cables are simply represented by lumped RL elements because of the short length of the cabling for shipboard power systems.

In fact, the models discussed above are for dynamic characteristics of system devices based on PSCAD/RSCAD, which is a general-purpose time domain simulation tool for studying dynamic behavior of electrical network. But a lot of work regarding terrestrial power systems has been done using PSS/E, which is a standard software package for transmission analysis. To extend the techniques for terrestrial power systems to the application of shipboard power systems and to compare the results, it would be better if a shipboard power system could be built with PSS/E. However, there are big

differences in the component specification between these two models. It is not feasible to build such a notional E-ship model with PSS/E at this time, since a large number of user-define components would need to be developed, and beyond the work in this thesis. Therefore, only the static model of integrated shipboard power system will be considered in the following discussion.

3.6 Numerical Solution

The differential-algebraic equations (DAEs) are deduced for system dynamic models. A large number of algorithms have been proposed for the numerical solution of the DAEs. Basically two approaches are used in dynamic simulation, namely simultaneous-implicit (SI) and partitioned-explicit (PE) methods [62]. The SI approach is more stable than PE methods, since it can handle "stiff" equations very well.

The trapezoidal rule is applied for implicit integration, which is introduced as following.

Consider the differential equation 3.19

$$\frac{dx}{dt} = f(x,t) \tag{3.19}$$

With $x = x_n$ at $t = t_n$, the solution for x at $t = t_{n+1}$ may be expressed in integral form as Equation 3.20.

$$x_{n+1} = x_n + \frac{\Delta t}{2}[f(x_n,t_n) + f(x_{n+1},t_{n+1})] \tag{3.20}$$

In general, $x^{(k+1)} = x^{(k)} - [J^{(k)}]^{-1} f(x^{(k)})$ (3.21)

Where, k is the iteration count, and $[J] \triangleq \frac{\partial f}{\partial x}$ is called the Jacobian.

With an initial value of $x^{(0)}$, step corresponding to Equation 3.21 is repeated and at the end of each iteration compute $\max_i \left| f_i(x^{(k+1)}) \right|$. If this is $< \varepsilon$, where ε is the specified tolerance, the iterations have converged.

3.7 Summary

This section specifies modeling and simulation requirements for voltage stability assessment. The description of each model type, especially, the modeling of DC links and control modes, has been presented based on its steady-state and dynamic behavior. The notional E-ship model has been investigated and summarized for the future research. The numerical methods follow. More detailed information about system configuration and modeling will be introduced in the following chapters and the additional data can be found in Appendix B: Test System Data.

CHAPTER IV

PROCEDURE OF VOLTAGE STABILITY ASSESSMENT

The objectives of voltage stability analysis discussed previously are to determine the state of the current system, to estimate its proximity to voltage instability, and to identify the mechanism involved in voltage instability, which is the concern examined during system planning and operational studies. This motivates the development of a practical assessment procedure and the design of a proper security margin and criteria. This procedure should be performed to monitor the state of a system periodically, on demand, and upon the occurrence of significant changes, to ensure system security against the occurrence of predefined contingencies. In general, voltage stability *margins* are defined as the difference between the value of a key system parameter at the current operating condition and at the voltage stability critical point. Voltage stability *criterion* defines how much margin is deemed sufficient for voltage security of the system [21]. The approach for voltage stability assessment in this research is to use steady-state methods and the time-domain simulation as the complementary methods to address different aspects of phenomenon in voltage instability.

This chapter provides details for some generalized guidelines for the procedure of voltage stability assessment. The next chapter will present the mathematical terminology to specify the security margin or voltage stability indicators.

4.1 General Assessment Procedure

Voltage stability procedure uses steady-state methods to calculate voltage stability margins for the base case and all contingencies. The critical contingencies which do not meet voltage stability criterion are identified. Then, the time-domain simulation method is used to benchmark the steady-state analysis results. The remedial measures will be designed by using both steady-state and time-domain methods for the critical contingencies. Figure 4.1 shows the basic procedure of voltage stability assessment.

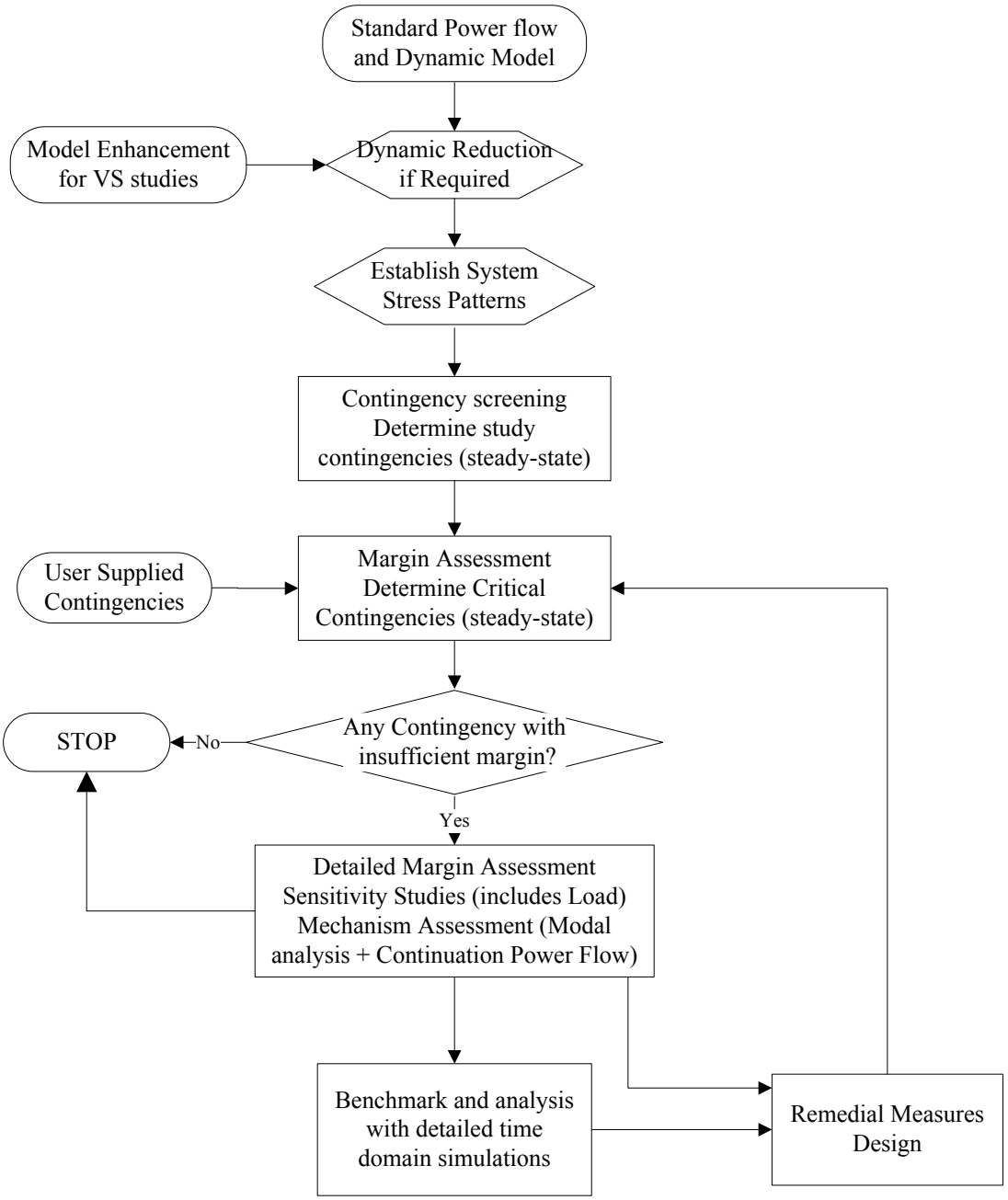

Figure 4.1 A Basic Procedure of Voltage Stability Assessment

Any change to increase the system stress pattern will trigger the execution of voltage stability assessment. It is impractical and unnecessary to analyze the impact of every conceivable contingency since only a limited number of contingencies might impose an immediate threat to voltage stability. Contingency screening is configured to

include or exclude contingencies to be suitable for special regulatory requirements. It is required to know whether the system operating conditions meet the voltage stability criteria, and how far the system should be from the borderline of voltage instability when subjected to any of the selected contingencies. Detailed contingency analysis will be executed by a steady-state method associated with the characteristics of interest. In this study, two typical methods, namely modal analysis and continuation power flow, will be performed for this purpose. If it is found that the system does not have sufficient voltage stability margin for one or more selected contingencies, preventive control should be determined to move the system state in such a way as to create sufficient margin, and corrective control will be taken to maintain voltage stability in case severe contingencies happen [21].

In theory, either power flow based (static) tools or time-domain simulation (dynamic) tools can be used to evaluate voltage stability. The calculated margins using different tools should be very close, provided that consistent device models are used in both programs. However, because of its high CPU time requirements, it is impractical to calculate voltage stability margin for all contingencies by using the time-domain simulation. A practical approach is using a power flow based tool to calculate voltage stability margin for the base case and all contingency cases, and only using time-domain simulation to benchmark power flow results, following a few selected critical contingencies.

4.2 Power Flow Based (Static) Assessment

Using a power flow based analysis method to evaluate the voltage stability for base case or for all contingencies mainly consists of two steps.

- *Establish a system snapshot*. This snapshot closely approximates a point along the time domain trajectory, and can be obtained by solving a set of system steady-state algebraic equations with appropriate models for controls and limits. The related equations which represent the network, steady-state generators and loads characteristics have been discussed in Chapter 3.

- *Determine voltage stability and calculate voltage stability margin at the snapshot.* Modal analysis is used to determine voltage stability at the selected snapshot. The flow chart of modal analysis is shown in Figure 4.2, and the details are available in [6]. In this method, the reduced steady-state Jacobian matrix (J_R) represents the linearized relationship between the incremental changes in bus voltage magnitude (ΔV) and bus reactive power injection (ΔQ). The participation factors for buses, branches and generators are calculated based on the right and left eigenvectors of J_R. The participation factors can determine which physical elements are associated with each mode, and identify the mechanism of potential voltage instability.

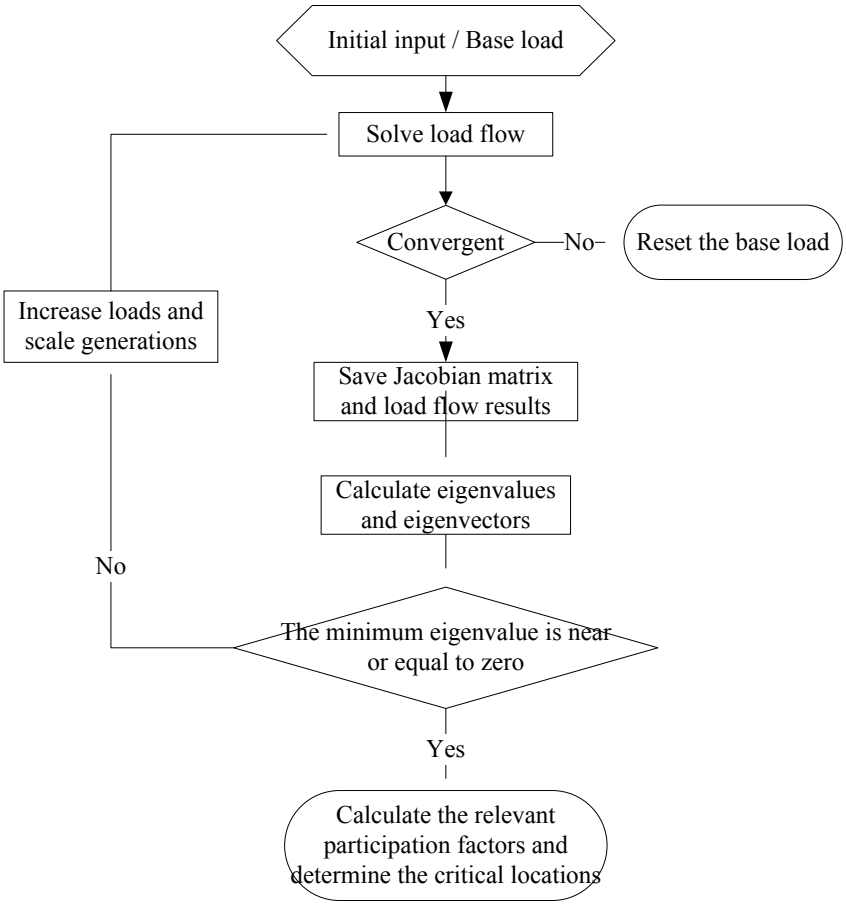

Figure 4.2 Flow Chart of Modal Analysis

Voltage stability margin can be calculated by computing PV curves (see Figure 4.3). The power flow is solved for base case at the each loading level. A contingency is applied and the power flow is solved to locate the post-contingency critical point. The increase in the pre-contingency system load from the initial operating point to the post-contingency critical point is the voltage stability margin for that contingency.

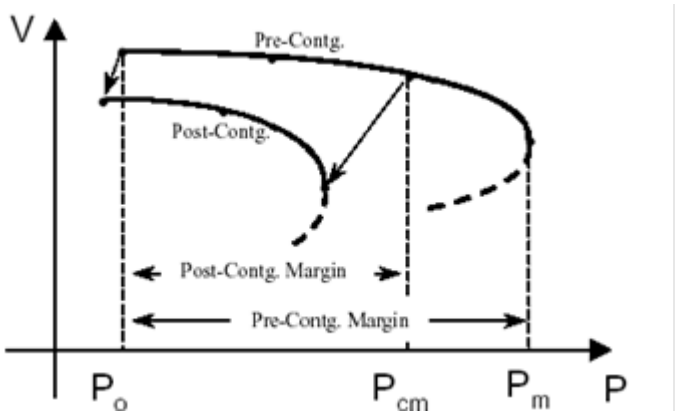

Figure 4.3 Pre- and Post-Contingency PV Curves and VS Margins [21]

Load and generation in selected areas are increased in a predefined manner to find the distance to voltage instability. The full power flow solution is performed at each loading level to obtain bus voltages. A voltage limit is reached when the power flow solution fails to converge. Continuation power flow method [13] is an alternative to overcome the convergence problem at operating conditions near the stability limit so as to obtain the power flow solutions for both stable and unstable points. PV plots show the sensitivity of bus voltages with loads (slope), the distance to instability (voltage stability margin), and the voltage at which instability occurs (critical voltage). QV curves are the other classical approach for voltage stability, to obtain the plot of bus voltage vs reactive power injection.

4.3 Dynamic Assessment

Time-domain simulation is essential for studies of the coordination of controls and protection in remedial measures design, especially under the situation of critical contingencies. Time-domain simulation involves the solution of two sets of equations: differential and algebraic equation sets. Usually numerical integration methods are used for the solution of the differential equations while L-U decomposition is used for the

algebraic equations. Figure 4.4 is the flow chart of numerical method for time-domain simulation. At the beginning of dynamic simulation, the states and variables need initialization based on the steady-state simulation. When any fault or switch operation occurs, system structure changes or reconfigures and the differential and algebraic equations will be modified to update the network solution. Calculations of $y(t+\Delta t)$ and $x(t+\Delta t)$ are the key steps in the time-domain simulation, since it is related to the state and variable values accumulated in previous steps as well as the accuracy of numerical method applied. Sometimes there is a need for state estimation for the current step. Simulation will be terminated at the end of predefined simulation time period or when the solution is divergent.

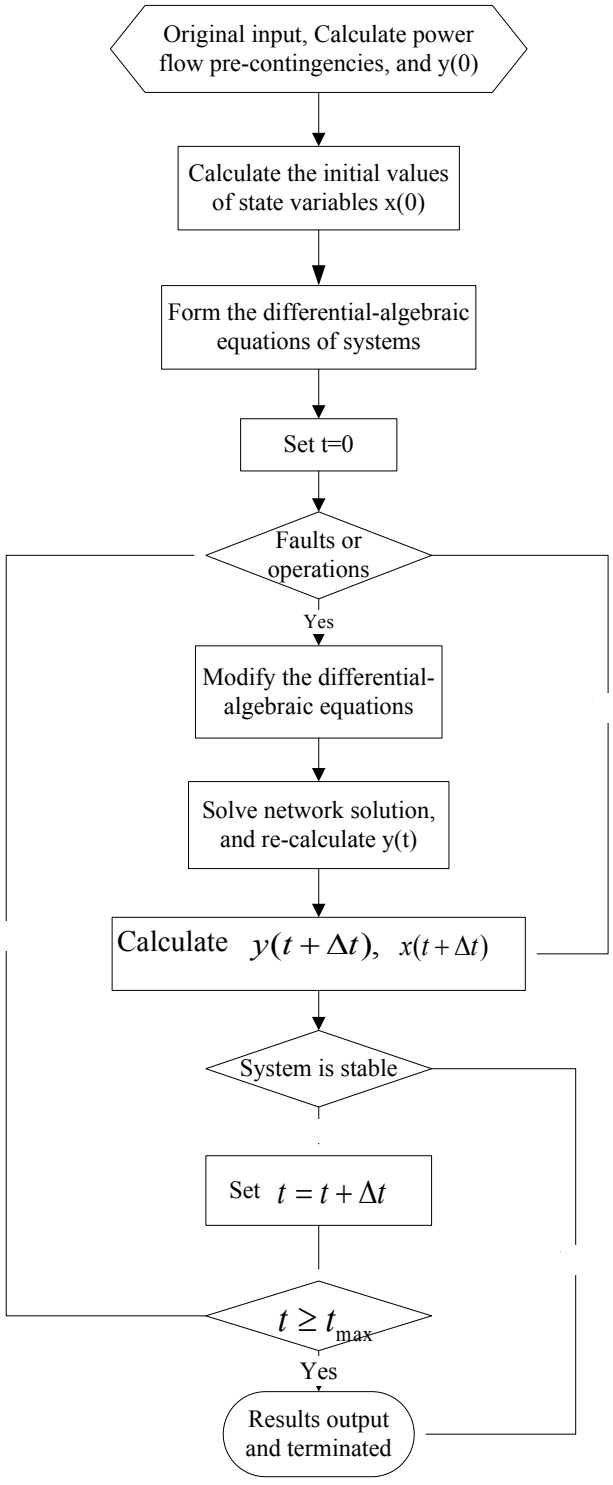

Figure 4.4 Flow Chart of Numerical Method for Time-Domain Simulation

4.4 Voltage Stability Assessment Tools

In recent years, a range of tools and techniques have been developed for voltage stability assessments. Some of these tools used in the operation of large complex systems have been described by their respective developers, such as CPF/EQTP from Iowa State University, UWPFLOW from University of Waterloo, and VSA from Siemens [21]. For research purposes, MATLAB will be used as the main tool to specify user-defined components or to write codes of voltage stability indicators. MATPower and Power System Toolbox (PST) are two packages of open resources available online, which can calculate the standard power flow accuracy, and provide a platform for static voltage stability assessment. PSS/E is a commercial program widely used in the power industry, which provides advanced and proven methods to verify the power flow results obtained from research tools, and performs dynamic simulation and fault analysis for transient voltage stability assessment.

4.4.1 MATPower

MATPower is a package of MATLAB M-files for solving power flow and optimal power flow problems [63]. It was initially developed by Power System Engineering Research Center (PSERC) at Cornell University for solving MATLAB-based power flow and optimal power flow. It is intended as a simulation tool for researchers and educators, and was designed to give the best performance possible while keeping the code simple to understand and modify.

4.4.2 Power System Toolbox (PST)

PST was developed by Joe Chow of Rensselaer Polytechnic Institute to enable users to perform power system analysis with MATLAB [64]. It consists of a set of

coordinated MATLAB M-files, power system application demo files and data files. PST can be used to perform load flow functions and dynamic functions. There are a number of demo files which provide sample power system applications, and users can use the demos as templates to construct their own applications.

4.4.3 Power System Simulator for Engineering Tool (PSS/E)

PSS/E is the well-established software tool offered by Siemens for electrical transmission analysis. It provides the advanced and proven methods in many technical areas, including power flow, optimal power flow, fault analysis, and dynamic simulation. In addition, the function of automate procedure can process the actions in "batch mode", such as running dynamic simulation. An embedded Python interpreter makes a faster development and more extensions possible.

In this research, MATPower is used to analyze the power flow of AC system, and PST can be performed for the power flow with DC links. Because of their open resources, Jacobian matrix can be figured out from the code of Newton-Raphson method, and the eliminated variable method is added to include the DC effect. Thus modal analysis method and the second order performance indicator are developed with M-file for static voltage stability assessment. The continuation power flow is also realized with M-files to calculate the loading margin.

Since PSS/E provides the well-established and proven methods. The power flow results obtained from the open-code programs will be verified in PSS/E. Contingency screen and dynamic simulation will be performed in PSS/E for its automate procedure. The response of dynamic components can be illustrated clearly during the dynamic simulation.

4.5 Summary

This chapter introduces the basic procedure of voltage stability assessment, and describes the main steps of steady-state and dynamic simulation. The flow charts of the related analysis methods are illustrated, and the brief introduction of involved research tools follows.

CHAPTER V

DEVELOPMENT OF VOLTAGE STAIBLITY INDICATORS

Voltage stability indicators are used to define a scalar magnitude that can be monitored as system parameters change. The basic concepts and classifications of voltage stability indicators have been reviewed in Section 2.3. This chapter concentrates on describing and comparing two classical indicators widely used in voltage stability assessment and a performance indicator proposed in this study, taking the different DC configurations and dynamic characteristics of generation into account.

5.1 Two Classical Indicators and one Proposed Performance Indicator

A good indicator should be "smooth" and have a "predicable" shape so that acceptable predictions may be made. However, as it is observed that all indicators have their advantages and disadvantages, it is not practical to recommend a particular indicator as the only one to use. In this study, two classical indicators, singular value/eigenvalue and loading margin are jointly used as a compromise for voltage stability assessment. Singular value or eigenvalue tends to be a poor predictor of proximity to voltage collapse but at low computational costs, and provides additional information regarding the instability mechanism. Loading margin yields an accurate measure of distance to collapse but at high computational costs. Hence, the inexpensive but less accurate singular values or eigenvalues can be used as predicators in the computation of the exact loading margin, so that the accurate measures of distance to collapse may be obtained together with useful additional information at reduced computational costs.

In addition, singular values or eigenvalues exhibit large discontinuities in the presence of system control limit, which is inadequate to predict proximity to collapse. Hence, the additional information embedded in singular values is explored, and a second order performance indicator is proposed as an improvement to overcome this weakness.

The relevant information regarding the aforementioned indicators is summarized in Table 5.1 to provide a comprehensive comparison of these indicators.

Table 5.1 A Comparison of Indicators

Indicator	Base Model	Computation Costs	Profile	Collapse Predications
Singular/Eigenvalues	Any	Medium	Nonlinear discontinuous	Inadequate
Loading Margin	Any	High	smooth	Exact
2nd Order Performance Indicator	Power flow	Medium	Quasi-linear discontinuous	Adequate

5.1.1 Singular Values and Eigenvalues

The QV mode is defined as "a way of disturbing the system by imposing the reactive power injections (in given direction), which results in proportional bus voltage change (in the same direction)". The reduced steady-state Jacobian matrix (J_R) represents the linearized relationship between the incremental changes in bus voltage magnitude (ΔV) and bus reactive power injection (ΔQ). The singular value or eigenvalue decomposition for reduced Jacobian matrix can be written as Equation 5.1.

$$J_R = W \Lambda U^T = \sum_{i=1}^{n} w_i \mu_i v_i^T \tag{5.1}$$

Where W represents a complex matrix of right eigenvectors, U corresponds to the complex matrix of left eigenvectors, and Λ is a diagonal matrix of complex eigenvalues.

Singular value or eigenvalue is one of powerful indicators for voltage stability evaluation in the wide range of power systems, and can be computed with modal analysis. The procedure of modal analysis, the singular value or eigenvalue decomposition, and the calculation of related participation factors are described in [6].

In Equation 5.1, μ_i is the eigenvalue of the i^{th} eigenmode. The incremental modal voltage response to an incremental modal reactive power is determined by the eigenvalue of the mode. Voltage stability criterion is that all eigenvalues of J_R are positive. When the eigenvalue of a voltage variation mode is very small or near to zero, an infinitesimally small change in the modal reactive power will cause a large or infinite modal voltage magnitude change, and the mode is instable. The minimum eigenvalue, which is near to, equal to zero, or becomes negative, is the critical one, and it indicates how close a system operating point is to voltage instability. The component (bus, branch, or generator) participation factors computed based on the critical mode provide additional information on the critical system location of voltage instability. The component with the largest participation factor means that it has the largest involvement in voltage instability.

5.1.2 Loading Margin

Loading margin is the most basic and widely accepted indicator of voltage collapse, defined as the amount of additional load in a specific pattern of load increase for a particular operating point (pre- or post- contingency), where voltage collapse may occur. In PV/QV curves, the loading margin is the change in loading between the operating point and the nose of the curve.

In principle loading margin can be calculated by starting at the current operating point, making small increments in loading and re-computing load flows at each increment until the nose of curve is reached [21]. There are several choices in defining the loading margin. The change in loading can be measured by 1) the sum of the absolute changes in load power; 2) the changes in real power only with constant power factor; or 3) the amount of power transferred between two areas when studying the transfer capability.

Compared to the other voltage collapse indicators, loading margin is straightforward, well accepted and easily understood, which is an accurate indicator taking full account of power system nonlinearity and limits. Once loading margin has been obtained, it is easy and quick to compute its sensitivity with respect to any power system parameters or control. However, loading margin is more computationally expensive and requires the assumption of a direction of load change, which is not readily available sometimes.

5.1.3 The Second Order Performance Index

Singular values or eigenvalues discussed in Section 5.1.2 may be inadequate to predict proximity to collapse since they exhibit large discontinuities in the presence of system control limits such as generator capability or SVC capability. In this section, a "second order" performance index is developed and analyzed to find the embedded information in singular values to overcome this weakness.

The minimum singular value is a natural indicator for monitoring how close a power system is operating to the voltage instability. It would be interesting to know how changes in loading (p) affect the minimum singular value ($\sigma_{\min}$). Simulations show that the maximum singular value of the full Jacobian inverse J_{PF}^{-1}, (i.e., the inverse of the

minimum singular value of J_{PF}), defined as $\sigma_{\max}$ can be approximated with respect to the load variations λ, by the function as Equation 5.2 with suitable values of the scalar positive constants b, c, and d [21].

$$\sigma_{\max}(\lambda) = (b - d\lambda)^{1/c} \tag{5.2}$$

This type of functions has the characteristic that the ratio as Equation 5.3 is linear with respect to the varying parameter λ.

$$\frac{\sigma_{\max}}{d\sigma_{\max}/d\lambda} = c\lambda - \frac{bc}{d} \tag{5.3}$$

Thus, the following indicator Equation 5.4 is proposed

$$i = \frac{1}{i_0}\frac{\sigma_{\max}}{d\sigma_{\max}/d\lambda} \tag{5.4}$$

Where i_0 is the value of Equation 5.3 at the starting loading point to normalize the indicator i. Since the denominator of Equation 5.4 tends to be infinite as the Jacobian becomes singular, and the index i approaches zero at the collapse point. Thus, appropriate prediction can be made of the distance to voltage collapse point based on the linear trend. The calculation of derivative, $d\sigma_{\max}/d\lambda$, in Equation 5.4 is described as following.

The net active and reactive power injection at the buses can be expressed as Equation 5.5.

$$\begin{cases} P_i = \sum_{k=1}^{n} |V_i||V_k|[G_{ik}\cos(\delta_i - \delta_k) + B_{ik}\sin(\delta_i - \delta_k)] \\ Q_i = \sum_{k=1}^{n} |V_i||V_k|[G_{ik}\sin(\delta_i - \delta_k) - B_{ik}\cos(\delta_i - \delta_k)] \end{cases} \tag{5.5}$$

Assume $F(u,\lambda)\underline{\underline{\Delta}}\begin{cases} P_i - \sum_{k=1}^{n} |V_i||V_k|(G_{ik}\cos\delta_{ik} + B_{ik}\sin\delta_{ik}) \\ Q_i - \sum_{k=1}^{n} |V_i||V_k|(G_{ik}\sin\delta_{ik} - B_{ik}\cos\delta_{ik}) \end{cases}$, then

$F(u,\lambda)=0$, where $\begin{cases} P_i = P_{Gi} - P_{Li} \\ Q_i = Q_{Gi} - Q_{Li} \end{cases}$, $u\underline{\underline{\Delta}}[\delta, V]^T$, $\lambda\underline{\underline{\Delta}}[P, Q]^T$.

Further, assume $p = k\lambda$ where k is the scalar parameter representing the loading direction. Then,

$$F(u,p)=0 \tag{5.6}$$

It is useful to know not only that the system is operating on the stable situation, but also how close it is to the bifurcation boundary. The natural extension from voltage/power sensitivity is embedded in the singular value of Jacobian F_u, and involves the minimum singular value of F_u.

The first order partial differentiation of Equation 5.6 is described as Equation 5.7.

$$\frac{\partial F(u,p)}{\partial u}\Delta u + \frac{\partial F(u,p)}{\partial p}\Delta p = 0 \tag{5.7}$$

As it is know that $Jacobian\underline{\underline{\Delta}}J_{PF} = \frac{\partial F(u,p)}{\partial u}$, and $\frac{\partial F(u,p)}{\partial p}$ is an identity matrix.

Hence,

$$J_{PF}\Delta u + \Delta p = 0 \Rightarrow \Delta u = -J_{PF}^{-1}\Delta p \tag{5.8}$$

This is the basic idea of Newton-Raphson power flow.

The notion of a singular matrix is intimately related to the ability to compute its inverse. Given the matrix J_{PF0}, the conditions on perturbation matrix ΔJ_{PF} are determined such that $J_{PF1} = J_{PF0} + \Delta J_{PF}$ is singular.

$$J_{PF1} = J_{PF0} + \Delta J_{PF} = J_{PF0}(1 + J_{PF0}^{-1}\Delta J_{PF}) \tag{5.9}$$

Assume J_{PF0} is non singular, to ensure J_{PF1} has an inverse, namely $J_{PF1}^{-1} = [J_{PF0}(1 + J_{PF0}^{-1}\Delta J_{PF})]^{-1} = (1 + J_{PF0}^{-1}\Delta J_{PF})^{-1} J_{PF0}^{-1}$ exists. Here, $\left\| J_{PF0}^{-1}\Delta J_{PF} \right\| < 1$ can guarantee J_{PF1}^{-1}, so, $\left\| \Delta J_{PF} \right\| < \dfrac{1}{\left\| J_{PF0}^{-1} \right\|} = \left\| J_{PF0}^{-1} \right\|^{-1}$. Hence, a measure of the nearness of matrix J_{PF0} to singularity is the number of $\left\| J_{PF0}^{-1} \right\|^{-1}$. In order to obtain numerical results, a particular norm must be chosen. The most natural choice is the spectral norm defined as Equation 5.10.

$$\left\| J_{PF} \right\|_2 = \sqrt{\lambda_{\max}(J_{PF}^T J_{PF})} = \sigma_{\max}(J_{PF}) \tag{5.10}$$

Where $\lambda_{\max}(J_{PF}^T J_{PF})$ is the maximum eigenvalue of symmetric matrix $(J_{PF}^T J_{PF})$, $\sigma_{\max}(J_{PF})$ is the largest singular value of J_{PF}.

For a square matrix $\sigma(J_{PF}^T J_{PF}) = \sigma(J_{PF} J_{PF}^T)$,

$\left\| J_{PF}^{-1} \right\|_2 = \sqrt{\lambda_{\max}[(J_{PF}^{-1})^T (J_{PF}^{-1})]} = \sqrt{\lambda_{\max}[(J_{PF} J_{PF}^T)^{-1}]} = \sigma_{\max}(J_{PF}^{-1}) = \sigma_{\min}^{-1}(J_{PF})$, hence,

$\left\| J_{PF} \right\|_2 = \sigma_{\max}(J_{PF})$, $\left\| J_{PF}^{-1} \right\|_2^{-1} = \sigma_{\min}(J_{PF})$.

The following extension in Equation 5.11 can be made according to the basic idea of Newton-Raphson power flow.

$$F(u_1, p_1) = F(u_0 + \Delta u, p_0 + \Delta p) = F(u_0, p_0) + \left.\frac{\partial F(u,p)}{\partial u}\right|_0 \Delta u + \left.\frac{\partial F(u,p)}{\partial p}\right|_0 \Delta p$$

$$\Delta F = F(u_1, p_1) - F(u_0, p_0) = \left.\frac{\partial F(u,p)}{\partial u}\right|_0 \Delta u + \left.\frac{\partial F(u,p)}{\partial p}\right|_0 \Delta p \tag{5.11}$$

On the other hand, the first order Taylor series on Jacobian is applied as Equation 5.12 for linearized approximation.

$$J_{PF}(u_1) = J_{PF}(u_0 + \Delta u) = J_{PF}(u_0) + \left.\frac{\partial J_{PF}(u)}{\partial u}\right|_0 \Delta u \tag{5.12}$$

Set $H \triangleq \frac{\partial J_{PF}(u)}{\partial u}$ is the Hessian matrix in three dimension ($n \times n \times n$), Therefore,

$$\Delta J_{PF} = J_{PF}(u_1) - J_{PF}(u_0) = H_0 \Delta u \tag{5.13}$$

Furthermore, the Jacobian matrix can be decomposed as $J_{PF} = R\Sigma S^T$, where R and S are orthonormal matrices, and Σ is a diagonal matrix whose elements σ are the singular values of J_{PF}. Hence, the following relationships exist as $RR^T = R^T R = 1$, $SS^T = S^T S = 1$, $R^{-1} = R$, $S^{-1} = S$. Let $J_{PF1} = R_1 \Sigma_1 S_1^T = (R_0 + \Delta R)(\Sigma_0 + \Delta\Sigma)(S_0 + \Delta S)^T$, expanding matrix multiplication, disregarding the second and third order perturbations, and Equation 5.14 can be obtained.

$$J_{PF1} = \underbrace{R_0 \Sigma_0 S_0^T}_{J_{PF0}} + R_0 \Delta\Sigma S_0^T + R_0 \Sigma_0 \Delta S^T + \Delta R \Sigma_0 S_0^T \tag{5.14}$$

Comparing Equation 5.13 and 5.14, Equation 5.15 can be obtained.

$$R_0 \Delta\Sigma S_0^T + R_0 \Sigma_0 \Delta S^T + \Delta R \Sigma_0 S_0^T = H\Delta u \tag{5.15}$$

Additional constraints are given by orthogonality of R and S as

$$R^T R = 1 \Rightarrow \begin{cases} R_0^T R_0 = 1 \\ R_1^T R_1 = 1 \end{cases}.$$

$$R_1^T R_1 = (R_0 + \Delta R)^T (R_0 + \Delta R) = (R_0^T + \Delta R^T)(R_0 + \Delta R)$$
$$= \underbrace{R_0^T R_0}_{=1} + R_0^T \Delta R + \Delta R^T R_0 + \underbrace{\Delta R^T \Delta R}_{\approx 0} = 1$$
$$\Rightarrow R_0^T \Delta R + \Delta R^T R_0 = 0 \Rightarrow R_0^T \Delta R = -\Delta R^T R_0 = [R_0^T \Delta R]^T.$$

For any matrix A, if $A = -A^T \Rightarrow a_{ij} = -a_{ji}$, when $i = j$, $a_{ii} = -a_{jj} = 0$, namely A is a matrix with zero diagonal element. So, $R_0^T \Delta R \triangleq \begin{bmatrix} 0 & & r_{ij} \\ & \ddots & \\ r_{ji} & & 0 \end{bmatrix}$, similarly, $\Delta S S_0^T \triangleq \begin{bmatrix} 0 & & s_{ij} \\ & \ddots & \\ s_{ji} & & 0 \end{bmatrix}$.

Equation 5.15 left side is multiplied by R_0^T, and the right side is multiplied by S_0, and the left terms can be expanded as Equation 5.16.

$$\begin{aligned} & R_0^T (R_0 \Delta \Sigma S_0^T + R_0 \Sigma_0 \Delta S^T + \Delta R \Sigma_0 S_0^T) S_0 \\ & = R_0^T R_0 \Delta \Sigma S_0^T S_0 + R_0^T R_0 \Sigma_0 \Delta S^T S_0 + R_0^T \Delta R \Sigma_0 S_0^T S_0 \\ & = \Delta \Sigma + \Sigma_0 \Delta S^T S_0 + R_0^T \Delta R \Sigma_0 \end{aligned} \tag{5.16}$$

Since Σ is a diagonal matrix, and the diagonal entries of $\Delta S^T S$ and $R^T \Delta R$ are zero, by inserting Equation 5.8 into Equation 5.15 and evaluating its entries, Equation 5.17 can be obtained.

$$\Delta \Sigma = R_0^T (H \Delta u) S_0 = -R_0^T (H J_{PF}^{-1} \Delta p) S_0 \tag{5.17}$$

The change in the r^{th} singular value of J_{PF} following the change of Δp is given by Equation 5.18.

$$\Delta \sigma_r = -[R_0^T (H J_{PF}^{-1} \Delta p) S_0]_{rr} \tag{5.18}$$

In particular, for the minimum singular value, Equation 5.19 is obtained.

$$\Delta \sigma_{\min} \approx c^T \Delta p \tag{5.19}$$

In order to use the $\sigma_{\max}$ of J_{PF}^{-1}, the corresponding increment $\Delta \sigma_{\max}$ can be calculated since $\sigma_{\max} = \dfrac{1}{\sigma_{\min}}$. Therefore,

$$\Delta\sigma_{\max} = c_{\max}^{T}\Delta p \approx (\sigma_{\max}^{2} c^{T})\Delta p \tag{5.20}$$

The entries of $c_{\max}$ are the partial derivatives of $\sigma_{\max}$ with respect to the active and reactive power injections. Loading changes can be related back to the desired parameter λ by $p = k\lambda$, associated with Equation 5.20, and the following relation can be obtained in Equation 5.21.

$$\frac{d\sigma_{\max}}{d\lambda} \approx c_{\max}^{T} k \tag{5.21}$$

Using the loading and generation pattern k suggested in [68], Equation 5.21 can take the following form as Equation 5.22.

$$\frac{d\sigma_{\max}}{d\lambda} = \sum_{j\in N_L}(c_{P\max j} + c_{Q\max j}\tan\varphi_j)\eta_j - \sum_{j\in N_G} c_{P\max j}\rho_j \tag{5.22}$$

Where N_G and N_L are the set of generators and load buses, respectively. $c_{P\max j}$ and $c_{Q\max j}$ are the entries in $c_{\max}$ related to the active and reactive power injections. η_j has the distribution coefficients of the total network load among its N_L load buses, and $\tan\varphi_j$ is the corresponding power factor; and ρ_j is the distribution coefficient of active power generation among N_G generator buses.

Computational efficiency of the technique presented here is associated with the computation costs of singular values, and singular vectors of power flow Jacobian and Hessian matrices. Given the terms of the active and reactive power injections, calculation of Jacobian and Hessian is a very straightforward process, albeit an extremely tedious one. For completeness, details on the calculation are introduced in the following paragraph.

The expression of the active power and reactive power injections is given as Equation 5.5. The first partial derivatives of the active power and reactive power injections $\frac{\partial P_i}{\partial \theta_k}$, $\frac{\partial P_i}{\partial |V_k|}$, $\frac{\partial Q_i}{\partial \theta_k}$, $\frac{\partial Q_i}{\partial |V_k|}$ are entries of the power flow Jacobian matrix, whose detailed expressions can be easily found in previous literature or textbook [69]. The second partial derivatives of the active power and reactive power injections which are entries of Hessian matrix, are listed as Equations 5.23-5.42.

$$\frac{\partial^2 P_i}{\partial |V_i|^2} = 2G_{ii} \tag{5.23}$$

$$\frac{\partial^2 P_i}{\partial |V_k|^2} = 0 \tag{5.24}$$

$$\frac{\partial^2 P_i}{\partial |V_i| \partial |V_k|} = G_{ik}\cos(\theta_i - \theta_k) + B_{ik}\sin(\theta_i - \theta_k) \tag{5.25}$$

$$\frac{\partial^2 P_i}{\partial \theta_i^2} = -|V_i| \sum_{k=1}^{n} |V_k| [G_{ik}\cos(\theta_i - \theta_k) + B_{ik}\sin(\theta_i - \theta_k)] \tag{5.26}$$

$$\frac{\partial^2 P_i}{\partial \theta_i \partial \theta_k} = |V_i||V_k| [G_{ik}\cos(\theta_i - \theta_k) + B_{ik}\sin(\theta_i - \theta_k)] \tag{5.27}$$

$$\frac{\partial^2 P_i}{\partial \theta_k^2} = |V_i||V_k| [-G_{ik}\cos(\theta_i - \theta_k) - B_{ik}\sin(\theta_i - \theta_k)] \tag{5.28}$$

$$\frac{\partial^2 P_i}{\partial |V_i| \partial \theta_i} = \sum_{k=1}^{n} |V_k| [-G_{ik}\sin(\theta_i - \theta_k) + B_{ik}\cos(\theta_i - \theta_k)] \tag{5.29}$$

$$\frac{\partial^2 P_i}{\partial |V_i| \partial \theta_k} = |V_k| [G_{ik}\sin(\theta_i - \theta_k) - B_{ik}\cos(\theta_i - \theta_k)] \tag{5.30}$$

$$\frac{\partial^2 P_i}{\partial |V_k| \partial \theta_i} = |V_i| [-G_{ik}\sin(\theta_i - \theta_k) + B_{ik}\cos(\theta_i - \theta_k)] \tag{5.31}$$

$$\frac{\partial^2 P_i}{\partial|V_k|\partial\theta_k} = |V_i|[G_{ik}\sin(\theta_i-\theta_k) - B_{ik}\cos(\theta_i-\theta_k)] \tag{5.32}$$

$$\frac{\partial^2 Q_i}{\partial|V_i|^2} = -2B_{ii} \tag{5.33}$$

$$\frac{\partial^2 Q_i}{\partial|V_k|^2} = 0 \tag{5.34}$$

$$\frac{\partial^2 Q_i}{\partial|V_i|\partial|V_k|} = G_{ik}\sin(\theta_i-\theta_k) - B_{ik}\cos(\theta_i-\theta_k) \tag{5.35}$$

$$\frac{\partial^2 Q_i}{\partial\theta_i^2} = -|V_i|\sum_{k=1}^{n}|V_k|[G_{ik}\sin(\theta_i-\theta_k) - B_{ik}\cos(\theta_i-\theta_k)] \tag{5.36}$$

$$\frac{\partial^2 Q_i}{\partial\theta_i\partial\theta_k} = |V_i||V_k|[G_{ik}\sin(\theta_i-\theta_k) - B_{ik}\cos(\theta_i-\theta_k)] \tag{5.37}$$

$$\frac{\partial^2 Q_i}{\partial\theta_k^2} = |V_i||V_k|[-G_{ik}\sin(\theta_i-\theta_k) + B_{ik}\cos(\theta_i-\theta_k)] \tag{5.38}$$

$$\frac{\partial^2 Q_i}{\partial|V_i|\partial\theta_i} = \sum_{k=1}^{n}|V_k|[G_{ik}\cos(\theta_i-\theta_k) + B_{ik}\sin(\theta_i-\theta_k)] \tag{5.39}$$

$$\frac{\partial^2 Q_i}{\partial|V_i|\partial\theta_k} = -|V_k|[G_{ik}\cos(\theta_i-\theta_k) + B_{ik}\sin(\theta_i-\theta_k)] \tag{5.40}$$

$$\frac{\partial^2 Q_i}{\partial|V_k|\partial\theta_i} = |V_i|[G_{ik}\cos(\theta_i-\theta_k) + B_{ik}\sin(\theta_i-\theta_k)] \tag{5.41}$$

$$\frac{\partial^2 Q_i}{\partial|V_k|\partial\theta_k} = -|V_i|[G_{ik}\cos(\theta_i-\theta_k) + B_{ik}\sin(\theta_i-\theta_k)] \tag{5.42}$$

Compared to other indicators, this indicator is more expensive to compute, as several matrix and vector manipulations and products are required, besides the

computation of the minimum singular value. However, it seems feasible to extend the technique to encompass other system models by removing certain modeling assumptions on the derivation process. In addition, the computed singular values and vectors can also be used to evaluate certain control actions.

5.2 Voltage Stability Indicators in DC Systems

At first, the typical DC configurations are discussed to illustrate the development of indicators in DC systems.

5.2.1 Typical DC configurations

DC systems are traditionally analyzed based on the single-infeed DC configuration. Though simplified, it can capture many of the important phenomena in DC systems. In this section, two typical DC configurations, namely a single-infeed DC configuration and a single-infeed DC with a parallel AC line, are discussed to obtain the basic power flow equations in order to calculate the voltage stability sensitivity, singular values or eigenvalues.

In the following figures, the notation of the symbols is self-explanatory from visual inspection. Although impedance angles are represented by generic notation in the figures, they are assumed to be 90^0 in this study to simplify the analytical derivation.

5.2.1.1 Single-Infeed DC configurations

The quasi-static model of single-infeed DC configuration is shown in Figure 5.1. AC and DC systems are modeled by steady-state algebraic equations. In particular, the AC system is represented by a constant Thevenin equivalent. The Thevenin AC voltage magnitude is assumed to remain constant throughout the analysis. This assumption is

deemed justified by the relatively fast response of the DC controller for small changes such that excitation voltage control in the AC system has not yet responded.

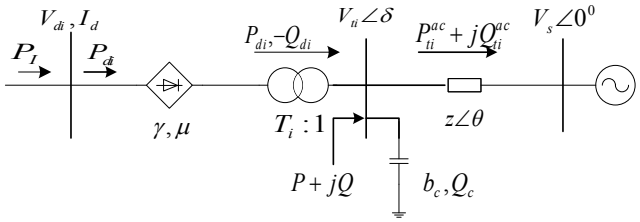

Figure 5.1 A Quasi-Static Model for the Single-Infeed DC Configuration

Power flow equations at inverter AC and DC buses are obtained as Equations 5.43-5.45.

$$\Delta P_{di} = P_I - P_{di} \tag{5.43}$$

$$\Delta P_{ti} = P + P_{di} - P_{ti}^{ac} \tag{5.44}$$

$$\Delta Q_{ti} = Q - Q_{di} - Q_{ti}^{ac} + Q_c \tag{5.45}$$

The static or quasi-static models can correctly capture and model important aspects of voltage stability. To give a correct description of some important issues a dynamic model is required. When the dynamic effects of the machine and its excitation voltage control are to be factored into voltage stability analysis, the Thevenin voltage source is replaced with a synchronous machine and an exciter shown as Figure 5.2.

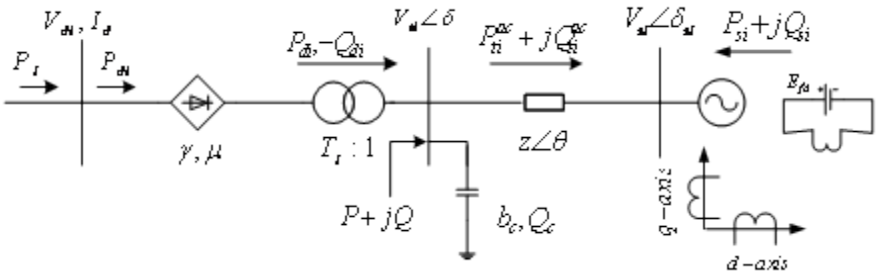

Figure 5.2 A Dynamic Model for the Single-Infeed DC Configuration

Similar to power flow equations for steady-state analysis, in the dynamic case, the machine bus is assigned as a PQ load bus with the machine power injections treated as voltage dependent loads. Consequently, the machine ac bus voltage magnitude and angle are chosen as state variables in addition to converter terminal voltage. The power flow model is therefore derived as Equations 5.46 - 5.50.

$$\Delta P_{di} = P_I - P_{di} \tag{5.46}$$

$$\Delta P_{ti} = P + P_{di} - P_{ti}^{ac} \tag{5.47}$$

$$\Delta P_{si} = P_{si} + P_{ti}^{ac} \tag{5.48}$$

$$\Delta Q_{ti} = Q - Q_{di} - Q_{ti}^{ac} + Q_c \tag{5.49}$$

$$\Delta Q_{si} = Q_{si} + Q_{ti}^{ac} \tag{5.50}$$

5.2.1.2 A Single-Infeed DC Configuration with a Parallel AC Line

The other typical DC configuration is a single-infeed DC configuration with a parallel AC line shown as Figure 5.3.

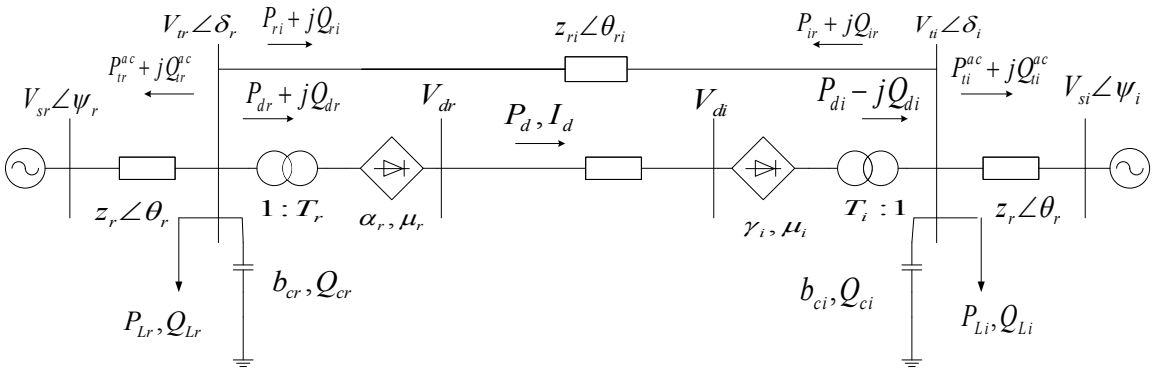

Figure 5.3 A Single-Infeed DC Configuration with A Parallel AC Line

Based on the model above, the power flow equations for rectifier and inverter can be obtained as Equations 5.51- 5.54.

$$0 = P_{dr} + P_{tr}^{ac} + P_{ri} + P_{Lr} \tag{5.51}$$

$$0 = Q_{dr} + Q_{tr}^{ac} + Q_{ri} + Q_{Lr} - Q_{cr} \tag{5.52}$$

$$P_{di} = P_{ti}^{ac} + P_{ir} + P_{Li} \tag{5.53}$$

$$0 = Q_{di} + Q_{ti}^{ac} + Q_{ir} + Q_{Li} - Q_{ci} \tag{5.54}$$

5.2.2 Voltage Stability Concepts in DC Systems

Table 5.2 Concept Comparison between AC and DC Systems

Concept	AC systems	DC systems	Expression
Short Circuit Ratio (SCR)	The ratio between AC short circuit capacity and nominal power level of equipment, such as large motor, DC converter, and SVC	the ratio between the short-circuit capacity of the AC network at the commutation bus and the nominal DC power level	$SCR = \frac{1}{Z}$
Effective Short Circuit Ratio (ESCR)	SCR and take shunt reactive equipment at the device location into account, especially with HVDC	SCR but reducing the short circuit capacity of the AC network with the capacitive shunt compensation at the commutation bus	$ESCR = \frac{1}{Z} - Q_c$
Maximum Power	Power is maximum when the magnitude of load impedance equals the magnitude of source impedance	Analogous characteristics of direct current I_d vs. dc power P_d	$V_{crit} = E/2$
Tap changer instability	Tap changing to reflect additional load conductance to the primary system results in reduced power	The sensitivity of dc voltage to the change in converter transformer tap ratio	--
Voltage Sensitivity/ Stability Factor	Predict voltage control problems in generator QV curves	Measure AC/DC voltage control and stability	Refer to [21] for AC system, [1] for DC system

Additional insight on voltage stability can be gained by exploring these concepts which have parallels in purely AC systems. The concept comparison [1] between AC and DC systems is shown in Table 5.2.

Two classical indicators of AC systems introduced in Section 5.2.1 and 5.2.2 have their counterparts in DC systems, but with different explanation from physical viewpoint. In purely AC systems, voltage stability margins are quantified as system loadability, and VQ or PV plots are typically used for such an evaluation. However, in DC systems, voltage stability is investigated in the context of decreasing the system strength of its

constituent AC/DC systems and not a continual increase in system load. Thus, VQ and VP plots are not relevant. Hence, only the application of singular values and eigenvalues is extended for voltage stability assessment of AC/DC systems in this study.

5.2.3 Jacobian Matrix in AC/DC Systems

To obtain the full/reduced Jacobian matrix of hybrid AC/DC systems, the eliminated variable method [56] is introduced in this study, which treats the real and reactive power consumed by inverters as voltage dependent loads so that the effect of DC links can be included in the existing AC Jacobian. The additional insight into the interaction between AC and DC parts of the system can be gained with this method.

5.2.3.1 Quasi-Static Single-Infeed DC Configuration

For the Quasi-Static single-infeed DC configuration shown as Figure 5.1, and power flow equations given as Equations 5.55-5.58, P_{di} and Q_{di} are not related to δ_i, and P and Q are not voltage-dependent inputs, namely, not relevant to δ_i and V_{ti}, hence, $\partial P_{di}/\partial\delta_i$, $\partial Q_{di}/\partial\delta_i$, $\partial P/\partial\delta_i$, $\partial Q/\partial\delta_i$ $\partial P/\partial V_{ti}$, and $\partial Q/\partial V_{ti}$ are all zero. Therefore,

$$J_{P\delta} = \frac{\partial P_{ti}}{\partial \delta_i} = -\frac{\partial P_{ti}^{ac}}{\partial \delta_i} \tag{5.55}$$

$$J_{PV} = \frac{\partial P_{ti}}{\partial V_{ti}} = \frac{\partial P_{di}}{\partial V_{ti}} - \frac{\partial P_{ti}^{ac}}{\partial V_{ti}} \tag{5.56}$$

$$J_{Q\delta} = \frac{\partial Q_{ti}}{\partial \delta_i} = -\frac{\partial Q_{ti}^{ac}}{\partial \delta_i} \tag{5.57}$$

$$J_{QV} = \frac{\partial Q_{ti}}{\partial V_{ti}} = -\frac{\partial Q_{di}}{\partial V_{ti}} - \frac{\partial Q_{ti}^{ac}}{\partial V_{ti}} \tag{5.58}$$

Where, the calculation of $\frac{\partial P_{di}}{\partial V_{ti}}$ and $\frac{\partial Q_{di}}{\partial V_{ti}}$ refers to Appendix A: Partial Derivatives of AC/DC Systems.

AC partial derivatives $\frac{\partial P_{ti}^{ac}}{\partial \delta_i}, \frac{\partial Q_{ti}^{ac}}{\partial \delta_i}$ $\frac{\partial P_{ti}^{ac}}{\partial V_{ti}}$, and $\frac{\partial Q_{ti}^{ac}}{\partial V_{ti}}$ can be solved, based on the power flow equations for AC lines given as Equation 5.59.

$$\begin{cases} P_{ti}^{ac} = [V_{ti}^2 \cos\theta_i - V_{ti} V_{si} \cos(\delta_i + \theta_i)] / |z| \\ Q_{ti}^{ac} = [V_{ti}^2 \sin\theta_i - V_{ti} V_{si} \sin(\delta_i + \theta_i)] / |z| - b_c V_{ti}^2 \end{cases} \tag{5.59}$$

Thus, the full Jacobian matrix $J_{PF} = \begin{bmatrix} J_{P\delta} & J_{PV} \\ J_{Q\delta} & J_{QV} \end{bmatrix}$ and the reduced Jacobian matrix of hybrid AC/DC systems $J_R = J_{QV} - J_{Q\delta} J_{P\delta}^{-1} J_{PV}$ can be obtained, and eigenvalue decomposition can be performed.

5.2.3.2 Dynamic Single-Infeed DC Configuration

A comparison of the models between quasi-static and dynamic single-infeed DC configurations shows that the differences lie in Equations 5.11 and 5.13 due to the models of machine AC bus. Consequently the machine AC bus voltage magnitude V_{si} and phase angle δ_{si} are chosen as state variables in addition to $[V_{ti}, \delta_{ti}]$. Similar to the calculation process for quasi-static single-infeed DC configurations, the partial derivatives based on power flow model given by Equations 5.46-5.50 can be obtained as Equations 5.60-5.63.

$$J_{P\delta} = \begin{bmatrix} \frac{\partial P_{si}}{\partial \delta_i} \\ \frac{\partial P_{ti}}{\partial \delta_i} \end{bmatrix} = \begin{bmatrix} \frac{\partial P_{si}}{\partial \delta_i} + \frac{\partial P_{ti}^{ac}}{\partial \delta_i} \\ -\frac{\partial P_{ti}^{ac}}{\partial \delta_i} \end{bmatrix} \tag{5.60}$$

$$J_{PV} = \begin{bmatrix} \frac{\partial P_{si}}{\partial V_i} \\ \frac{\partial P_{ti}}{\partial V_i} \end{bmatrix} = \begin{bmatrix} \frac{\partial P_{si}}{\partial V_i} + \frac{\partial P_{ti}^{ac}}{\partial V_i} \\ \frac{\partial P_{di}}{\partial V_i} - \frac{\partial P_{ti}^{ac}}{\partial V_i} \end{bmatrix} \tag{5.61}$$

$$J_{Q\delta} = \begin{bmatrix} \overline{\dfrac{\partial \delta_i}{\partial Q_{ti}}} \\ \dfrac{\partial Q_{ti}}{\partial \delta_i} \end{bmatrix} = \begin{bmatrix} \overline{\partial \delta_i} & \dfrac{\partial Q_{ti}^{ac}}{\partial \delta_i} \\ & -\dfrac{\partial Q_{ti}^{ac}}{\partial \delta_i} \end{bmatrix} \tag{5.62}$$

$$J_{QV} = \begin{bmatrix} \dfrac{\partial Q_{si}}{\partial V_i} \\ \dfrac{\partial Q_{ti}}{\partial V_i} \end{bmatrix} = \begin{bmatrix} \dfrac{\partial Q_{si}}{\partial V_i} + \dfrac{\partial Q_{ti}^{ac}}{\partial V_i} \\ \dfrac{\partial Q_{di}}{\partial V_i} - \dfrac{\partial Q_{ti}^{ac}}{\partial V_i} \end{bmatrix} \tag{5.63}$$

Where all entries have been computed in Section 5.3.3.1, except $\frac{\partial P_{si}}{\partial \delta_i}$, $\frac{\partial Q_{si}}{\partial \delta_i}$, $\frac{\partial P_{si}}{\partial V_i}$, and $\frac{\partial Q_{si}}{\partial V_i}$, which depend on the machine model chosen for dynamic simulation, and will affect some results of voltage stability assessment. The calculation of $\frac{\partial P_{si}}{\partial \delta_i}$, $\frac{\partial Q_{si}}{\partial \delta_i}$, $\frac{\partial P_{si}}{\partial V_i}$, and $\frac{\partial Q_{si}}{\partial V_i}$ refers to [39]. Thereby, eigenvalue decomposition and modal analysis can be applied for dynamic single-infeed DC configuration.

5.2.3.3 A Single-Infeed DC Configuration with A Parallel AC Line

In fact, the calculation of partial derivatives based on the model given as Equations 5.51-5.54 is the same as the procedure introduced in Section 5.3.3.1, but taking both rectifier and inverter terminals into account. So, it is easy to obtain the following entries for Jacobian matrix. Then, modal analysis is performed for voltage stability assessment.

$$J_{P\delta} = \begin{bmatrix} \dfrac{\partial P_i}{\partial \delta} \\ \dfrac{\partial P_r}{\partial \delta} \end{bmatrix},\ J_{PV} = \begin{bmatrix} \dfrac{\partial P_i}{\partial V} \\ \dfrac{\partial P_r}{\partial V} \end{bmatrix},\ J_{Q\delta} = \begin{bmatrix} \dfrac{\partial Q_i}{\partial \delta} \\ \dfrac{\partial Q_r}{\partial \delta} \end{bmatrix},\ J_{QV} = \begin{bmatrix} \dfrac{\partial Q_i}{\partial V} \\ \dfrac{\partial Q_r}{\partial V} \end{bmatrix} \tag{5.64}$$

5.3 Summary

In this chapter, two classical indicators, singular values/ eigenvalues and loading margin, have been introduced as a compromise for voltage stability assessment. The second order performance indicator is proposed as an improvement for singular values/ eigenvalues. Concepts involving in voltage stability of DC systems have been explored by comparing their parallels in purely AC systems, so as to extend the application of modal analysis for voltage stability assessment of hybrid AC/DC systems. Quasi-static and dynamic single-infeed DC configurations and a single-infeed DC with a parallel AC line configuration are illustrated in details and given their power flow models. The calculation procedure of partial derivatives of power flow modals is described to obtain Jacobian matrix of hybrid AC/DC systems for modal analysis.

CHAPTER VI

SYSTEM STUDY AND STEADY STATE SIMULATION

The previous chapters have discussed the modeling and simulation considerations of static and dynamic simulation of hybrid AC/DC systems, illustrated the procedure of voltage stability assessment, and shown the development of voltage stability indicators. This chapter describes steady-state simulation of the Western System Coordinating Council (WSCC) system with three different study cases to demonstrate the procedure of static voltage stability assessment and to explain how the previously discussed indicators are jointly used for voltage instability prediction. The next chapter will describe the modified IEEE one-area RTS-96 system to demonstrate the procedure of transient voltage stability assessment for base case and all contingencies.

Additional information on the system data is available in Appendix B: Test System Data.

6.1 System 1: WSCC 3-Machine, 9-Bus System

The Western System Coordinating Council (WSCC) model, consisting of nine buses, three generators and three loads [62], is a popular system widely used in the literature, which is considered to investigate the static voltage stability for three cases of study, including the system with 1) only AC system; 2) DC link in power control mode; and 3) DC link in current control mode. In this work, a gradual loading change is set to trigger the procedure of static assessment. Load flow is performed to get a snapshot of system initial status. The critical location and contributing factors are identified and a

rough margin is obtained by using modal analysis. The loading margin is calculated accurately by PV plots. The prediction of minimum eigenvalues is improved by using the developed second order performance indicator.

6.1.1 Description of System

The WSCC system without DC link is shown as Figure 6.1. Loads are assumed to have constant power factor. The loading level is scaled by a fixed factor, which represents the percentage of actual load with respect to the base load, namely $\text{actual load} = \lambda \times \text{base load}$. The generators are scaled by the same factor correspondingly.

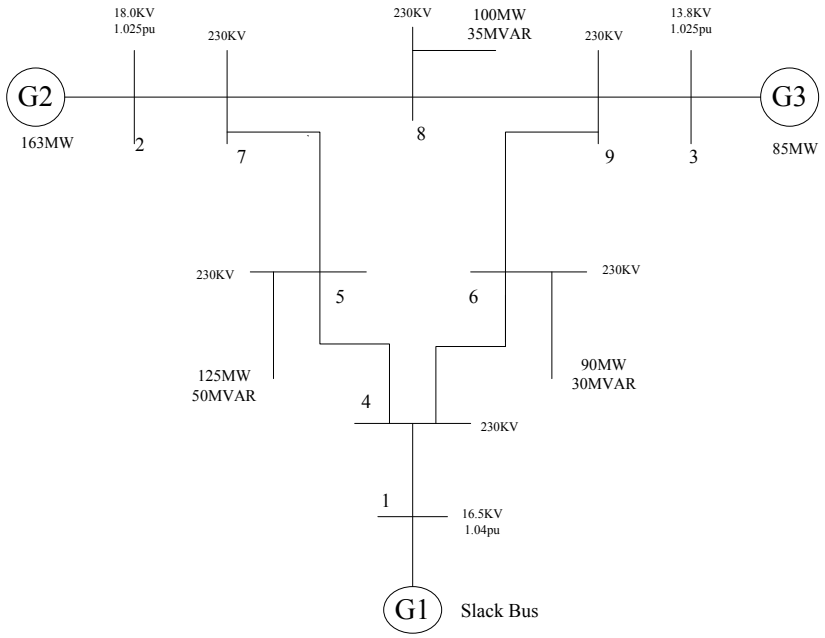

Figure 6.1 WSCC 3-Machine 9-Bus System with only AC system

To investigate the effect of DC link on the voltage stability, a two-terminal DC link is added between buses 4 and 9 shown as Figure 6.2. The parameters of the DC line are set as the followings.

P=100MW, I=250A, $V_{sckedule} = 400kV$, rectifier firing angle $\alpha \in [10^0, 25^0]$, inverter extinction angle $\gamma \in [15^0, 25^0]$, and control mode is "Power" and "Current" respectively.

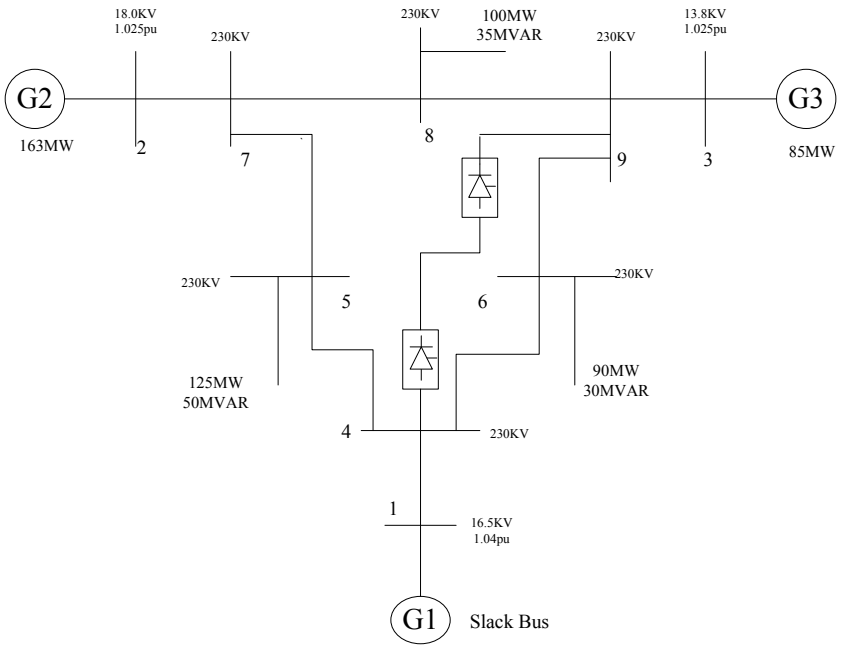

Figure 6.2 WSCC 3-Machine 9-Bus System with DC49 Link

Load flow calculation, modal analysis, PV plot and the second order performance indicator are implemented on both systems to show the static assessment procedure.

6.1.2 Load Flow of Base Case

The load flow is calculated in PSS/E. The obtained results of base case are summarized as Tables 6.1, 6.2, and 6.3. Table 6.1 is the bus voltage magnitude and phase angles, and Table 6.2 is the generator output for three cases of study. Table 6.3 is the comparison of DC link transmission capability with different control modes. It shows that DC link without any reactive power compensation impairs voltage stability, because both rectifier and inverter are consumption points, absorbing reactive power. In this case, current control mode is better than power control mode, given the conditions of the same

setting value, as the former provides higher bus voltage magnitude, and less transmission power loss. However, power control mode can provide more transmission capability, which means it can transmit more active power than current control does. In practice, power control is often considered with the appropriate local reactive power compensation to improve the voltage stability.

Table 6.1 Bus Voltages of WSCC Base Case

Bus #	**Type**	**Only AC system**	**DC49 in service, No shunt**	
			Power control	**Current control**
1	(Swing)	1.04	1.04	1.04
2	(P-V)	$1.025\angle 9.28^0$	$1.025\angle 14.59^0$	$1.025\angle 14.04^0$
3	(P-V)	$1.025\angle 4.66^0$	$1.025\angle 13.77^0$	$1.025\angle 12.83^0$
4	(P-Q)	$1.0258\angle -2.22^0$	$0.9979\angle -2.52^0$	$1.0012\angle -2.47^0$
5	(‘’)	$0.9956\angle -3.99^0$	$0.9668\angle -2.55^0$	$0.9703\angle -2.69^0$
6	(‘’)	$1.0127\angle -3.69^0$	$0.9793\angle -0.87^0$	$0.9835\angle -1.15^0$
7	(‘’)	$1.0258\angle 3.72^0$	$1.0147\angle 8.97^0$	$1.0162\angle 8.42^0$
8	(‘’)	$1.0159\angle 0.73^0$	$1.0015\angle 7.51^0$	$1.0035\angle 6.81^0$
9	(‘’)	$1.0324\angle 1.97^0$	$1.0145\angle 11.03^0$	$1.0168\angle 10.09^0$
40	Rectifier	--	$0.9979\angle -2.52^0$	$1.0012\angle -2.48^0$
90	Inverter	--	$1.0145\angle 11.03^0$	$1.0168\angle 10.09^0$

Table 6.2 Generator Output of WSCC Base Case

Bus #	Type	Only AC system		DC49 in service, No shunt			
				power control		Current control	
		P_G (pu)	Q_G (pu)	P_G (pu)	Q_G (pu)	P_G (pu)	Q_G (pu)
1	(Swing)	0.716	0.27	0.791	0.777	0.78	0.717
2	(P-V)	1.63	0.067	1.63	0.249	1.63	0.225
3	(P-V)	0.85	-0.109	0.85	0.205	0.85	0.163
Total		3.196	0.228	3.271	1.231	3.26	1.105

Table 6.3 Transmission Capability of DC49 Link of WSCC Base Case

Control mode	Control setting Value	$V_{schedule}$ (kV)	P (MW)		Q(MVAR)	
			40->90	90->40	40->90	90->40
Power	P=100MW	400	100	-99.5	26.3	32.3
Current	I=250A	400	90	-89.6	23.7	28.6

6.1.3 Modal Analysis

The eigenvalues and eigenvectors of the system Jacobian matrix, as well as the associated participation factors are calculated in modal analysis with the user-defined M-files in MATLAB. The minimum eigenvalues at the different loading levels are summarized as Table 6.4.

Table 6.4 Minimum Eigenvalues at Different Loading Levels

Load factor (λ)	Minimum Eigenvalues		
	Only AC system	DC49 in service, No shunt	
		Power control	Current control
1.0	5.957341	5.824135	5.849111
1.1	5.881292	5.708734	5.738398
1.2	5.791532	5.574953	5.609984
……	……	……	……
1.9	4.561902	3.597905	3.745106
2.0	4.225344	2.886257	3.109206
2.1	3.795877	1.519947	2.035590
2.13	N/A	0.422221	N/A
2.15	N/A	N/A	0.707844
2.2	3.209587	13.221030	7.371165
2.25	0.592559	N/A	N/A
2.3	2.272621	16.33776	3.183091
2.4	6.105680	31.323630	16.14360
Critical mode	4	4	4

The load factor is defined as Equation 6.1.

$$\text{Load Factor} = \frac{\text{Predicted Load}}{\text{Base Load}} \tag{6.1}$$

The increase step of the load factor ($\Delta\lambda$) is set as 0.1 initially. After the critical zone is found, this step is narrowed to 0.01 in order to calculate the minimum eigenvalue more accurately, shown as yellow highlight in Table 6.4. It can see that the critical loading levels are $2.25\times$ base load, $2.13\times$ base load, and $2.15\times$ base load for the cases with DC out of service, DC in power control, and DC in current control, respectively.

The critical mode can also be identified in modal analysis as the minimum eigenvalue is near or equal to zero at the collapse. In this study, the critical modes of three study cases are all mode 4. After identifying the critical mode, the stressed bus and the weak branch can be investigated by the calculation of their associated participation factors. The bus participation factors are summarized in Table 6.5, and the branch participation factors in Table 6.6.

Table 6.5 Bus Participation Factors at the Critical Mode

Bus No.	Bus participation factors		
	Only AC system	DC49 in service, No shunt	
		Power control	Current control
4	0.476759	0.498712	0.493680
5	0.070304	0.060696	0.060840
6	0.244333	0.231463	0.235650
7	0.028856	0.026990	0.028799
8	0.155782	0.135032	0.110866
9	0.023982	0.047119	0.070212

From Table 6.5, it can conclude that mode 4 is a localized mode since buses 4, 6, and 8 have large participation factors while the other buses with values close to zero participation factors. Bus 4 is the most stressed bus, and an effective remedial action may be considered at this bus to stabilize the critical mode. It should be noted that there is usually more than one weak mode associated with different parts of the system, and the

mode associated with the minimum eigenvalue may not be at risk as the system is stressed.

From Table 6.6, it can be seen that branch #1 (from bus 1 to bus 4) consumes the most reactive power in response to an incremental change in reactive load, which means branch #1 is a weak link or highly loaded. The other two weak links are branch #2 (from bus 4 to bus 5) and branch #3 (from bus 4 to bus 6). All of these three branches are connected with bus 4, the most stressed bus. Hence these branches may be considered for the contingency selection and for remedial measures to alleviate voltage stability problem.

Table 6.6 Branch Participation Factors at the Critical Mode

Branch No.	Branch participation factors		
	Only AC system	DC49 in service, No shunt	
		Power control	Current control
1 (from bus 1 to bus 4)	1	1	1
2 (from bus 4 to bus 5)	0.496089	0.516802	0.520405
3 (from bus 4 to bus 6)	0.303738	0.403551	0.397623
4 (from bus 5 to bus 7)	0.168777	0.202984	0.182327
5 (from bus 6 to bus 9)	0.131590	0.208157	0.188201
6 (from bus 7 to bus 8)	0.021446	0.033196	0.037817
7 (from bus 8 to bus 9)	0.030669	0.009007	0.013228
8 (from bus 2 to bus 7)	0.106846	0.128486	0.119614
9 (from bus 3 to bus 9)	0.073702	0.118329	0.106845

6.1.4 Loading Margin

In modal analysis, bus 4 has been identified as the most stressed bus, and the critical loading levels have been predicted approximately. It is required to verify the results by using PV plots, which can measure the loading margin more accurately. The continuation power flow method specified in the M-files is used to trace the PV curves at the most stressed bus, namely bus 4. The voltage magnitude profiles with different

loading levels, namely 200%, 300%, and 400%, at bus 4 are shown as Figures 6.3-6.5 below.

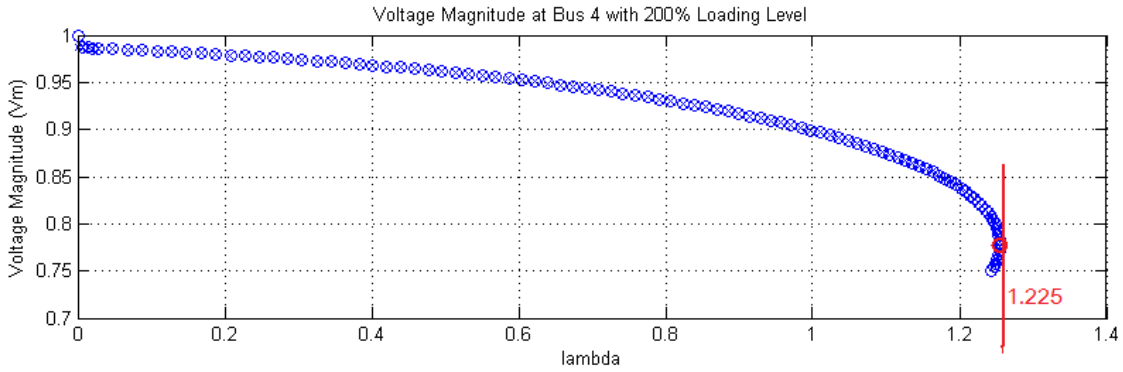

a) With 200% Base Load

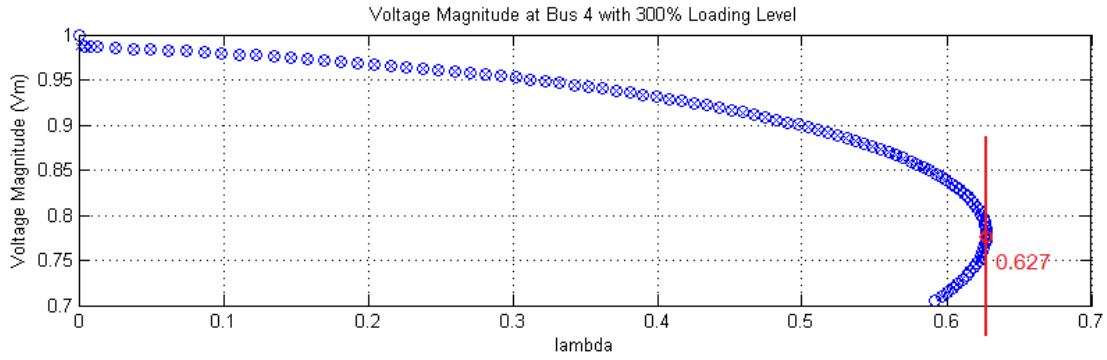

b) With 300% Base Load

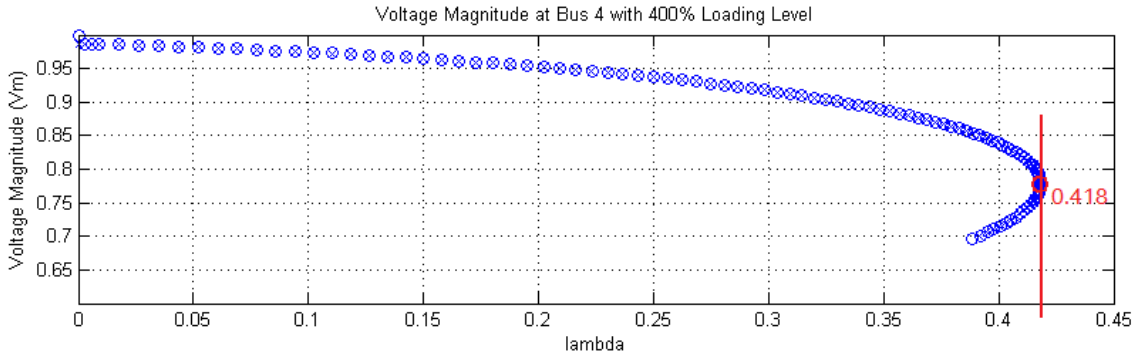

c) With 400% Base Load

Figure 6.3 Voltage Magnitude Profiles at Bus 4 of WSCC with only AC system

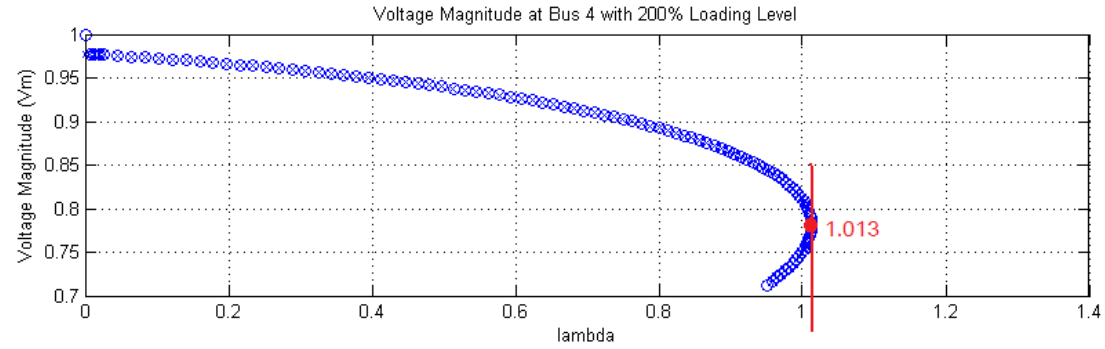

a) With 200% Base Load

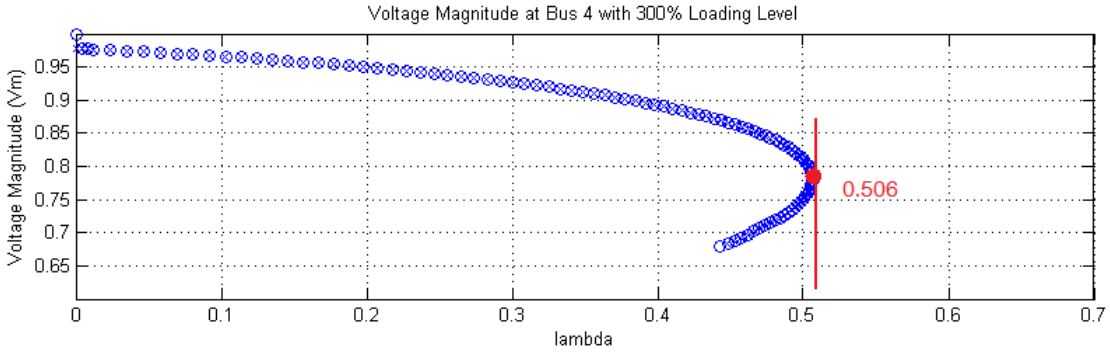

b) With 300% Base Load

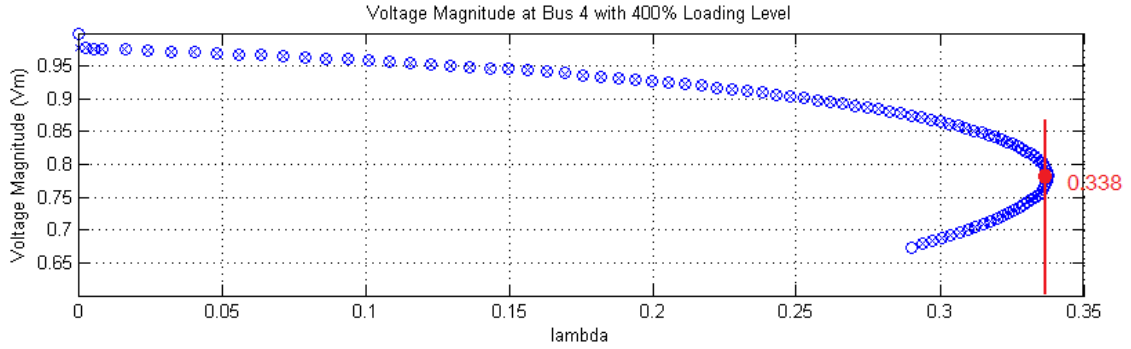

c) With 400% Base Load

Figure 6.4 Voltage Magnitude Profiles at Bus 4 of WSCC with DC49 in Power Control

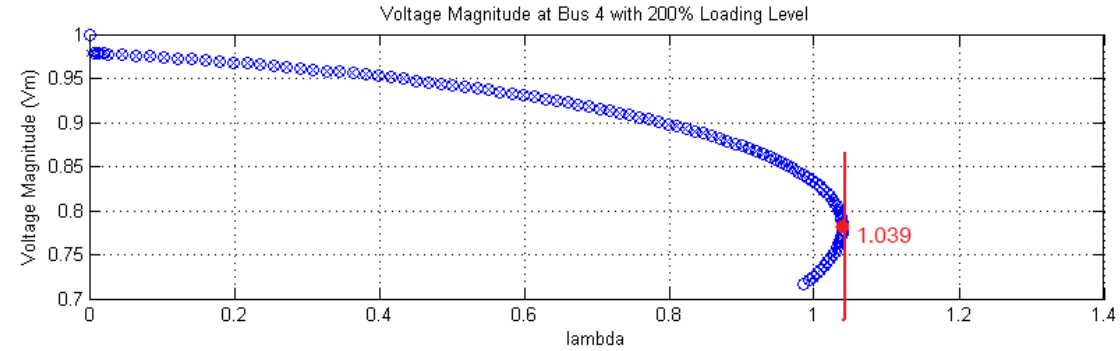

a) With 200% Base Load

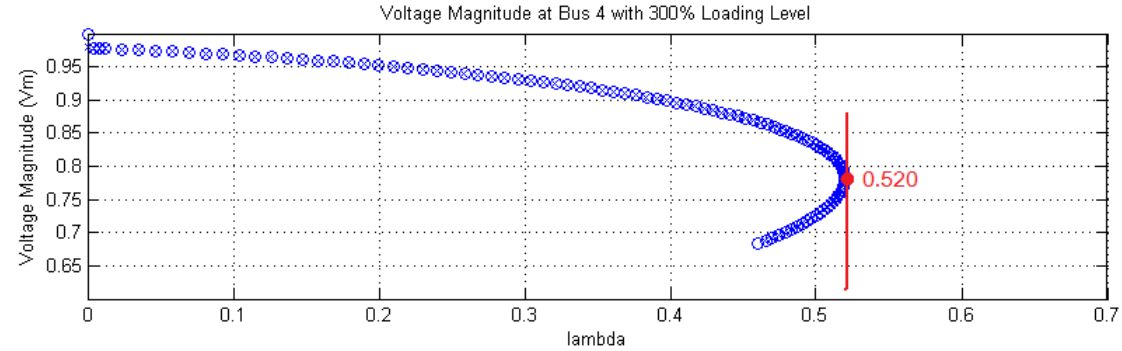

b) With 300% Base Load

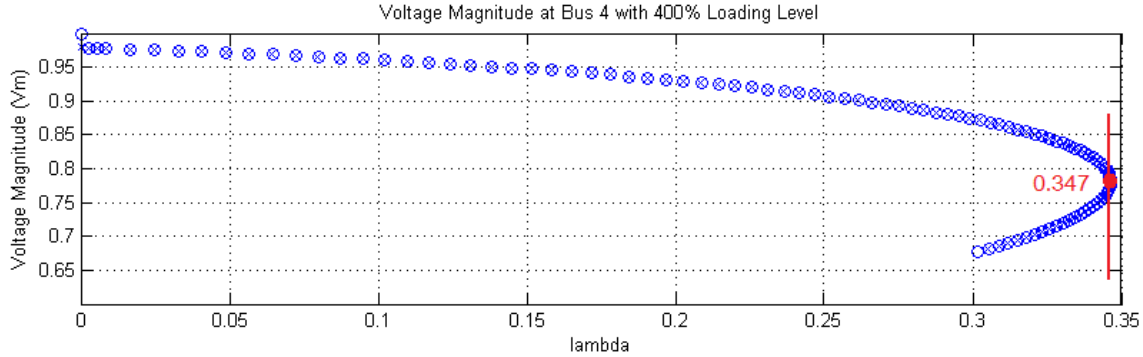

c) With 400% Base Load

Figure 6.5 Voltage Magnitude Profiles at Bus 4 of WSCC with DC49 in Current Control

Figures 6.3-6.5 are voltage magnitude profiles at bus 4 for WSCC with different cases of study, namely only AC system, DC in power control, and DC in current control. Each figure includes three PV plots, namely plots a), b) and c) corresponding to the loading level at 200%, 300%, and 400% base load, respectively.

The margin loading factor is defined as Equation 6.2.

$$\text{Margin Loading Factor} = \frac{\text{Maximum Load - Base Load}}{\text{Base Load}} \tag{6.2}$$

From Figure 6.3-6.5, the margin loading factors can be calculated and summarized as Table 6.7, where Error = $Value in Table 6.4 - Average$.

Table 6.7 Margin Loading Factors at Bus 4

Loading level (* Base Load)	Margin loading factor		
	Only AC system	DC49 in service, No shunt	
		Power control	Current control
200%	1.225	1.013	1.039
300%	0.627 *2	0.506*2	0.520*2
400%	0.418*3	0.338*3	0.347*3
Average	1.244	1.013	1.040
Value in Table 6.4	1.25	1.13	1.15
Error	0.006	0.117	0.110

In Table 6.7, the averages of loading margin are $1.244 \times \text{Base Load}$, $1.013 \times \text{Base Load}$, and $1.040 \times \text{Base Load}$ for the three different study cases, respectively. The results are matched with the corresponding loading factors of 2.25, 2.13, and 2.15 in modal analysis method as Table 6.4. In addition, although the predicted loading levels are different at each PV plot, bus loadability (bus load limit) should be the same, given the same network configuration and the operating condition.

6.1.5 The Second Order Performance Index

The minimum eigenvalues obtained from the modal anlaysis summarized in Table 6.4 can be plotted as Figure 6.6. It shows that the trend of minimum eigenvalue with the

increase of loading level is nonlinear, and it is difficult to predict the voltage stability margin from the current operating snapshot.

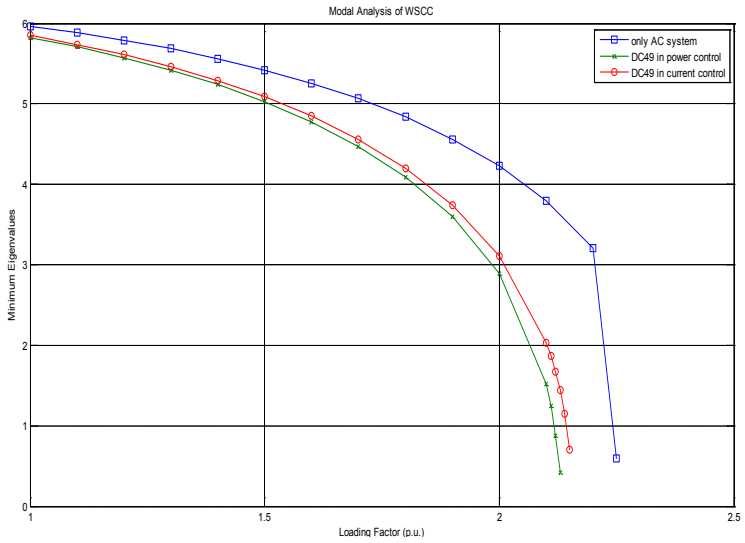

Figure 6.6 Modal Analysis Results of WSCC

Therefore, the developed second order performance indicators are calculated as an improvement. The polynomial of degree 1.0 is also tried to fit the calculated value in a least squares sense. The calculated values and the polynomial fitting values are shown in Figures 6.6- 6.8.

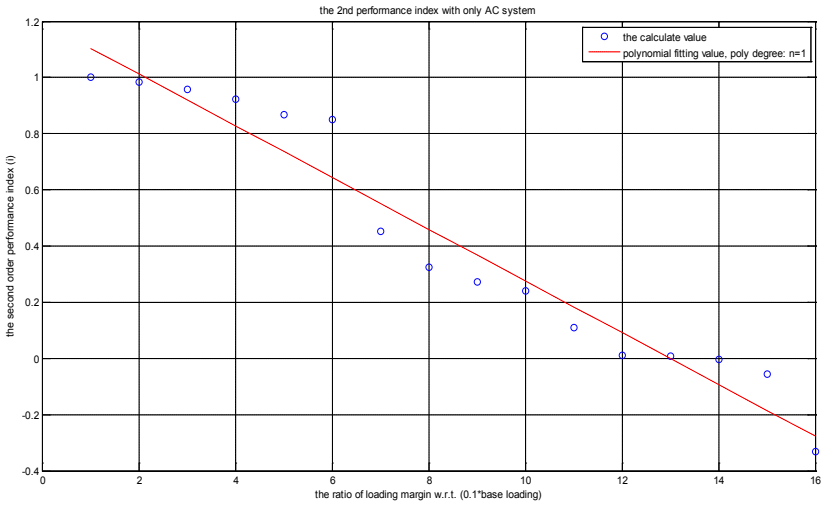

Figure 6.7 The 2nd Performance Indicator of WSCC with only AC system

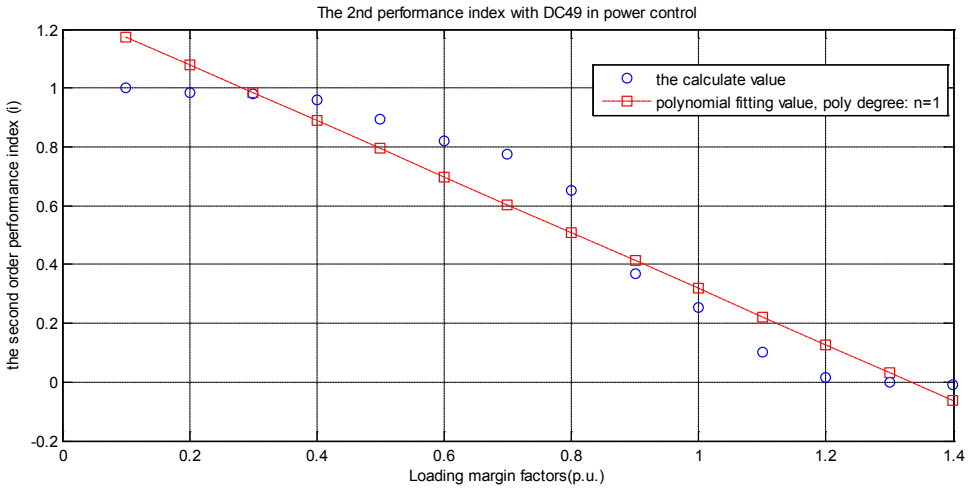

Figure 6.8 The 2nd Performance Indicator of WSCC with DC49 Power Control

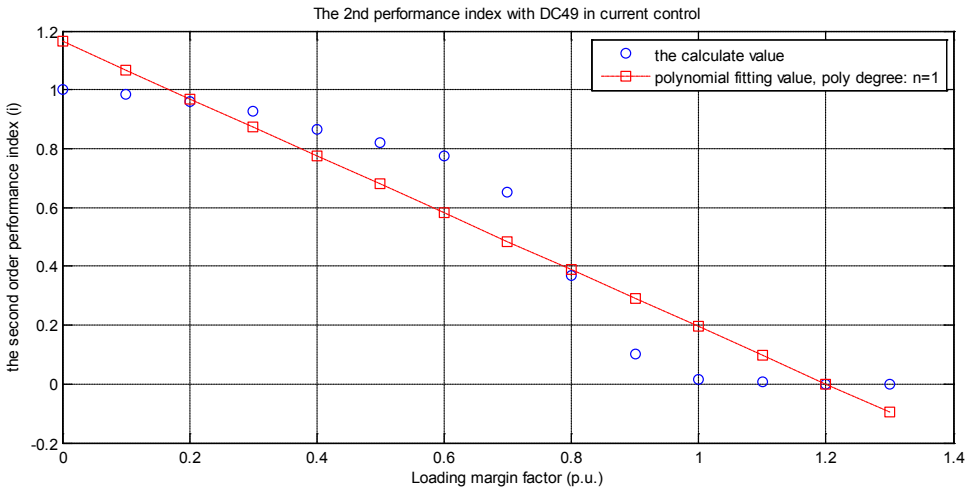

Figure 6.9 The 2nd Performance Indicator of WSCC with DC49 Current Control

Figures 6.6-6.8 show that based on the 2nd performance indicator, loading margins are $1.30 \times \text{Base Load}$, $1.10 \times \text{Base Load}$, and $1.20 \times \text{Base Load}$ for the cases of WSCC with only AC system, with DC49 in service power control, and with DC49 in service current control, respectively. The second order performance indicator starts from 1.0 at the initial loading point, then decreases and is close to zero at the critical point with the loading level increases. The second order performance index shows the approximate linearity and the associated prediction can be made based on this linear trend. This approximation introduces an error which is specified as Equation 6.3.

$$Error = |CalculatedValue - PolyfittingValue| \tag{6.3}$$

The maximum errors based on Figures 6.7-6.9 are 0.1695, 0.1749 and 0.1632 for three cases of study. It occurred to the initial loading level. These errors may be caused by the factors, which have been discussed in the development of indicator in Chapter 5.

- Assumption is made in the linearity of the second order performance indicator.
- The approximation is introduced in the manipulation of matrices.

The second order performance indicator is less accurate than modal analysis since it has introduced some assumption and approximation in its development. It may cost more computational time in the calculation at the beginning several point to find the appropriate fitting polynomial. Once the fitting function has been built, it can be straightforward to predict its proximity to voltage instability by its linear feature.

6.2 System 2: Integrated Shipboard Power System

The integrated AC/DC power system architecture used in this work is the benchmark naval-ship power system given in Figure 6.10. The architecture consists of five generators, five AC to DC rectifiers, one DC to AC inverter, five propulsion motors, one AC load, six AC cables and six DC cables. There is no DC load in this architecture, since it is difficult to tap power off along the DC line in PSS/E. The system data refers to Appendix B: Test System Data.

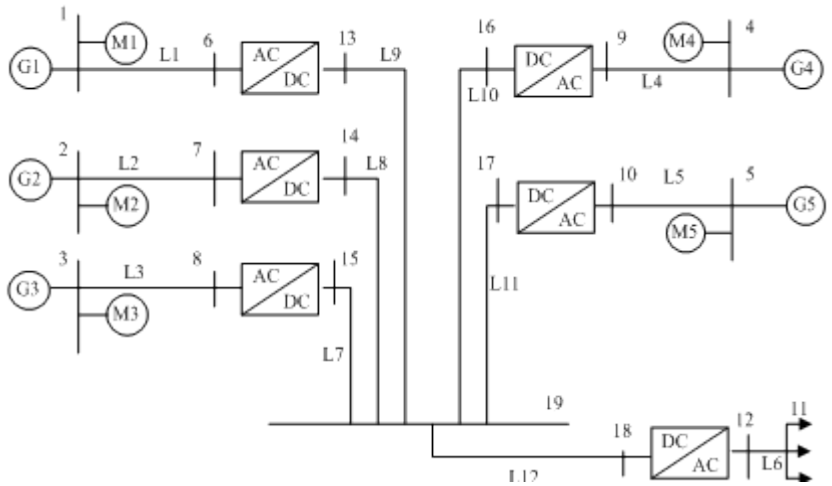

Figure 6.10 Benchmark Integrated Shipboard Power System

6.2.1 Load Flow Analysis

This model has been built in PSS/E. Load flow analysis has been performed for base case and for the contingency, where the rectifier between buses 10 and 17 is blocked. The similar results can be obtained when the other four rectifiers are blocked individually. If the inverter is blocked, the whole DC line will be blocked, and the AC terminals will become five independent subsystems. DC power, voltage and current have been set to 1.0 p.u, and the inverter DC bus (bus 18) has been set as the voltage regulating bus. The load flow results for base case and the contingency are summarized as Tables 6.8 and 6.9.

Table 6.8 Voltages at DC Buses of Integrated Shipboard Power System

Operating Condition		Voltages at DC Line (p.u.)		
		Bus 13	Bus 19	Bus 18
Base Case	Power	1.0653	1.0544	1.0
	Current	1.0696	1.0580	1.0
Contingency	Power	1.0550	1.0440	1.0
	Current	1.0580	1.0464	1.0

Table 6.9 Transmission Capability of DC Links of Integrated Shipboard Power System

Operating Condition		Rectifier				Inverter			
		P (p.u.)		I (p.u.)	Q (p.u.)	P (p.u.)		I (p.u.)	Q (p.u.)
		13->19	19->13	13->19		19->18	18->19	19->18	
Base Case	Power	1.0	-0.99	0.938	0.290	4.949	-4.693	4.694	2.413
	Current	1.07	-1.058	1.0	0.292	5.290	-5.0	5.0	2.639
Contingency	Power	1.0	-0.99	0.948	0.291	3.958	-3.792	3.792	1.862
	Current	1.058	-1.046	1.0	0.296	4.186	-4.0	4.0	2.032

Based on Table 6.8, it can see that current control provides higher voltages at DC buses than power control. From Table 6.9, it shows that current control provides higher transmission capability and higher current. But there is a tradeoff that higher current

means higher line loss, and higher voltage means higher reactive power consumption at converters. Both of control modes do not cause voltage stability problem, and power control has an advantage in terms of cable requirements and reactive power compensation.

6.2.2 Modal Analysis

Similar to Section 6.1.3, a gradual change in loading level is assumed, and the loading factor is defined as Equation 6.1. Modal analysis is performed for base case with power control, and the results are shown as Figure 6.11, where it shows that the critical loading level of base case with power control model is around $22.5 \times BaseLoad$.

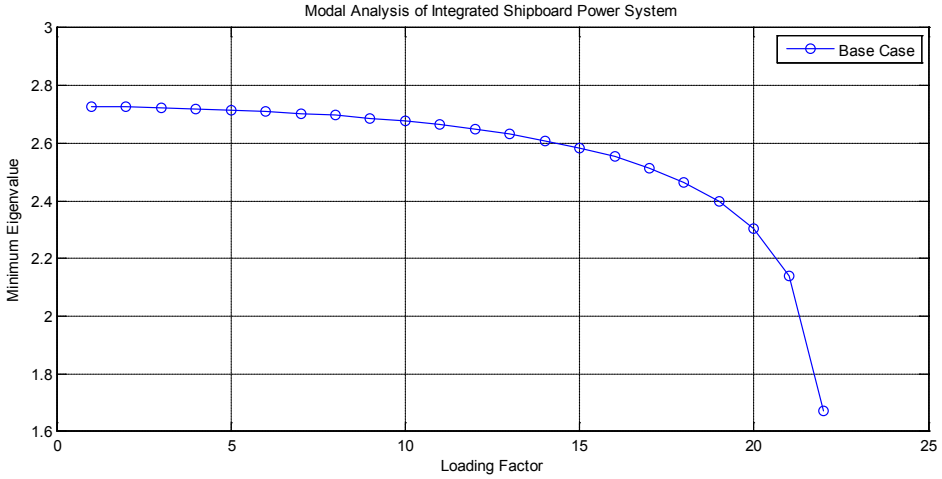

Figure 6.11 Modal Analysis Results of Integrated Shipboard Power System

6.2.3 Loading Margin

Bus 19 is a bus connected to all of the converter links, where loading margin is measured. The voltage magnitude is calculated for base case with power control shown as Figures 6.12.

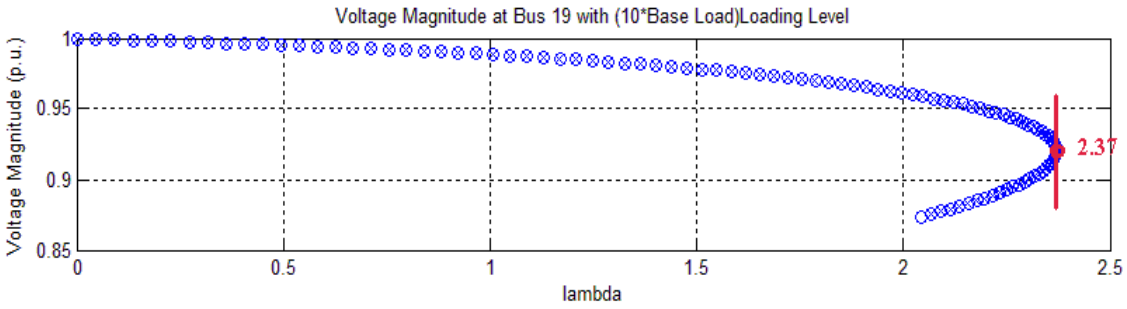

a) With 10 * Base Load

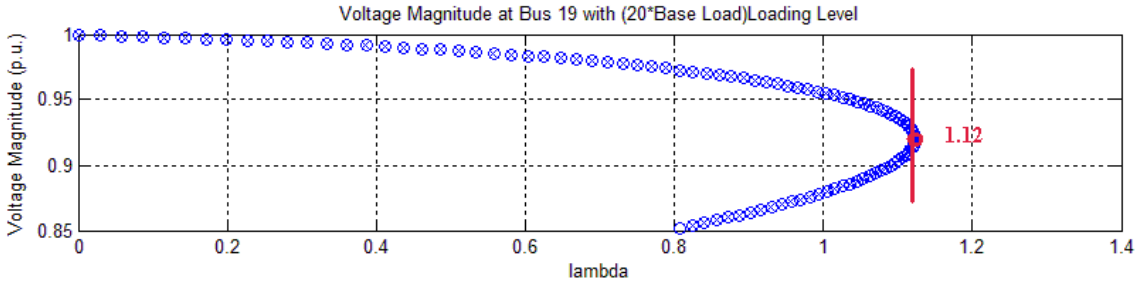

b) With 20* Base Load

Figure 6.12 Voltage Magnitude Profiles at Bus 19 of Integrated Shipboard Power System

The margin load factor is defined as Equation 6.2.

In Figure 6.12 a) Margin loading factor = 2.37*(10-1) = 21.23;

In Figure 6.12 b) Margin loading factor= 1.12*(20-1) = 21.28.

Hence, the average critical loading level for base case with power control is 22.25, corresponding to the result obtained from modal analysis (22.5) in Section 6.2.2.

Two points have to be noted in voltage stability assessment for the integrated shipboard power system.

- If any DC link in this configuration is blocked, it will make the generator connected to this link "island". How to handle this "island" is expected to be investigated in the future work.

- The Hessian matrix is the key factor in second order performance indicator. The calculation of Hessian matrix for multi-infeed DC configuration is also of interest for future work.

In addition, more information regarding the shipboard power system is expected to be available.

6.3 Summary

This chapter describes the static voltage stability assessment procedure of WSCC system. Firstly, load flow analysis is performed for three study cases, namely with only AC system, with DC links in power control, and with DC links in current control, to obtain the snapshots for initializing voltage stability assessment. Modal analysis is used to identify the critical mode, the most stressed bus and the weak linked branch by minimum eigenvalues and maximum participation factors. Then, the continuation power flow method is used to trace PV curves at the most stressed bus to measure the loading margin accurately. At last the second order performance indicator is deployed to estimate the critical point by the linear trend as the improvement to the modal analysis.

DC links can degrade the voltage stability of power systems without reactive power compensations. The DC link with power control can provide more active power transfer capability, but can cause more transmission loss and a lower voltage stability level. In contrast, DC link with current control can provide the higher voltage stability level and less transmission loss, but less active power transfer capability. In practice, the reactive power compensation is considered properly to take advantages of various control modes. The simulation results of three methods have been compared by each other.

The static voltage stability assessment procedure is also applied for the benchmark shipboard power system with multi-infeed DC configuration. The load flow, modal analysis and loading margin are performed to predict the critical loading level. The

obtained results are consistent for the base case. More research work is expected to solve some technical problems regarding “islanding” and Hessian matrix for contingencies.

CHAPTER VII

SYSTEM STUDY AND DYNAMIC SIMULATION

This chapter describes the modified IEEE one-area Reliability Test System – 1996 (RTS -96) [66] to demonstrate the procedure of transient voltage stability assessment. Load flow analysis will be performed for the base case, AC contingency analysis will be implemented to select the critical ones in the specified list, and PV and QV plots will be calculated for base case and the selected contingencies. How the dynamic simulation is used to bench mark the steady-state simulation results will be explained, and the coordination of controls, compensation or protections in remedial measures will be studied.

The data of RTS-96 are available for download from the webpage maintained by the University of Washington [67].

7.1 System 2-1: Modified IEEE One-Area RTS-96 Static Simulation

The Reliability Test System was proposed to provide a basic system sufficiently broad for testing or comparing methods for reliability analysis of power systems. In this study several modifications are introduced in power flow data to make it more suitable for voltage stability analysis. These changes and underlying assumptions are considered to highlight the aspects of problems related to voltage control and reactive power compensation.

7.1.1 Description of Modified RTS-96

RTS-96 corresponds to the IEEE 1976 Reliability Test System [68], and was extended to represent multi-area systems in 1996 version by interconnecting copies of one-area RTS-96. The system presented here is the so-called "one-area RTS-96", equivalent to the 1979 Reliability Test System, whose single-line diagram in PSS/E is shown as Figure 7.1.

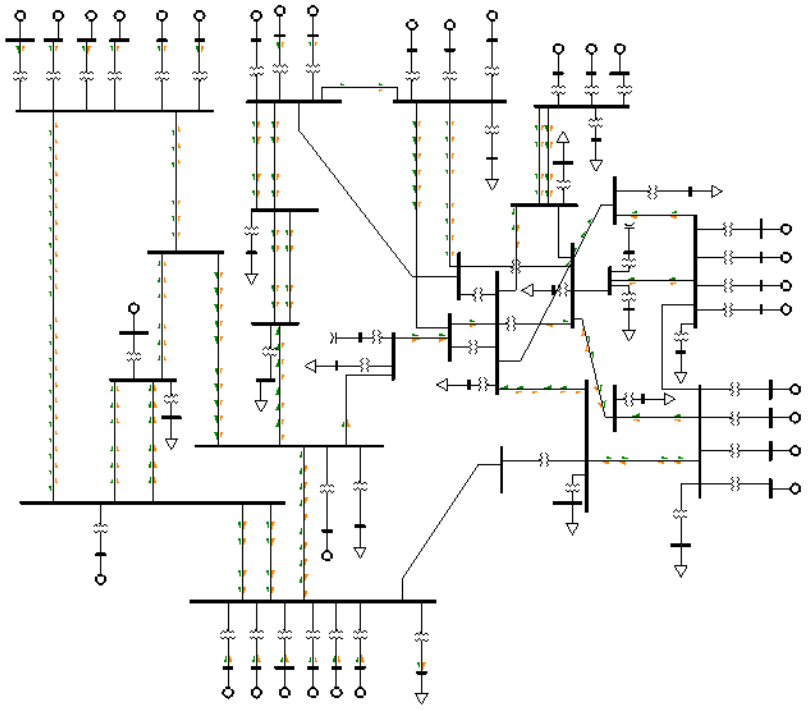

Figure 7.1 The Single Line Diagram of Modified IEEE One-Area RTS-96 in PSS/E

The introduced modifications are summarized below.

- Synchronous condenser at bus 114 was replaced by an SVC with the same nominal range (-50/+200MVar), so that the reactive power output of this device becomes voltage dependent.

- Shunt at bus 106 was replaced by an SVC with a range of (-50/+100MVar), which introduces an additional voltage control capability and is required to avoid voltage collapse during dynamic simulation.

- Step-up transformers of generators and SVCs are represented assuming 5 tap positions, and no OLTC. All other transformers are represented with +/-10% OLTC transformers with 33 steps (0.625% per step).

- Loads are no longer connected to the 138kV or 230kV but to 13.8kV by step-down transformers with OLTC control.

Table 7.1 A List of System Components

	Buses	Plants	Machines	Machine owners	
Total	75	32	32	32	
Maximum	4000	1200	1440	2880	
	Switched Shunts	Loads	Transfers	Mutuals	Facts Devices
Total	2	17	0	0	0
Maximum	500	8000	500	2000	20
Transformers					
	Branches	Two-Winding	Three-Winding	Zero Impedance	Branch Owners
Total	90	56	0	0	90
Maximum	10000	1600	400	200	20000
Multi-Section Line					
	Groupings	Sections	2-Term DC	N-Term DC	VSC DC
Total	0	0	0	0	0
Maximum	400	1000	30	5	20

Table 7.1 lists the components in the modified IEEE one-area RTS-96 system and the maximum simulation capacity provided by PSS/E simulation environment. The load flow analysis and AC contingency analysis are performed by using PSS/E.

7.1.2 Load Flow Analysis of the Base Case

Table 7.2 RTS-96 Base Case Summary

Total	Generation	PQ Load	I Load	Y Load	Shunts	Charging	Losses	Swing
MW	3200.2	3135.0	0.0	0.0	0	0	65.2	398.7
MVAR	1349.9	638.0	0.0	0.0	-39.1	547.7	1298.6	182.7

Load flow is analyzed to initialize the system status for dynamic simulation. The load flow results for the base case are summarized as Table 7.2, which provides an idea of system current loading level. The voltage information of the base case will be discussed with the voltage information of contingencies in Section 7.1.3.

7.1.3 AC Contingency Analysis

The large disturbances instead of a small disturbance, such as the outage of generators and opening circuits, have been set to trigger the procedure of transient voltage stability assessment. Before AC contingency analysis is performed to screen contingencies for transient voltage stability assessment, subsystems and contingency lists need to be specified and different solution options need to be compared.

7.1.3.1 Description of Subsystems and Solution Options

To calculate the distribution factor, two subsystems, namely "138kV only" and "230kV only", are defined, which only include the buses at 138kV or 230kV, and exclude the buses at 18kV and 13.8kV. The contingency list is specified as "*open the single circuit in the subsystem of '138kV only' and '230kV only'*" and "*decrease generation by 100 percent*", which means the contingencies of generation outage and

opening single circuit at high voltage side are considered, and the other contingencies are beyond the scope of this work.

Different solution options of load flow analysis have been set up for all specified contingencies. When the divergence happened, the largest mismatch at the bus and total mismatch of system have been recorded and compared as Table 7.3 to obtain the optimal solution.

The largest mismatch is the convergence criterion for power flow model. It should be less than a preset tolerance, typically 1×10^{-5} p.u. if the solution is convergent. From Table 7.3, it shows that the most optimal solution can be obtained by using a full Newton Raphson solution and the non-divergent power flow solution. The transformer taps are locked, but the switched shunts are allowed to respond during contingency analysis. QV and PV plots will be calculated by using the same solution.

Table 7.3 A Comparison of Different Solution Options for Divergent Contingencies

Solution options		Contingency #4 From 112 to123	Contingency #6 From 114 to 116	Contingency #10 From 115 to 124	Contingency #30 From 106 to 110
Lock shunt	Largest Mismatch (MW)	83.28	118.93	115.69	130.40
	Total Mismatch (MVA)	373.10	450.09	549.18	820.22
Lock shunt + Non Divergent	Largest Mismatch (MW)	38.99	67.58	50.70	65.31
	Total Mismatch (MVA)	158.19	379.33	394.43	286.95
Enable shunt	Largest Mismatch (MW)	N/A	90.97	851.72	4.01
	Total Mismatch (MVA)		468.18	8051.10	13.34
Enable shunt+ Non Divergent	Largest Mismatch (MW)	N/A	29.33	48.70	13.79
	Total Mismatch (MVA)		247.04	353.13	56.33

7.1.3.2 Results of AC Contingency Analysis

Voltage range and deviation in subsystems "230kV only" and "138kV only" have been monitored to screen the contingencies. The solutions of four opening-single-circuit contingencies are divergent, but no divergent solution for generator outages. Hence, four opening-single-circuit contingencies do not meet the stability criterion, and will be selected for voltage stability assessment. Although all generator-outage contingencies can satisfy the requirements of stability, three of them with the lowest voltage range still have been selected to compare with the opening-single-circuit contingencies. These seven selected contingencies have been defined as ***contingency #4*** (230kV circuit between

buses 112 and 123), ***contingency #6*** (230kV circuit between buses 114 and 116), ***contingency #10*** (230kV circuit between buses 115 and 124), ***contingency #30*** (138kV circuit between 106 and 110), ***Gen1017***, ***Gen30123***, and ***Gen40102***.

7.1.4 Modal Analysis

Modal analysis is performed for the base case, four selected opening-single-circuit contingencies and three selected generator-outage contingencies, in order to obtain the general information regarding voltage stability margin. The critical loading levels for the base case and for the selected contingencies are summarized in Table 7.4. The minimum eigenvalues at the different loading levels are shown in Figure 7.2.

Table 7.4 RTS-96 Critical Loading Levels

	Critical Loading Level (*Base Loading)
Base Case	1.72
Contingency #4	1.66
Contingency #6	1.70
Contingency #10	1.49
Contingency #30	1.40
Gen10107	1.66
Gen30123	1.69
Gen40102	1.67

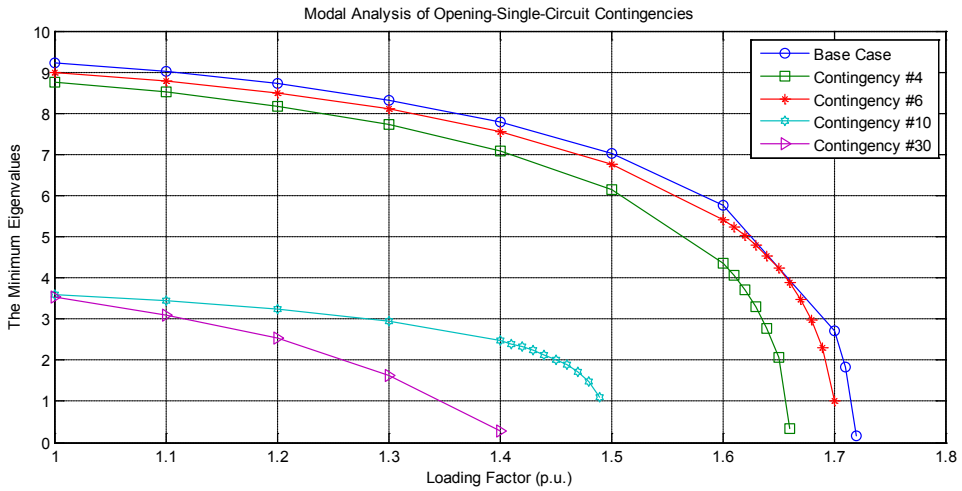

a) Base Case and four Opening-Single-Circuit Contingencies

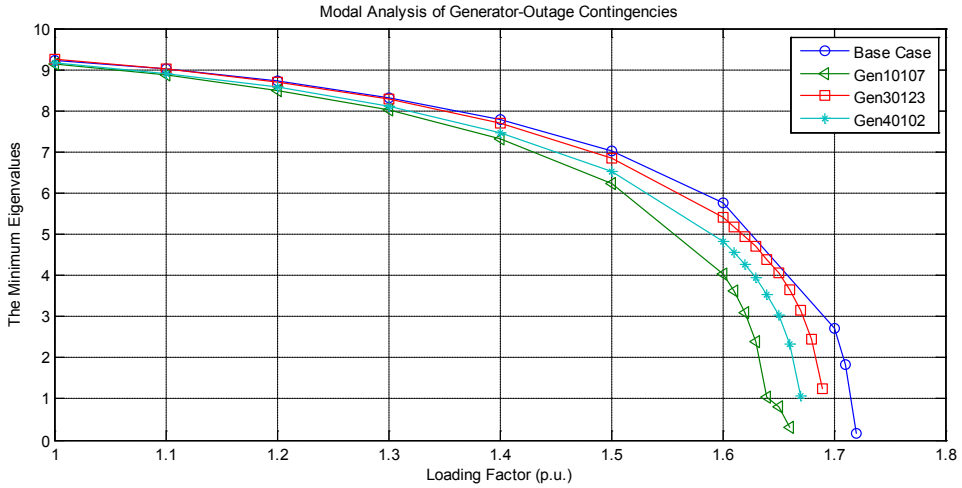

b) Base Case and three Generator-Outage Contingencies

Figure 7.2 The Minimum Eigenvalues at Different Loading Levels of RTS-96

From Table 7.4, it can see that contingency #30 has the lowest critical loading level (1.4*Base Load). In Figure 7.2, the minimum eigenvalues at the different loading levels for contingency #30 are nearest to zero. Therefore, the worst contingency is contingency #30, namely opening the circuit between buses 106 and 110, since this cable has a large charging capacitor (2.459 p.u.), and no line reactors are connected to it at the initial data. In order to make this system more realistic, line reactors were added at each

terminal of the cable (0.75 p.u. in each end) to decrease over-voltage during energization and load rejection.

7.1.5 QV and PV Plots

QV plot at bus 110 is calculated for the base case and the selected contingencies to obtain the reactive power margin shown as Figure 7.3.

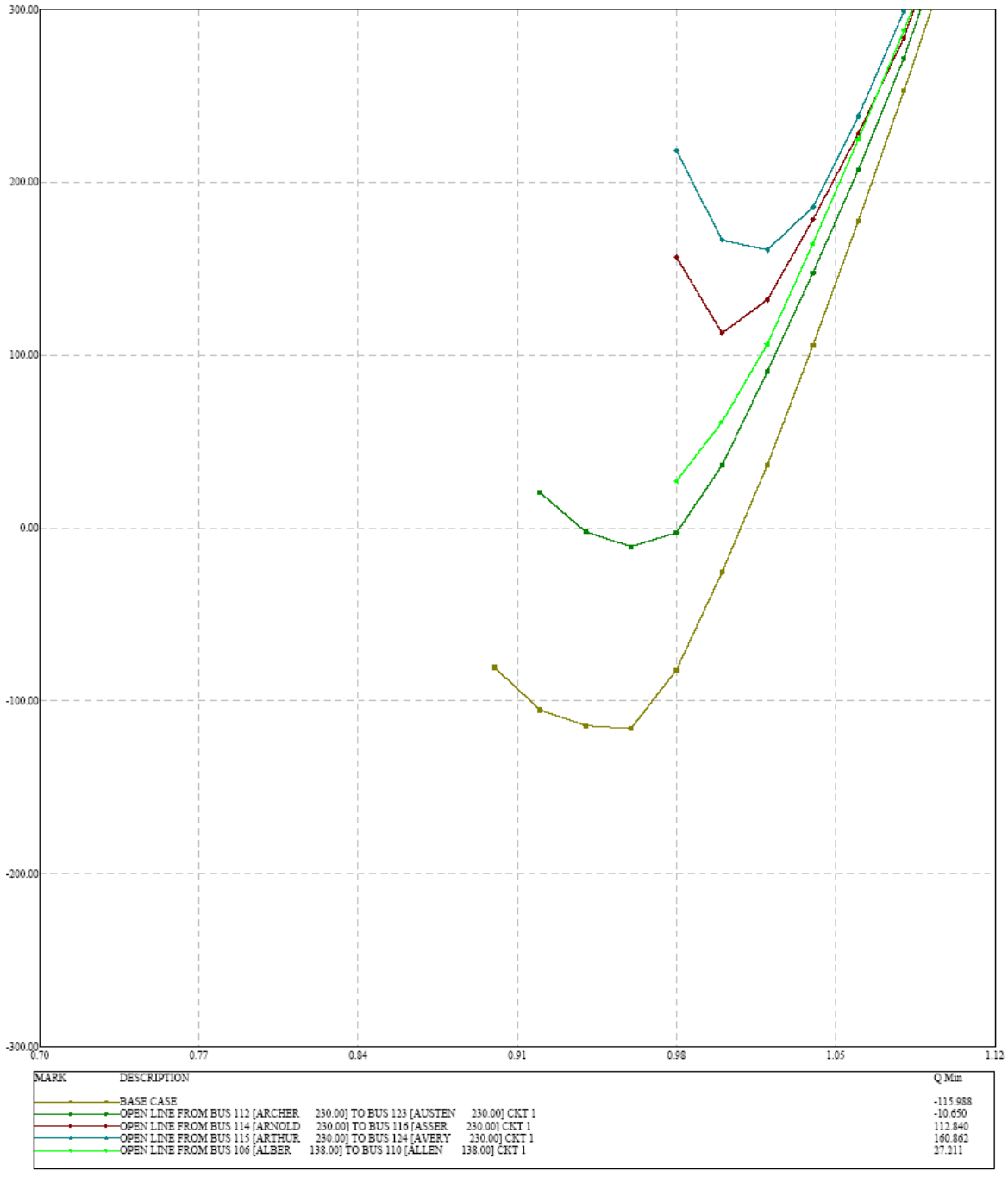

a) Open Single Circuit

Figure 7.3 QV Plot at Bus 110

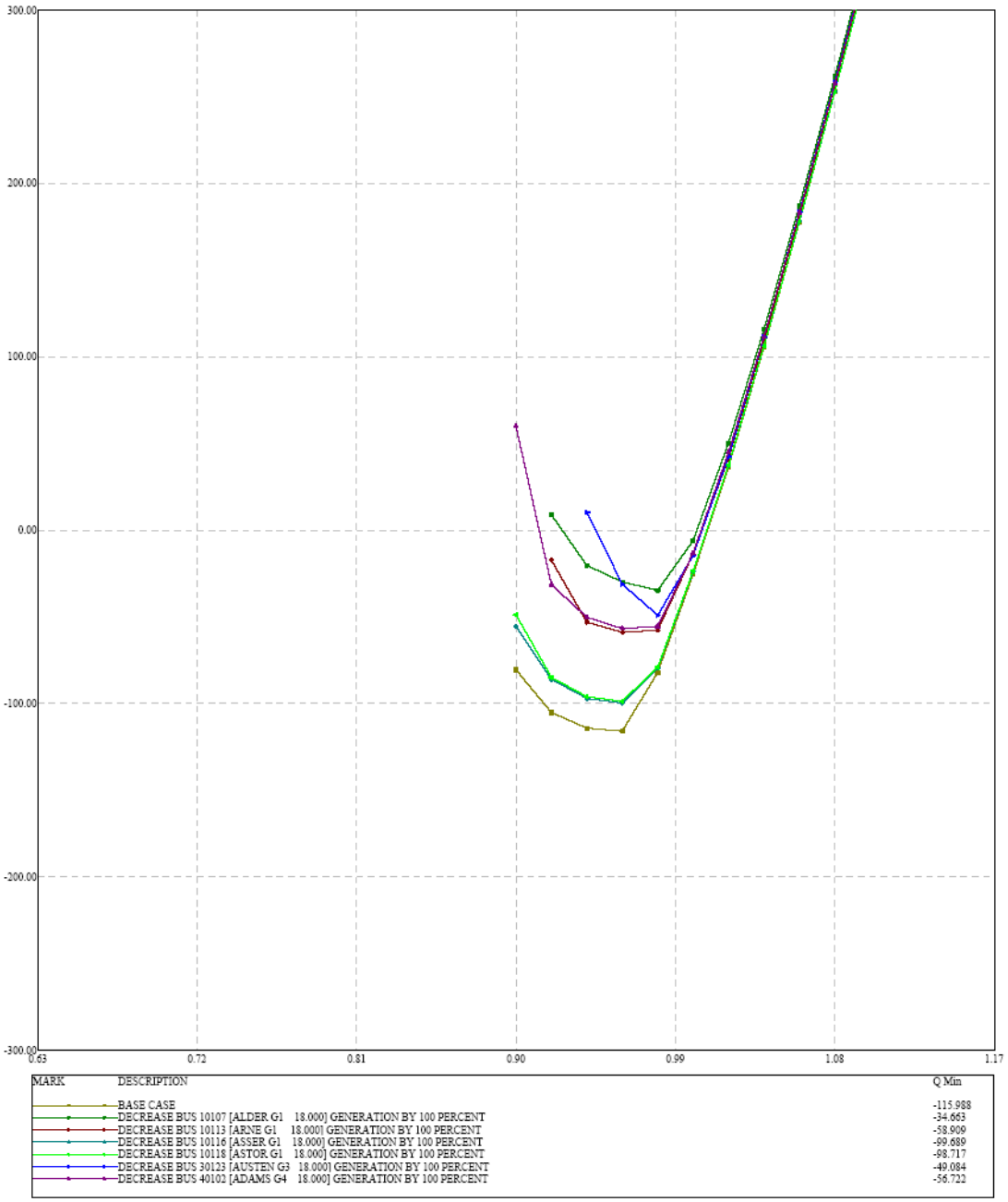

b) Generator Outage

Figure 7.3 (Continued)

Figure 7.3 shows that the reactive power margin in the base case is around 116MVar, dropping to 10.65MVar for contingency #4. Voltage collapse is identified for

contingency #6, contingency #10 and contingency #30, where the reactive power deficiencies are 112.84MVar, 160.86MVar and 27.21MVar, respectively. In fact, the QV curve associated with contingency #30 is incomplete, since the power flow solution cannot converge at voltages below 0.98 p.u.. The reactive power margins are 34.66Mvar for Generator10107, 49.08MVar for Generator 30123, and 56.72MVar for Generator 40102.

PV plot analysis considers the transfers from generation (230kV) to load (138kV) network, which means that the generation connected to 230kV area is increased with the additional power being transferred to the loads connected to 130kV area. PV plots at bus 110 are calculated for the base case and the selected contingencies as Figure 7.4.

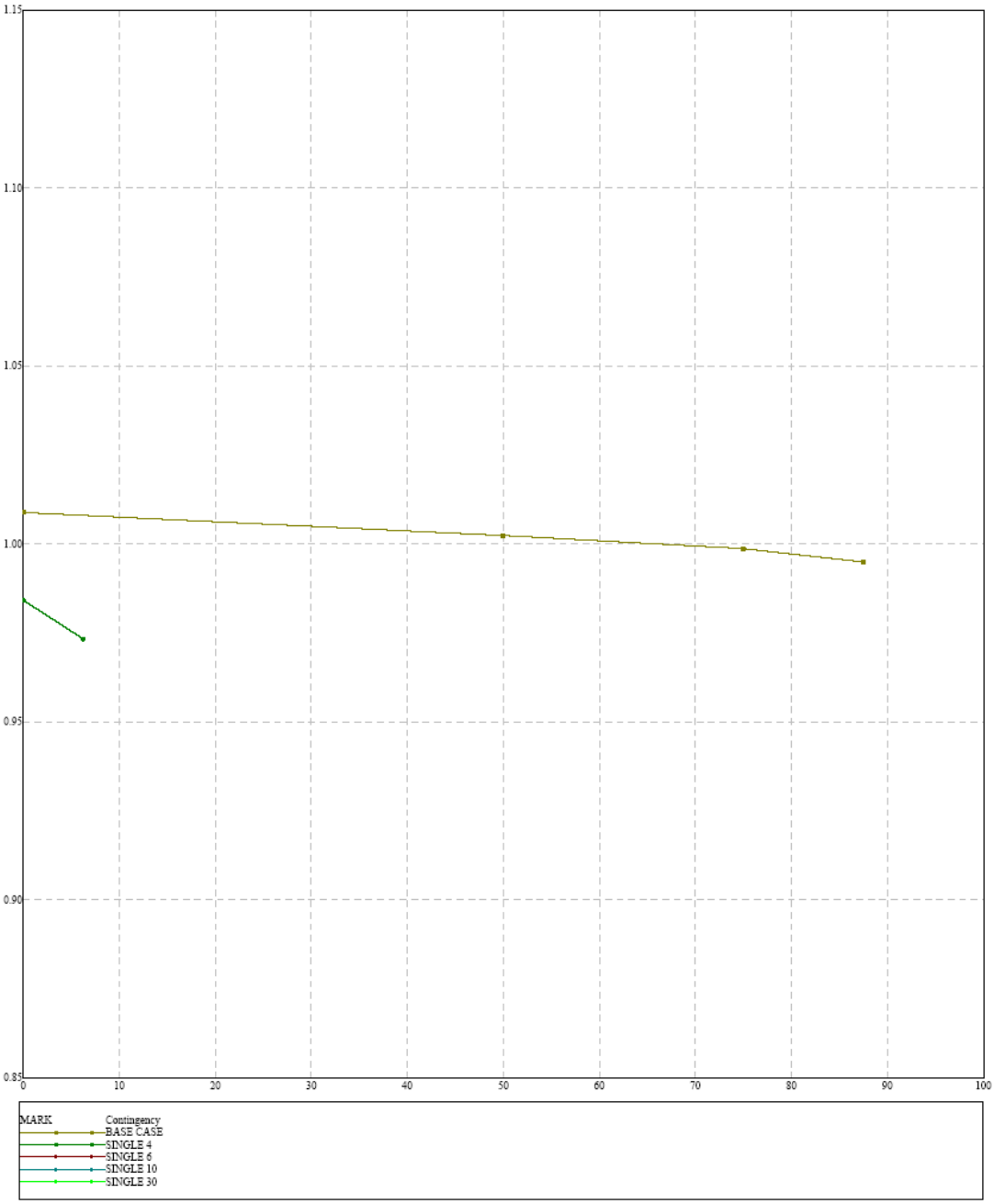

Figure 7.4 PV Plot at Bus 110

Figure 7.4 shows that the maximum transfer calculated is 87.5MW for the base case, and contingency #4 resulted in a maximum incremental transfer of just 6.25MW. There are no curves for contingencies #6, #10, and #30, which means that no incremental transfer is possible for these contingencies.

7.1.6 The Second Order Performance Indicator

The second order performance indicator is implemented to provide a complement for modal analysis in Section 7.1.4. The results for the base case and four opening-single-circuit contingencies are shown in Figure 7.5.

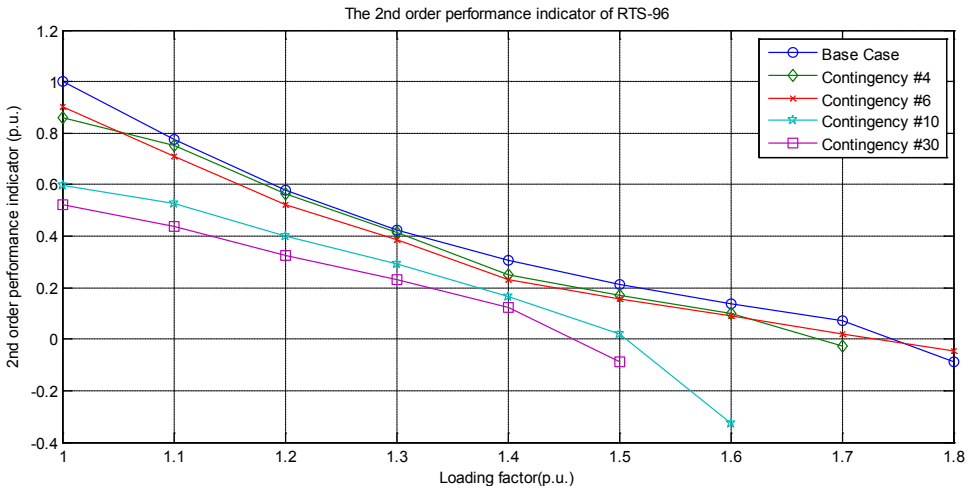

Figure 7.5 The 2nd Order Performance Indicators of RTS-96

Figure 7.5 shows the similar tendency of proximity to voltage collapse for the base case and the selected contingencies, which is corresponding to the results obtained from modal analysis. This proximity is quite rough, but shows linearity. More work regarding polynominal fitting is needed if this indicator is applied for voltage stability prediction.

7.2 System 2-2: Modified IEEE One-Area RTS-96 Dynamic Simulation

The typical models and data for all the elements in dynamic simulation are proposed as described in the following. The additional explanation of parameters and the associated block diagrams are available in [61].

- *Generators*: Hydro turbines are represented by the salient pole machine model (GENSAL); thermal units are represented by the round-rotor machine model (GENROU).

- *Excitation systems*: 1968 IEEE type 1 excitation system model (IEEET1) and 1981 IEEE type AC1 excitation system model (EXAC1) models correspond to AC rotating exciters. There is other bus-fed static exciter (SCRX).

- *Turbine/Speed governors*: The hydro turbines are represented by the hydro turbine governor model (HYGOV), while the steam units are represented by the 1981 IEEE type1 turbine governor model (IEEEG1) and the parameters for the steam turbines consider a single reheater. Those machines without such model are simulated with constant mechanical power.

- *Static VAR Compensators*: Two static VAR compensators (SVC) are involved in this case. One is connected to bus 10114, and rated -50/+200MVar. The other is connected to bus 10106 and rated -50/+100MVar. Both of them are represented by the SVC model for switched shunts (CSSCS1).

In order to investigate of dynamic characteristics of single component, the response of the individual component to disturbance needs to be studied so that the simulation time can be set properly for dynamic simulation. Typically the response of excitation system and speed governor is considered for dynamic simulation. Buses 10101, 10107, 10121 and 10122 are chosen to represent the different types of excitation systems or speed governors in this test system.

7.2.1 Response of Excitation System

The test system consists of three types of excitation systems (EXAC1, IEEET1, and SCRX). The open circuit step test has been used to test the control tuning of excitation systems. The machine terminal voltages (seen in Figure 7.6) and generator main field voltages (in Figure 7.7) at buses 10101, 10121, and 10107 are shown to present the response of EXAC1, IEEET1 and SCRX, respectively. It can be seen that the voltage regulator provides a fast response with the minimal overshoot.

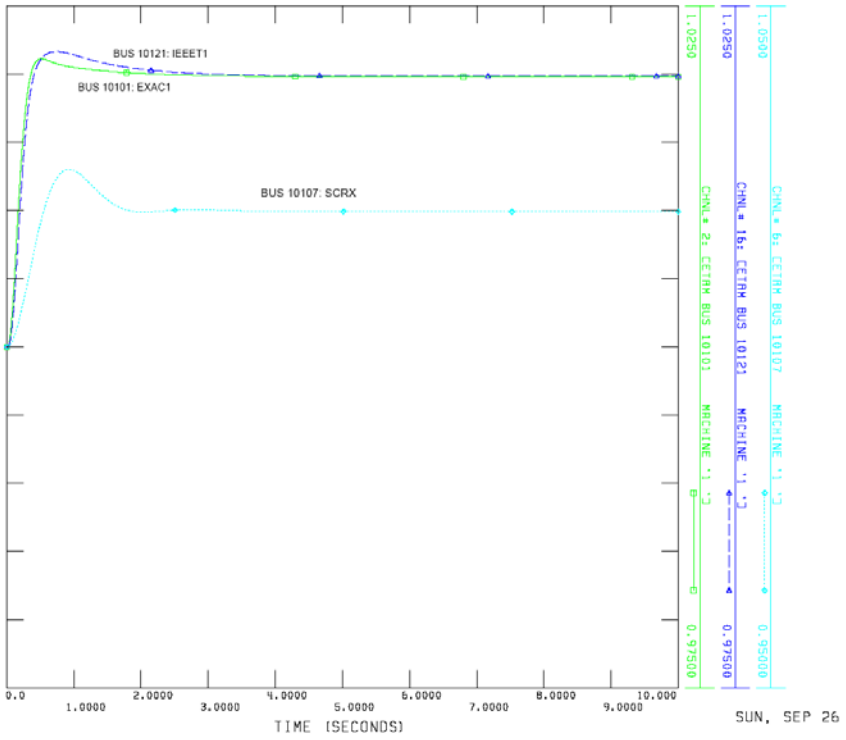

Figure 7.6 Machine Terminal Voltages at Buses 10101, 10121 and 10107

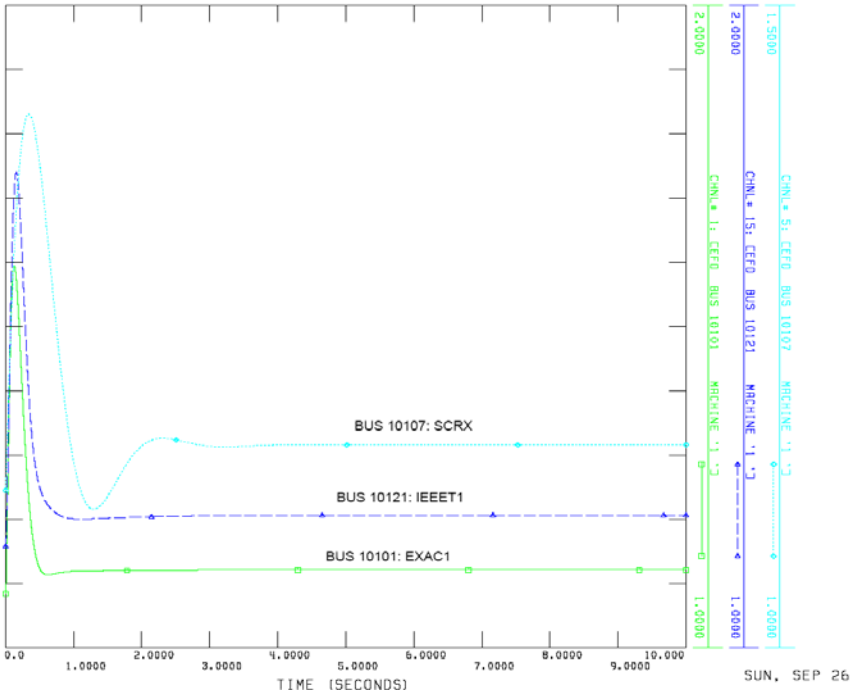

Figure 7.7 Generator Main Field Voltages at Buses 10101, 10121 and 10107

7.2.2 Response of Speed Governor

The test system consists of two types of speed governors (IEEEG1and HYGOV). A sudden change in the load demand has been applied to show the reaction of speed governor. The turbine mechanical power (in Figure 7.8) and the machine speed deviation from nominal (in Figure 7.9) at buses 10121 and 10122 are shown to present the response of IEEEG1 and HYGOV, respectively. It can be seen that speed (frequency) reaches a new steady state in about 15 seconds without restoring to its nominal value. This deviation is proportional to the steady state droop in the model and the magnitude of the step change in load. In addition, the response of the hydro units is slower.

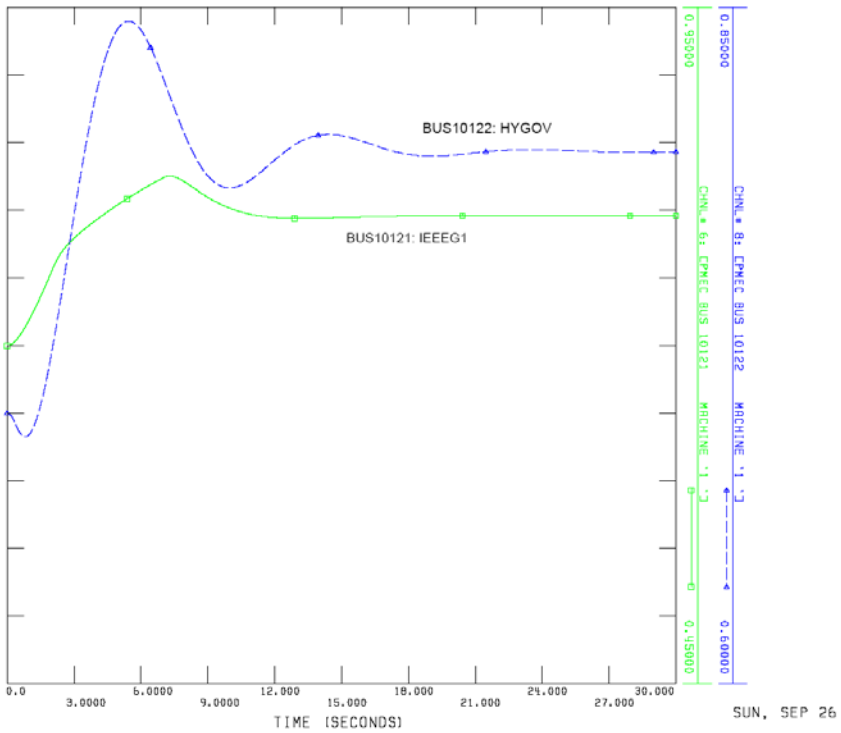

Figure 7.8 Turbine Mechanical Power at Buses10121 and 10122

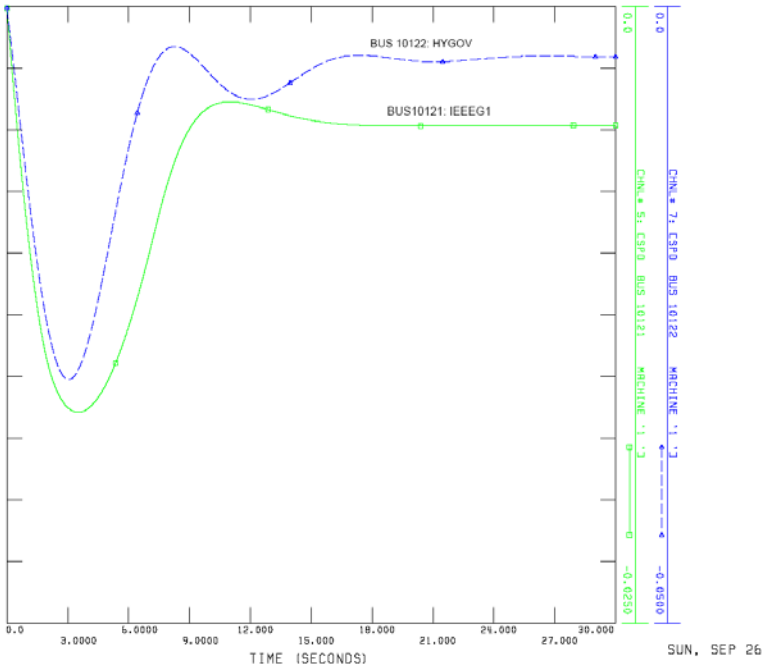

Figure 7.9 Machine Speed Deviation at Buses 10121 and 10122

There are other dynamic characteristics of components which may take longer time to be active in the response to voltage stability. For example, the maximum excitation limiter becomes affected at around $t = 50s$ and reduces the field voltage, resulting in a reduction in reactive power output.

The most critical contingency identified in AC contingency analysis will be applied for transient voltage stability assessment, whose results will be compared with those of static voltage stability assessment. The dynamic simulation of pre-contingency system will run to 1.0 second before the circuit between buses 106 and 110 is open to trigger the simulation of post-contingency system. The dynamic simulation will continue to 120 seconds so that the system can reach the stable status after being subjected to disturbance, taking the possible dynamic characteristics into considerations.

7.2.3 Extend Modal Analysis to Dynamic Simulation

An attempt has been made to extend modal analysis to dynamic simulation, where the static model of generator is incorporated with the representation of synchronous machine and its voltage control. Dynamic voltage stability indicator here follows the concept of modal analysis, which has been discussed in Chapter 5. Basically, the machine buses are assigned as PQ loads with the machine power injection treated as voltage dependent loads. Table 7.5 gives an example to summarize the system pre- and post-contingency conditions, where the effect of dynamic characteristics has been included. In Table 7.5, bus 106 is the concerned critical point, bus 1106 is a load bus, and buses 10101, 10107, 10121 and 10122 are generator buses representing the different excitation systems or speed governors.

Based on Table 7.5, it can be seen that generator active power outputs at buses 10101, 10107, 10121 and 10122 remain the values for both pre- and post-contingency cases with or without SVC dynamics, but reactive power outputs increase for post-contingency case. The active and reactive power consumed at load bus 1106 decrease for post-contingency case without SVC dynamics, but recover to the initial status with the support of SVC dynamics. The voltages at generator terminal buses remain constant for all discussed cases, the voltage at the load bus drops, and the voltage at the critical bus drops even more.

Table 7.5 A Summary of System Pre- and Post-Contingency Conditions

		Voltage (p.u.)		Active Power (MW)		Reactive Power (MVar)	
		Pre-	Post-	Pre-	Post-	Pre-	Post-
Bus 106	No SVC	1.025	0.891	--	--	--	--
	SVC		0.978				
Bus 1106	No SVC	1.035	0.962	149.6	139.02	30.8	26.60
	SVC		1.028		148.58		30.38
Bus 10101	No SVC	1.029	1.027	10	9.99	7.34	10.48
	SVC		1.028		10		9.28
Bus 10107	No SVC	1.037	1.041	80	79.99	49.15	51.69
	SVC		1.037		80		51.57
Bus	No SVC	1.047	1.046	398.66	398	182.74	192.98
10121	SVC			398.63	400		191.65
Bus 10122	No SVC	1.003	1.003	50	49.87	3.75	4.42
	SVC			49.99	50.2		4.36

Modal analysis is extended to the applications of the system in the conditions of pre-contingency and post-contingency with or without SVC support, to predict the voltage stability for these four cases of study. The analysis results are summarized in Table 7.6.

The results in Table 7.6 show the decreasing trend of the minimum eigenvalues with the increasing loading levels. It also shows that the voltage stability level is even higher after the contingency occurred, because of the combined effect of excitation system, speed governor, load reduction, OLTC, and SVC dynamic. In addition, based on the analysis in Section 7.3.1, it can conclude the excitation is a fast response while the governor is a slow response, MEL is slower. However, it is very hard to differentiate these effect of dynamic characteristics on voltage stability without referring to any assessment results. Therefore, the time domain simulation comes to application.

Table 7.6 The Results of Modal Analysis Extended to Dynamic Simulation

Loading level (*Base Load)	Minimum Eigenvalue			
	Pre-Contingency		Post-Contingency	
	No SVC	SVC	No SVC	SVC
1.0	8.383008	8.383152	8.424100	8.424128
1.1	8.0306967	8.030629	8.087635	8.087725
1.2	7.5270954	7.526713	7.607723	7.607723
1.3	6.7801722	6.779235	6.900581	6.900579
1.4	5.5418913	5.539631	5.750243	5.750183
1.5	2.2404548	2.226122	3.063616	3.064147
1.6	0.5545889	0.021486	0.026007	21.07059

7.2.4 Time Domain Simulation of Outage of the Cable between Buses 106 and 110

The most critical contingency and the time sequence mentioned in Section 7.2.3 are implemented in the time domain simulation. The voltages at buses 106 and 1106, as well as the active and reactive power at bus 1106 are shown as Figures 7.10 through 7.12.

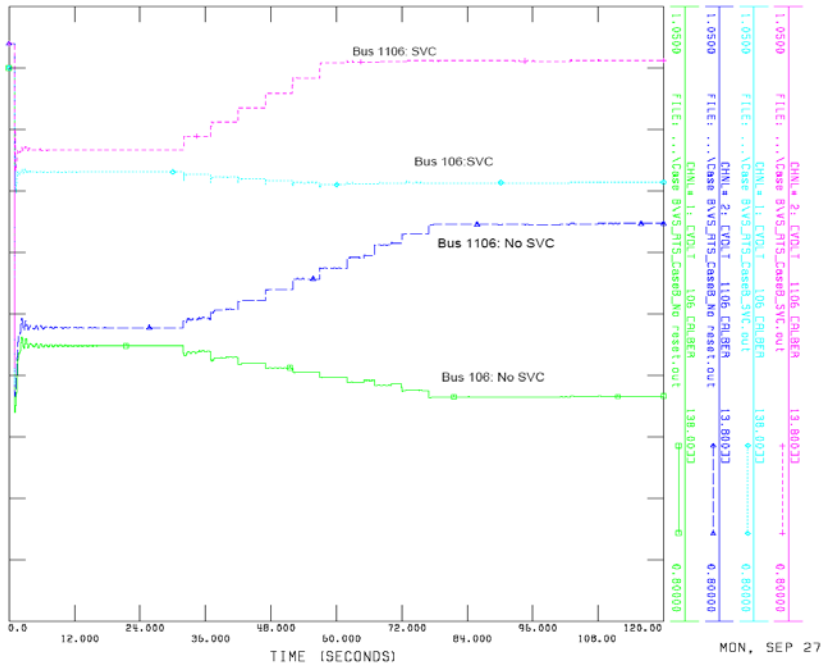

Figure 7.10 Voltages at Buses 106 and 1106

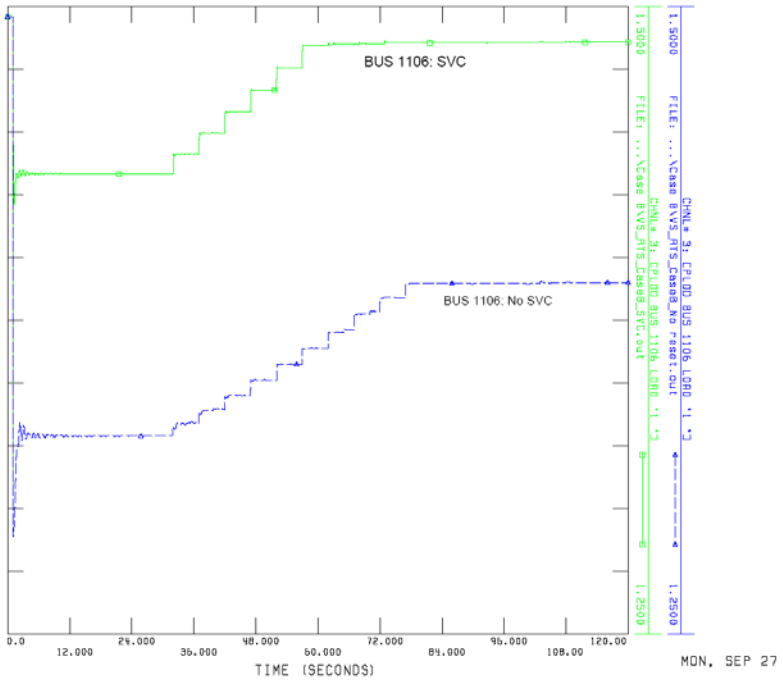

Figure 7.11 Active Power at Load Bus 1106

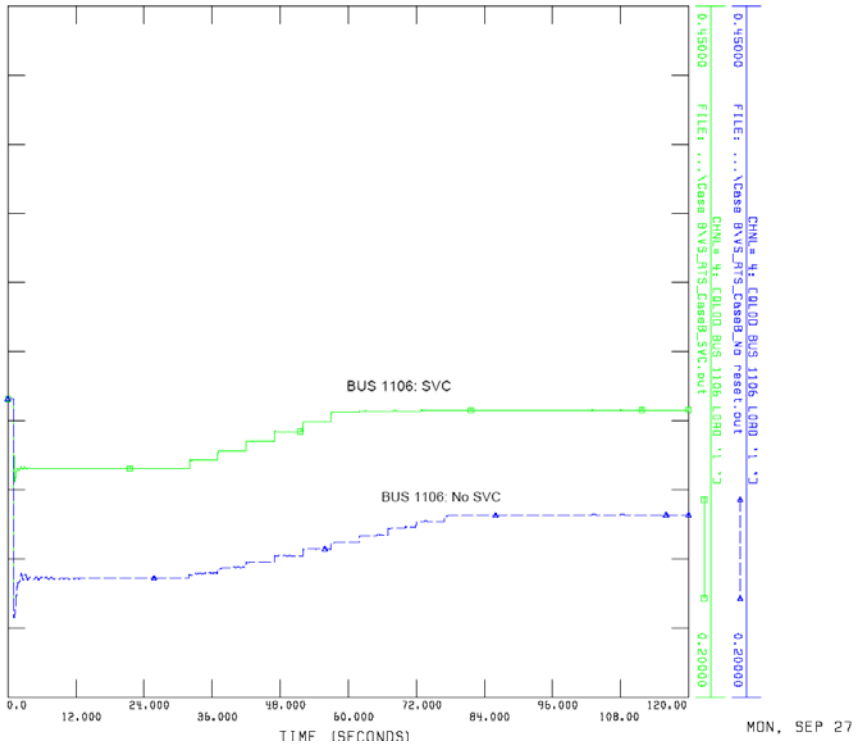

Figure 7.12 Reactive Power at Load Bus 1106

From analysis results in Section 7.2.3, it can conclude that the power flow solution did not converge, and QV plot showed a voltage collapse condition for contingency #30 in static assessment. But in Figure 7.10, the voltage at the load bus 1106 is higher than the initial condition due to the response of SVC combined with the response of OLTC, while the voltage at buses 106 and 1106 did not recover if SVC is blocked (switched shunt is held constant at its initial value). Hence, the dynamic characteristic of SVC is critical to avoid a voltage collapse around bus 106. The active (in Figure 7.11) and reactive (in Figure 7.12) load power demand is reduced, and the voltage stabilizes at around 0.9 p.u. If load recovery is taken into account, voltages will decrease even more. The influence of load model in dynamic simulation, such as the effect of induction motors is the other phenomenon of interest to be investigated in the future work.

7.3 Summary

This chapter describes the procedure of transient voltage stability assessment for RTS-96. The system description is introduced and the contingency lists are specified for load flow and AC contingency analysis. The critical contingencies have been selected by screening the contingency lists. Modal analysis, QV plot and PV plot are performed for the base case and the selected contingencies. The most critical contingency is identified, and the associated reactive power margin and transfer capability are calculated. Modal analysis has been extended for application of transient voltage stability. Although it provides some general information of voltage stability, the time-domain simulation is still necessary to differentiate the response of dynamic characteristics of components in transient voltage stability assessment.

CHAPTER VIII

CONCLUSIONS AND FUTURE WORK

Voltage stability is a concern with the operation of a terrestrial power system close to its limit, and is of interest in a shipboard power system in terms of its survivability. Voltage stability is gaining importance and becoming more complicated, with the integration of DC links into AC systems to improve the flexibility of power transmission and distribution. The objectives of voltage stability assessment are to determine the current system state, to estimate its proximity to instability, and to identify the involved areas and contributing factors. All of these goals can be achieved by extending existing methods and developing new algorithm, model and formulation.

8.1 Conclusions

The proposed methodology in this work is a comprehensive and systematical method for voltage stability assessment. In this method, the eliminated variable method is introduced to include the DC effect into AC systems. This method has basis of the single-infeed DC configuration, and it is also a generalization of a multi-infeed DC configuration. It is an easy way to calculate the partial derivatives of AC/DC systems, so as to obtain the Jacobian matrix for AC/DC systems, independent of DC configurations. Modal analysis is a useful voltage stability assessment method suitable for a wide range of systems, and provides information regarding the critical operating mode, contributing buses, branches and generators.. Usually the modal analysis is used for a “pure” AC system. After being combined with the eliminated variable method, the modal analysis

can be extended for hybrid AC/DC systems.. In addition, the dynamic characteristics of a generator can be easily added by handling the generator "PV" bus with a voltage-dependent "PQ" load. Correspondingly, modal analysis can be extended for applications of dynamic simulation. This is a reliable method for fast voltage stability assessment.

In modal analysis, the minimum eigenvalue is the indicator for assessment, but it is nonlinear and discontinuous when the system devices hit their limits. In this work, the second order performance indicator is proposed to overcome this weakness. An effective algorithm of Hessian matrix based on the power flow model was developed to derive this indicator. This indicator shows the linearity, and it is straightforward to estimate the proximity based on this linear trend. This method is an improvement of modal analysis, and can be a complement for the fast voltage stability assessment.

The modal analysis and its AC/DC extension and the developed indicator have been implemented in the WSCC 3-machine 9-bus system in different control modes, namely only AC system, with DC in power control, and with DC in current control. The results verified these tools to be effective by calculating the loading margin. The loading margin is the widely used and accurate method for static voltage stability assessment. The dynamic extension of modal analysishas also been applied in the transient voltage stability assessment of the modified IEEE one-area RTS-96 system. It shows a general trend toward voltage instability, but cannot differentiate the response of dynamic characteristics. Hence, the detailed time-domain simulation was performed to benchmark the results from the static assessment, and to provide the information of response of dynamic components.

The specific contributions of this research work are summarized below:

- The eliminated variable method was introduced to solve the load flow and calculate the Jacobian matrix of hybrid AC/DC power systems. By combining it with the eliminated variable method, the classical modal analysis can be extended for the voltage stability assessment of hybrid AC/DC power systems. This method is straightforward for implementation and easy for modification for the existing software program for AC systems.

- An effective Hessian matrix was developed to investigate the embedded information in singular values of system Jacobian matrix. A second order performance indicator was proposed and developed as an improvement of the modal analysis for the fast prediction of voltage stability.

- The widely used modal analysis was applied for an integrated shipboard power system with a multi-infeed DC configuration.

8.2 Future Work

As with any research, there is always something more to be done. This proposed work also poses several additional problems. First, the converter model, especially the multi-terminal converter model, is a challenge, and can be investigated further. Further work may involve the investigation of more dynamic characteristics for transient voltage stability assessment. For example, the dynamic phenomenon of the complex load model is an important factor to voltage instability. Second, since there is very limited shipboard power system model available, the application of this method related to a larger, more detailed shipboard power system is expected to be investigated further when more information becomes available.

Enhancing testing and improvement is required for the developed stability indicator. During the derivation procedure, several matrices and vectors have been calculated, which provide the embedded information used to evaluate certain control. However, these manipulations and products are more time intensive to compute so changes in their formulation are necessary to make it faster. There is a trade off in the

accuracy and computational cost. Hence, the developed indicator should be compared with other indicators to demonstrate its effectiveness and the involved tradeoffs. This indicator is also expected to be tested for larger terrestrial power systems and shipboard power systems.

REFERENCES

[1] C. W. Taylor, *Power System Voltage Stability*, EPRI Power System Engineering Series, McGraw Hill, 1994.

[2] N. Doerry, "Next Generation Integrated Power System Technology Development Roadmap", Final Report, November 2007, Available from U.S. Navy Electronic Commerce Online.

[3] B. M. Weedy and B. R. Cox, "Voltage Stability of Radial Power Links", *Proc. IEE*, Vol. 115, pp. 528-536, April, 1968.

[4] V. A. Venikov, V. A. Stroev, V. I. Idelchick, and V. I. Tarasov, "Estimation of Electric Power System Steady-State Stability in Load Flow Calculation", IEEE Trans. On Power Apparatus and Systems, vol. PAS-94, pp. 1034-1041, May/June 1975.

[5] V. Ajjarapu and B. Lee, "Bibliography on Voltage Stability", *IEEE Transactions on Power Systems*, Vol. 13, Issue 1, Feb. 1998, pp. 115-125.

[6] Prahba Kundur, *Power System Stability and Control*, EPRI Power System Engineering Series, McGraw Hill, 1994.

[7] B. Anderson, and C. Barker, "A New Era in HVDC", *IEE Review*, Vol. 46, Issue 2, March 2000, pp. 33-39.

[8] IEEE/CIGRE Joint Task Force on Stability Terms and Definitions, "Definition and Classification of Power System Stability", *IEEE Transactions on Power Systems*, Vol. 19, No. 2, May 2004, pp. 1387-1401.

[9] T. V. Cutsem and C. Vournas, *Voltage Stability of Electric Power Systems*, Power Electronics and Power Systems Series, Kluwer Academic Publisher, 1998.

[10] North American Electric Reliability Council, *Transmission Transfer Capability: A reference Document for Calculating and Reporting the Electric Power Transfer Capability of Interconnected Electric System*, May 1995.

[11] T. Nord, "Voltage Stability in an Electric Propulsion System for Ships", *M. S. Thesis*, Royal Institute of Technology, Sweden, 2006.

[12] Y. Wang, da Silva, L. C. P., W. Xu, and Y. Zhang, "Analysis of Ill-conditioned Power Flow Problems Using Voltage Stability Methodology", *Generation, Transmission and Distribution, IEE Proceedings*, Vol. 148, Issue 5, 2001, pp. 384-390.

[13] V. Ajjarapu and C. Christ, "The Continuation Power Flow: A Tool for Steady State Voltage Stability Analysis", *IEEE Transactions on Power Systems*, Vol. 7, No. 1, February 1992, pp. 416-423.

[14] X. Zhang, P. Ju, and E. Handschin, "Continuation Three-Phase Power Flow: A Tool for Voltage Stability Analysis of Unbalanced Three-Phase Power Systems", *IEEE Transactions on Power Systems*, Vol. 20, No. 3, August 2005, pp. 1320-1329.

[15] V. A. Venikov, V. A. Stroer, and et. al., "Estimation of Electrical Power System Steady-State Stability", *IEEE Transactions on Power Apparatus and Systems*, Vol. PAS-94, No. 3, May/June 1975, pp. 1034-1040.

[16] H. G, Kwatoy, A. K, Pasrija, andL. Y. Bahar, "Static Bifurcation in Electric Power Network Loss of Steady-State Stability and Voltage Collapse", *IEEE Transactions on Circuits and System*, Vol. CAS-33, No.10, 1986, pp. 981-982.

[17] B. Gao, G. K. Morison, and P. Kundur, "Voltage Stability Evaluation Using Modal Analysis", *IEEE Transaction on Power Systems*, vol. 7, NO. 4, Nov. 1992, pp. 1529-1542.

[18] A. Tiranuchit and R. J. Thomas, "A Posturing Strategy Against Voltage Stabilities in Electric Power System", *IEEE Transactions on Power Systems*, Vol. 3, No. 1, February 1988, pp. 87-93.

[19] A. Klos and A. Kerner, "The Nonuniqueness of Load Flow Solution", *Proceeding of PSCC-5.3.1/8*, Cambridge, 1975.

[20] A. Yokoyama and Y. Sekine, "A Static Voltage Stability Index Based on Multiple Load Flow Solution", *Proceedings: Bulk Power System Voltage Phenomena – Voltage Stability and Security: EPRI Report EL – 6183*, January 1989.

[21] IEEE Working Group on Power System Stability, *Voltage Stability Assessment: Concepts, Practices and Tools*, IEEE PSE Power System Stability Subcommittee Special Publication SP101PSS, 2002.

[22] V. Ajjarapu, and B. Lee, "Bifurcation Theory and its Application to Nonlinear Dynamic Phenomena in an Electrical Power System", *IEEE Transactions on Power Systems*, Vol. 7, Feb. 1992, pp. 424-431.

[23] S. Ayasun, C. O. Nwankpa, and H. G. Kwatny, "Computation of Singular and Singularity Induced Bifurcation Points of Differential-Algebraic Power System Model", *IEEE Transactions on Circuits and Systems I: Regular Papers*, Vol. 51, Aug. 2004, pp. 1525-1538.

[24] S. K. Khaitan, J. D. McCalley, and Qinming Chen, "Multifrontal Solver for Online Power System Time-Domain Simulation", *IEEE Transactions on Power Systems*, Vol. 23, Nov. 2008, Page(s): 1727 – 1737.

[25] Kuo Lung Lian, and T. Noda, "A Time-Domain Harmonic Power-Flow Algorithm for Obtaining Nonsinusoidal Steady-State Solutions", *IEEE Transactions on Power Delivery*, Vol. 25, July 2010, pp. 1888-1898.

[26] Garng M. Huang, Liang Zhao, and Xuefeng Song, "A New Bifurcation Analysis for Power System Dynamic Voltage Stability Studies", *IEEE Power Engineering Society Winter Meeting*, Vol . 2, Jan 27-31, 2002, pp. 882-887.

[27] Y. C. Su, S. J. Cheng, and J. Y. Wen, "Power System Dynamic Stability Analysis and Stability Type Discrimination", *Universities Power Engineering Conference, 2006, UPEC'06, Proceeding of the 41st International*, Vol. 2 Sept 6-8, 2006, pp 516-520.

[28] Diaz de Leon, J. A. II, and C. W. Taylor, "Understanding and Solving Short-term Voltage Stability Problems", Power Engineering Society Summer Meeting, 2002 IEEE, Vol. 2, July 2002, Page(s): 745 – 752.

[29] R. M. Monteiro Pereira, Adelino J. C. Pereira, C. M. Machado Ferreira, and F. P. Maciel Barbosa, "Dynamic Voltage Stability Assessment of an Electric Power Network using Composite Load Models", *Universities Power Engineering Conference*, 2008, UPEC, 2008, 43rd, International, Sept. 1-4,2008, pp 1-5.

[30] **A.** Borghetti, R. Caldon, **A.** Mari and C. **A.** Nucci, "On Dynamic Load Models for Voltage Stability Studies", *IEEE Transactions on Power Systems*, Vol. 12, No. 1, February 1997, pp. 293-303.

[31] A. E. Hammad, "Stability and Control of HVDC and AC Transmissions in Parallel", *IEEE Transactions on Power Delivery*, Vol. 14, No. 4, October 1999, pp. 1545-1554.

[32] D. J. Shoup, J.J. Paserba, and C.W. Taylor, "A survey of current practices for Transient Voltage Dip/Sag Criteria Related to Power System Stability", *Proceedings of IEEE/PES Power System Conference and Exposition*, 10-13 October 2004, New York.

[33] C. W. Taylor, "Concept of Undervoltage Load Shedding for Voltage Stability", *IEEE Transactions on Power Systems*, Vol. 7, No. 2, April 1992, pp. 480-488.

[34] G. D. Irisarri, X. Wang, J. Tong, and S. Moktari, "Maximum Loadability of Power Systems using Interior Point non-linear Optimization Method", *IEEE Transactions on Power Systems*, Vol. 12, No. 1, February 1997, pp. 162-172.

[35] K. Iba, H. Suzuki, M. Egawa, and T. Watanabe, "Calculation of Critical Loading Condition with Nose Curve using Homotopy Continuation Method", *IEEE Transaction on Power Systems*, vol. 6, no. 2, May 1991, pp. 584-593.

[36] T. V. Cutsem, "A Method to Compute Reactive Power Margins with Respect to Voltage Collapse", *IEEE Transaction on Power Systems*, Vol. 6, No. 1, February 1991, pp. 145-156.

[37] C. J. Parker, I. F. Morrison, and D. Sutanto, "Application of an Optimization Method for Determining the Reactive Margin from Voltage Collapse in Reactive Power Planning", *IEEE Transactions on Power Systems*, Vol. 11, No. 3, August 1996, pp. 1473-1481.

[38] F. L. Alvarado, I, Dobson, and Y. Hu, "Computation of Closest Bifurcations in Power Systems", pp. 5.23-5.38 in L. H. Fink, editor, *Proc. Bulk Power System voltage Phenomena – Voltage Stability and Security*, EL-6183, EPRI, January 1989.

[39] Denis Lee Hau Aik, and G. Andersson, "Quasi-Static Stability of HVDC Systems Considering Dynamic Effects of Synchronous Machines and Excitation Voltage Control", *IEEE Transactions on Power Delivery*, Vol. 21, No. 3, July 2006, pp.1501-1514.

[40] Y. Mansour, editor, "Suggested Techniques for Voltage Stability Analysis", *Technique Report 93TH0620-5PWR*, IEEE/PES, 1993.

[41] P. A. Lof, T. Smed, G. Andersson, and D. J. Hill, "Fast Calculation of a Voltage Stability Index", *IEEE Transactions on Power Systems*, Vol. 7, No. 1, February 1992, pp. 54-64.

[42] I. Dobson, "Observations on the Geometry of Saddle Node Bifurcations and Voltage Collapse in Electrical Power Systems", *IEEE Transactions on Circuits and Systems - I*, vol. 39, no. 3, March 1992, pp. 240-243.

[43] S. Greene, I. Dobson, and F. L. Alvarado, "Sensitivity of the Loading Margin to Voltage Collapse with Respect to Arbitrary Parameters", *IEEE Transactions on Power Systems*, vol. 12, no. 1, February 1997, pp. 262-272.

[44] Y. Ramura, H. Mori, and S. Iwamoto, "Relationship between Voltage Instability and Multiple Load Flow Solutions in Electric Power Systems", *IEEE Transactions on Power Apparatus and Systems*, vol. 102, no. 5, May 1983, pp. 1115-1125.

[45] C. A. Canizares, A. Z. de Souza, and V. H. Quintana, "Comparison of Performance Indices for Detection of Proximity to Voltage Collapse", *IEEE Transactions on Power Systems*, Vol. 11, no. 3, August 1996, pp. 1441-1250.

[46] A. C. Z. de Souza, C. A. Canizares, and V. H. Quintana, "New Techniques to Speed up Voltage Collapse Computations using Tangent Vectors", *IEEE Transactions Power Systems*, vol. 12, no. 3, August 1997, pp. 1380-1387.

[47] Theodore Wildi, *Electrical Machines, Drives, and Power Systems (5th Ed.)*, Pearson Education, 2002.

[48] John G. Ciezki and Robert W. Ashton, "Selection and Stability Issues Associated with a Navy Shipboard DC Zonal Electric Distribution System", *IEEE Transactions on Power Delivery*, Vol. 15, No. 2, April 2000, pp. 665-669.

[49] M. D. Heffernan, K. S. Turner, J. Arrillaga and C. P. Arnold, "Computation of AC-DC System Disturbances, Parts I, II and III", *IEEE Transactions on Power Apparatus and Systems*, Vol. PAS-100, No. 11, November 1981, pp.4341-4346.

[50] J. Reeve and R. Adapa, "A New Approach to Dynamic Analysis of AC Networks Incorporating Detailed Modelling of DC Systems, Parts I and II", *IEEE Transactions on Power Delivery*, Vol. PD-3, No. 4, October 1988.

[51] PSS®NETOMAC program description, software solutions. Available: http:// www.energy.siemens.com.

[52] J. Reeve, G. Fahmy and B. Stott, "Versatile load flow method for multi-terminal HVDC systems", *IEEE Transactions on Power Apparatus and Systems*, Vol. PAS-96, No.3, 1977, pp. 925-33

[53] H. Fudeh and C.M. Ong, "A simple and efficient AC-DC load flow method for multi-terminal DC systems", *IEEE Transactions on Power Apparatus and Systems*, Vol. PAS-100, No 7, 1981, pp. 4389-4396

[54] D.A. Braunagel, L.A. Kraft and J.L. Whysong, "Inclusion of DC converter and transmission equations directly in a Newton Power Flow", *IEEE Transactions on Power Apparatus and Systems*, PAS-95, No 1, 1976, pp. 76-88

[55] M.M. El.Marsafawy and R.M. Mathur, "A new, fast technique for load-flow solution of integrated multi-terminal DC/AC systems", *IEEE Transactions on Power Apparatus and Systems*, PAS-99, No 1, 1980, pp. 246-255

[56] T. Smed, G. Andersson, G.B. Sheble, and L.L. Grigsby, "A new approach to AC/DC power flow", *IEEE Transactions on Power Systems*, Vol. 6, No 3, 1991, pp. 1238-1316

[57] Denis L.H. Aik and G. Andersson, "Nonlinear Dynamics in HVDC Systems", *IEEE Transactions on Power Delivery*, Vol. 14, No. 4, 1999, pp. 1417-1426.

[58] IEEE Task Force Report, "Load Representation for Dynamic Performance Analysis", *IEE Transactions on Power Systems*, Vol.8, May 1993, pp.472-482.

[59] IEEE Task Force Paper, "Standard Load Models for Power Flow and Dynamic Performance Simulation", *IEEE Transactions on Power Systems*, Vol. 10, No. 3, August 1995, pp. 1302-1313.

[60] *IEEE Guide for Synchronous Generator Modeling Practices in Stability Analyses*, IEEE Standard 1110-1991, March 21, 1991.

[61] PSS/E™ 30.2 Program Application Guide, Volume II, Siemens PTI.

[62] Peter W. Sauer, and M. A. Pai, *Power System Dynamics and Stability*, Prentice Hall, 1998.

[63] MATPower User's Manual, Available: http://www.pserc.cornell.edu/matpower/

[64] Power System Toolbox description, Available: http://www.ecse.rpi.edu/pst/PST.html

[65] PSS/E description, Available: http://www.energy.siemens.com/hq/en/services/power-transmission-distribution/power-technologies-international/software-solutions/pss-e.htm

[66] Reliability Test System Task Force of the Application of Probability Methods Subcommittee – "The IEEE Reliability Test System- 1996", *IEEE Transactions on PWRS,* vol.14, no. 3, Aug. 1999, pp. 1010-1020

[67] RTS data description, Available: http://www.ee.washington.edu/research/pstca/rts/pg_tcarts.htm

[68] A. Berizzi, P. Bresesti, P. Marannino, G.P. Granelli, and M. Montagna, "System-area operating margin assessment and security enhancement against voltage collapse", *IEEE Trans. Power Systems*, vol. 11, No. 3, August 1996, pp 1451-1462

[69] Arthur R. Bergen, and Vijay Vittal, *Power Systems Analysis,* 2nd Edition, Prentice-Hall, Inc., 2000, pages 345-346

[70] CDR John V. Amy Jr, "Considerations in the Design of Naval Electric Power Systems", *Proceedings of IEEE Power Engineering Society Summer Meeting*, 25-25 July 2002, 1: 331-335

[71] C. Petry, and J. Rumburg "Zonal Electrical Distribution Systems: An Affordable Architecture for Future", *Naval Engineers Journal*, May 1993, 105:45-51

[72] J. G. Ciezki and R. W. Ashton "Selection and Stability Issues Associated with a Navy Shipboard DC Zonal Electric Distribution System", *IEEE Transactions on Power Delivery*. April 2000; 15(2):665-669

[73] N. Doerry (Naval Sea Systems Command, Washington DC), "Next generation integrated power system technology development roadmap" Final Report. November 2007. Available from: US Navy Electronic Commerce Online

[74] James A. Momoh, and Sahar, S. Kaddah, "Comparative Study between Two Voltage Stability Methods for Integrated Shipboard Power System with DC Zonal", *North American Power Symposium Conference 2002*, Vol. 1, pp. 294-299.

[75] CAPS @ Florida State University, *RTDS Notional E-ship Model Technical Guide*, Version 3.4, Tallahassee, Florida

APPENDIX A

PARTIAL DERIVATIVES OF AC/DC SYSTEMS

This appendix provides additional details related to the partial derivatives of ac/dc systems. Note that the variables not defined below are defined in the List of Symbols

When the DC link is included in the power flow equations, only the mismatch equations at the converter terminal AC buses have to be modified as Equations A.1-A.4.

$$\Delta P_{tr} = P_{tr}^{spec} - P_{tr}^{ac}(\theta, V) - P_{dr}(V_{tr}, V_{ti}, X_{dc}) \tag{A.1}$$

$$\Delta P_{ti} = P_{ti}^{spec} - P_{ti}^{ac}(\theta, V) + P_{di}(V_{tr}, V_{ti}, X_{dc}) \tag{A.2}$$

$$\Delta Q_{tr} = Q_{tr}^{spec} - Q_{tr}^{ac}(\theta, V) - Q_{dr}(V_{tr}, V_{ti}, X_{dc}) \tag{A.3}$$

$$\Delta Q_{ti} = Q_{ti}^{spec} - Q_{ti}^{ac}(\theta, V) - Q_{di}(V_{tr}, V_{ti}, X_{dc}) \tag{A.4}$$

Where, X_{dc} is a vector of internal dc variables and satisfies Equation A.5.

$$R(V_{tr}, V_{ti}, X_{dc}) = 0 \tag{A.5}$$

Here, R is a set of equations given by Equations 3.4-3.6 and four control specifications, which are determined by control modes listed in Table A.1.

Power flow is solved after each iteration of Equation A.6.

$$\begin{bmatrix} \Delta P \\ \Delta Q \end{bmatrix} = \begin{bmatrix} H & N \\ J & L \end{bmatrix} \begin{bmatrix} \Delta \theta \\ \Delta V / V \end{bmatrix} \tag{A.6}$$

The Equations A.5 are solved for X_{dc} as Equation A.7.

$$X_{dc} = f(V_{tr}, V_{ti}) \tag{A.7}$$

The active and reactive powers consumed by the converters can be written as functions of V_{tr} and V_{ti}, as shown in Equation A.8.

$$P_{dr} = P_{dr}(V_{tr}, V_{ti}, X_{dc}) = P_{dr}(V_{tr}, V_{ti}, f(V_{tr}, V_{ti})) = P_{dr}(V_{tr}, V_{ti}) \tag{A.8}$$

Table A.1 Control Modes of DC Lines

Control mode	Specified Variables			
A	α_r	γ_i	V_{di}	P_{di}
B	T_r	γ_i	V_{di}	P_{di}
C	α_r	γ_i	T_i	P_{di}
D	T_r	γ_i	T_i	P_{di}
E	α_r	γ_i	T_r	P_{di}
F	α_r	T_i	V_{di}	P_{di}
G	α_r	T_i	T_r	P_{di}

By this means, Equation A.6 can be replaced by Equation A.9.

$$\begin{bmatrix} \Delta P \\ \Delta Q \end{bmatrix} = \begin{bmatrix} H & N' \\ J & L' \end{bmatrix} \begin{bmatrix} \Delta\theta \\ \Delta V / V \end{bmatrix} \tag{A.9}$$

Where,

$$N'(tr, tr) = V_{tr} \frac{\partial P_{tr}^{ac}}{\partial V_{tr}} + V_{tr} \frac{\partial P_{dr}(V_{tr}, V_{ti})}{\partial V_{tr}} \tag{A.10}$$

$$N'(tr, ti) = V_{ti} \frac{\partial P_{tr}^{ac}}{\partial V_{ti}} + V_{ti} \frac{\partial P_{dr}(V_{tr}, V_{ti})}{\partial V_{ti}} \tag{A.11}$$

$$N'(ti, tr) = V_{tr} \frac{\partial P_{ti}^{ac}}{\partial V_{tr}} - V_{tr} \frac{\partial P_{di}(V_{tr}, V_{ti})}{\partial V_{tr}} \tag{A.12}$$

$$N'(ti, ti) = V_{ti} \frac{\partial P_{ti}^{ac}}{\partial V_{ti}} - V_{ti} \frac{\partial P_{di}(V_{tr}, V_{ti})}{\partial V_{ti}} \tag{A.13}$$

Similarly, L' is modified as Equations A.14-A.17.

$$L'(tr,tr) = V_{tr}\frac{\partial Q_{tr}^{ac}}{\partial V_{tr}} + V_{tr}\frac{\partial Q_{dr}(V_{tr},V_{ti})}{\partial V_{tr}} \tag{A.14}$$

$$L'(tr,ti) = V_{ti}\frac{\partial Q_{tr}^{ac}}{\partial V_{ti}} + V_{ti}\frac{\partial Q_{dr}(V_{tr},V_{ti})}{\partial V_{ti}} \tag{A.15}$$

$$L'(ti,tr) = V_{tr}\frac{\partial Q_{ti}^{ac}}{\partial V_{tr}} + V_{tr}\frac{\partial Q_{di}(V_{tr},V_{ti})}{\partial V_{tr}} \tag{A.16}$$

$$L'(ti,ti) = V_{ti}\frac{\partial Q_{ti}^{ac}}{\partial V_{ti}} + V_{ti}\frac{\partial Q_{di}(V_{tr},V_{ti})}{\partial V_{ti}} \tag{A.17}$$

Several points are worth mentioning here. First, using $\Delta P/|V|$ and $\Delta Q/|V|$ rather than ΔP and ΔQ as bus mismatch reduces the number of operations needed in constructing the Jacobian coefficient matrix. Each ac system bus adds two constraints (i.e. $\Delta P/|V|, \Delta Q/|V|$) and two unknowns (i.e. $\Delta\theta$, $\Delta V/|V|$), while each dc system bus adds one unknown $\Delta P/|V|$ and one variable $\Delta V/|V|$.

To illustrate the procedure of partial derivatives in AC/DC systems, the analytical elimination is carried out in detail for some representative modes.

In general when two of the variables $[P_{dr} \quad P_{di} \quad V_{dr} \quad V_{di} \quad I_d]$ are specified, the other three can be computed from Equations 3.6-3.8. The partial derivative of reactive power can be calculated as Equation A.18.

$$\begin{aligned}\frac{\partial Q_d}{\partial V_t} &= \frac{\partial(\sqrt{S_d^2 - P_d^2})}{\partial V_t} = \frac{1}{2\sqrt{S_d^2 - P_d^2}} \cdot \frac{2S_d\partial S_d - 2P_d\partial P_d}{\partial V_t} \\ &= \frac{1}{Q_d}\left(S_d\frac{\partial S_d}{\partial V_t} - P_d\frac{\partial P_d}{\partial V_t}\right)\end{aligned} \tag{A.18}$$

<u>*Control mode A*</u>: $[\alpha_r \quad \gamma_i \quad V_{di} \quad P_{di}]$

The active power at the rectifier terminal can be calculated as Equation A.19. Based on Equations 3.4, 3.9 and 3.10, Equations A.20-A.21 can be obtained.

$$P_{dr} = V_{dr} I_d = (V_{di} + R_d I_d) I_d = P_{di} + R_d I_d^2 \tag{A.19}$$

$$\begin{aligned} S_{dr} &= k \frac{3\sqrt{2}}{\pi} T_r V_{tr} I_d = \frac{k}{\cos \alpha_r} (V_{dr} + \frac{3}{\pi} X_c I_d) I_d \\ &= \frac{k}{\cos \alpha_r} (V_{di} + R_d I_d + \frac{3}{\pi} X_c I_d) I_d = k_\alpha (P_{di} + P_L + Q_L) \end{aligned} \tag{A.20}$$

$$\begin{aligned} S_{di} &= k \frac{3\sqrt{2}}{\pi} T_i V_{ti} I_d = \frac{k}{\cos \gamma_i} (V_{di} + \frac{3}{\pi} X_c I_d) I_d \\ &= k_\gamma (P_{di} + P_L) \end{aligned} \tag{A.21}$$

Since P_{di} and V_{di} are specified, I_d is given by Equation 3.8, and P_{dr}, S_{dr}, and S_{di} are expressed in terms of four given specifications $[\alpha_r \quad \gamma_i \quad V_{di} \quad P_{di}]$, their partial derivatives w. r. t V_{tr} and V_{ti} are zero.

<u>*Control mode B*</u>: $[T_r \quad \gamma_i \quad V_{di} \quad P_{di}]$

Since P_{di} and V_{di} are specified, I_d, V_{dr}, P_{dr} and S_{di} are computed as the same as for mode A, except S_{dr}. Since T_r is specified, the partial derivative of S_{dr} w. r. t. V_{tr} is computed with Equation 3.9, and Equations A.22 and A.23 can be obtained.

$$V_{tr} \frac{\partial S_{dr}}{\partial V_{tr}} = V_{tr} (k \frac{3\sqrt{2}}{\pi} T_r I_d) = S_{dr} \tag{A.22}$$

$$V_{tr} \frac{\partial Q_{dr}}{\partial V_{tr}} = V_{tr} \frac{S_{dr}}{Q_{dr}} \frac{\partial S_{dr}}{\partial V_{tr}} = \frac{S_{dr}^2}{Q_{dr}} \tag{A.23}$$

<u>*Control mode C*</u>: $[\alpha_r \quad \gamma_i \quad T_i \quad P_{di}]$

Since T_i and P_{di} are specified, combine Equations 3.5 and 3.8 as Equation A.24.

$$P_{di} = \frac{3\sqrt{2}}{\pi} T_i V_{ti} \cos\gamma_i I_d - \frac{3}{\pi} X_c I_d^2 \tag{A.24}$$

Solve for I_d, and obtain Equation A.25.

$$I_d = \frac{\frac{3\sqrt{2}}{\pi} T_i V_{ti} \cos\gamma_i - \sqrt{(\frac{3\sqrt{2}}{\pi} T_i V_{ti} \cos\gamma_i)^2 - 4\frac{3}{\pi} X_c P_{di}}}{2\frac{3}{\pi} X_c} \tag{A.25}$$

To simplify the expression, assume $C_1 = \frac{T_i \cos\gamma_1}{\sqrt{2} X_c}$, $C_2 = \frac{\pi}{3X_c}$,then obtain Equation A.26.

$$\frac{\partial I_d}{\partial V_{ti}} = C_1 - \frac{C_1^2 V_{ti}}{\sqrt{(C_1 V_{ti})^2 - C_2 P_{di}}} \tag{A.26}$$

For further simplification, define $\partial I_I = \frac{V_{ti}}{I_d} \frac{\partial I_d}{\partial V_{ti}}$

Since P_{di} is given, both of its partials are zero, S_{di} is computed with Equation 3.10. Then, obtain Equations A.27-A.28.

$$V_{tr} \frac{\partial Q_{di}}{\partial V_{tr}} = 0 \tag{A.27}$$

$$V_{ti} \frac{\partial Q_{di}}{\partial V_{ti}} = \frac{1}{Q_{di}} (S_{di} \frac{\partial S_{di}}{\partial V_{ti}} - P_{di} \frac{\partial P_{di}}{\partial V_{ti}}) = \frac{S_{di}^2}{Q_{di}} (1 + \partial I_I) \tag{A.28}$$

Since $P_{dr} = P_{di} + R_d I_d^2$, Equation A.29-A.33 can be obtained.

$$V_{tr} \frac{\partial P_{dr}}{\partial V_{tr}} = 0 \tag{A.29}$$

$$V_{ti} \frac{\partial P_{dr}}{\partial V_{ti}} = V_{ti} 2R_d I_d \frac{\partial I_d}{\partial V_{ti}} = 2R_d I_d^2 \partial I_I = 2P_L \partial I_I \tag{A.30}$$

$$V_{tr}\frac{\partial Q_{dr}}{\partial V_{tr}} = 0 \tag{A.31}$$

$$V_{ti}\frac{\partial S_{dr}}{\partial V_{ti}} = 2\partial I_I k_\alpha (P_L + Q_L) \tag{A.32}$$

$$V_{ti}\frac{\partial Q_{dr}}{\partial V_{ti}} = \frac{2\partial I_I}{Q_{dr}}[k_\alpha S_{dr}(P_L + Q_L) - P_L P_{dr}] \tag{A.33}$$

Other modes

The partial derivatives for the other control modes can be derived analogously.

As a summary, if the tap changer controlling the control angle is specified (modes B, D, F, G), only the reactive power at that converter will depend on corresponding ac voltage; if the tap changer controlling the direct voltage is specified (mode C, D, E, G), all real and reactive powers will depend on the ac voltage at that terminal.

Table A.2 Partial Derivatives for Modes with the Direct Voltage Determined by T_i

Mode	$\frac{\partial P_{dr}}{\partial V_{tr}}$	$V_{tr}\frac{\partial Q_{dr}}{\partial V_{tr}}$	$V_{ti}\frac{\partial P_{dr}}{\partial V_{ti}}$	$V_{ti}\frac{\partial Q_{dr}}{\partial V_{ti}}$	$\frac{\partial P_{di}}{\partial V_{tr}}$	$\frac{\partial Q_{di}}{\partial V_{tr}}$	$\frac{\partial P_{di}}{\partial V_{ti}}$	$V_{ti}\frac{\partial Q_{di}}{\partial V_{ti}}$
A	0	0	0	0	0	0	0	0
B	0	$\frac{S_{dr}^2}{Q_{dr}}$	0	0	0	0	0	0
C	0	0	$2P_L\partial I_I$	$\frac{2\partial I_I}{Q_{dr}}[k_\alpha S_{dr}(P_L + Q_L) - P_{dr}P_L]$	0	0	0	$\frac{S_{dr}^2}{Q_{dr}}(1+\partial I_I)$
D	0	$\frac{S_{dr}^2}{Q_{dr}}$	$2P_L\partial I_I$	$\frac{2\partial I_I}{Q_{dr}}(S_{dr}^2 - 2P_L P_{dr})$	0	0	0	$\frac{S_{dr}^2}{Q_{dr}}(1+\partial I_I)$

Table A.3 Partial Derivatives for Modes with the Direct Voltage Determined by T_r

Mode	$V_{tr}\frac{\partial P_{dr}}{\partial V_{tr}}$	$V_{tr}\frac{\partial Q_{dr}}{\partial V_{tr}}$	$\frac{\partial P_{dr}}{\partial V_{ti}}$	$\frac{\partial Q_{dr}}{\partial V_{ti}}$	$V_{tr}\frac{\partial P_{di}}{\partial V_{tr}}$	$V_{tr}\frac{\partial Q_{di}}{\partial V_{tr}}$	$\frac{\partial P_{di}}{\partial V_{ti}}$	$V_{ti}\frac{\partial Q_{di}}{\partial V_{ti}}$
E	$2P_L\partial I_R$	$\frac{S_{dr}^2(1+\partial I_R)-2P_L\partial I_R P_{dr}}{Q_{dr}}$	0	0	0	$\frac{2\partial I_R}{Q_{di}}Q_L k_r S_{di}$	0	0
F	0	0	0	0	0	0	0	$\frac{S_{di}^2}{Q_{di}}$
G	$2P_L\partial I_R$	$\frac{S_{dr}^2(1+\partial I_R)-2P_L\partial I_R P_{dr}}{Q_{dr}}$	0	0	0	$\frac{S_{di}^2}{Q_{di}}\partial I_R$	0	$\frac{S_{di}^2}{Q_{di}}$

The partial derivatives for all modes in Table A.1 are summarized in Tables A.2 and A.3. Where,

$$\partial I_R = \frac{V_{tr}}{I_d}\frac{\partial I_d}{\partial V_{tr}} \tag{A.34}$$

$$I_d = C_3 V_{tr} - \sqrt{(C_3 V_{tr})^2 - C_4 P_{di}} \tag{A.35}$$

$$C_3 = \frac{3T_r \cos\alpha_r}{\sqrt{2}(\pi R_d + 3X_c)} \tag{A.36}$$

$$C_4 = \frac{\pi}{\pi R_d + 3X_c} \tag{A.37}$$

APPENDIX B

TEST SYSTEM DATA

B.1 WSCC 3-Machine 9-Bus System Dynamic Data

Table B.1 WSCC Machine Data

Parameters	M/C 1	M/C 2	M/C 3
H (secs)	23.64	6.4	3.01
D (pu)	1		
X_d (pu)	0.146	0.8958	1.3125
X_q (pu)	0.0969	0.8645	1.2578
$X_d^{'}$ (pu)	0.0608	0.1198	0.1813
$X_q^{'}$ (pu)	0.0969	0.1969	0.25
$X_d^{"}/X_q^{"}$ (pu)	0.02		
X_l (pu)	0.01		
$T_{d0}^{'}$ (sec)	8.96	6.0	5.89
$T_{q0}^{'}$ (sec)	0.31	0.535	0.6
$T_{d0}^{"}$ (sec)	0.35		
$T_{q0}^{"}$ (sec)	0.07		
S(1, 0)	0.2		
S(1, 2)	0.667		

Table B.2 WSCC Excitation System Data

Parameters	K_A	T_A	$V_{R\max}$	$V_{R\min}$	K_E	T_E	K_F	T_F
	400	0.03	4.687	-4.687	1.0	0.38	0.06	1.0
Parameters	$E_{fd\min}$	E_1	$S(E_1)$	E_2	$S(E_2)$			
	-3.78	2.835	0.17	3.78	0.24			

B.2 Benchmark Shipboard Power System

Table B.3 Generation Limits for Benchmark Shipboard Power System

Generator #	$P_{G\min}$	$P_{G\max}$	$Q_{G\min}$	$Q_{G\max}$	P_G	Q_G
1	0.8	4.0	-1.0	3.0	--	--
2	0.5	3.0	-0.5	2.0	1.8	--
3	0.5	3.0	-0.5	2.0	1.8	--
4	0.5	3.0	-0.5	2.0	1.8	--
5	0.5	3.0	-0.5	2.0	1.8	--

Table B.4 Parameters of Cables for Air Capable Naval-Ship Power System

Cable #	From	To	R (p.u.)	X (p.u.)	$P_{\max}$
1	1	6	0.06	0.15	1.5
2	2	7	0.06	0.2	1.5
3	3	8	0.06	0.2	1.5
4	4	9	0.06	0.2	1.5
5	5	10	0.06	0.2	1.5
6	11	12	0.011	0.07	1.0
7	13	19	0.09 (DC)	--	1.2
8	14	19	0.09 (DC)	--	1.2
9	15	19	0.085 (DC)	--	1.2
10	16	19	0.08 (DC)	--	1.2
11	17	19	0.08 (DC)	--	1.2
12	18	19	0.04 (DC)	--	0.8

Table B.5 Converters Data for the Air Capable Naval-Ship Power System

Converter #	From Bus	To Bus	Type	Voltage (Volts)		X_C (p.u.)
				HV	LV	
1	6	13	AC/DC	4160	1000	0.06
2	7	14	AC/DC	4160	1000	0.06
3	8	15	AC/DC	4160	1000	0.06
4	9	16	AC/DC	4160	1000	0.06
5	10	17	AC/DC	4160	1000	0.06
6	12	18	DC/AC	1000	755	0.04

Table B.6 Ship Service and Propulsion Loads

Bus #	P (p.u.)	Q (p.u.)
1	1.11	0.1
2	1.11	0.1
3	1.11	0.1
4	1.11	0.1
5	1.11	0.1
11	0.385	0.05